Sensory adaptation across cell classes in macaque cortical visual areas V1 and V2

A Dissertation

Presented to the Faculty of the Weill Cornell Graduate School

Of Medical Sciences

In Partial Fulfillment of the Requirements for the Degree of

Doctor of Philosophy

By

Daniel James Thengone

June 2017

SENSORY ADAPTATION ACROSS CELL CLASSES IN

MACAQUE CORTICAL VISUAL AREAS V1 AND V2

DANIEL JAMES THENGONE, PH.D

CORNELL UNIVERSITY, 2017

Effective representation of the sensory world is a complex task because the statistics of sensory events fluctuate over many timescales. Here we study how the brain uses recent stimulus history to alter its representations of sensory information in primate visual cortex, with a focus on the role of inhibition and whether adaptation acts at multiple sites. Adaptation to gratings induced changes in gain, bandwidth, and orientation preference in both excitatory and inhibitory cell types. We find that tuned inhibitory cells adapt in a manner that is distinct from their excitatory counterparts - effects that are consistent with the notion of adaptation-induced disinhibition of cortical interactions. We further show that some of the diversity of effects present at the population level reflects location on the orientation map: cells in pinwheel centers have generally larger adaptation-induced shifts. Moreover, a subset of untuned neurons become tuned after adaptation. Next, we find that adaptation effects in extrastriate area V2 go beyond effects inherited from striate area V1: specifically, attractive shifts to stimuli that are nearly orthogonal to the preferred direction are much larger in V2 compared to V1. The prominence of these attractive shifts correlates with classical perceptual after-effects. More broadly, this finding shows that adaptation modulates sensory processing at multiple cortical levels. Finally, modeling demonstrates that tuned inhibition and pre-synaptic adaptation are required to account for the observed magnitude, direction, and diversity of effects.

BIOGRAPHICAL SKETCH

Daniel James Thengone was born in Abu Dhabi, United Arab Emirates where his parents had immigrated from Kerala, India. Here he attended Sunrise English Private School till 8th grade. In 2003, the Thengone family immigrated to the United States, where Daniel graduated from the Scholars Program at Susan E. Wagner High School in Staten Island, New York. In 2007, he enrolled in the William E. Macaulay Honors College at CUNY Brooklyn, and graduated with a Bachelors of Sciences in Biology in 2011.

In 2012, Daniel enrolled in the doctoral program in the Brain and Mind Research Institute at Weill Cornell Graduate School, where he did his thesis research under the mentorship of Drs. Jonathan D. Victor and Nicholas D. Schiff. After working on multiple topics in computational neuroscience and systems neurology, Daniel will complete his graduate degree (Ph.D) in 2017.

For his graduate work, Daniel received two pre-doctoral fellowships: he was awarded the Ruth L. Kirschstein Pre-doctoral fellowship from the NIH/NEI, and was the inaugural recipient of the Fred Plum Fellowship in Systems Neurology and Neuroscience. Daniel was also a co-recipient of the 2017 Julian R. Rachele Prize – for an outstanding research paper.

“Nihil est in intellectu, quod non prius fuit in sensu”

to my parents, Elsy and James

ACKNOWLEDGEMENTS

I owe my deepest gratitude to my mentor Jonathan Victor. It has been a privilege for me to closely interact and to learn from Jonathan, who has been a consistent source of ideas, advice and support throughout the course of this thesis work. I am truly grateful for his patience with me as I developed my “hand-wavy” ideas to testable hypotheses, and for generously allowing me to make countless mistakes along the way. Through his incredible example, Jonathan has taught me numerous lessons in asking the right questions, thinking before acting (or coding), and tackling problems - all with ingenuity and enthusiasm. Though I may never grasp the high bar he has set, I have, and will continue to aim high, and gratefully struggle to reach this goal. I am forever indebted to Jonathan for his meticulous feedback, criticisms, remarks and guidance – they have not only refined this thesis work immensely, but have also indelibly shaped how I ask questions and approach problems, both in lab and life.

I owe my sincere thanks to Nicholas Schiff the opportunity to work on multiple projects along with my thesis. I have been fortunate to make some important and impactful discoveries with him. Watching Niko in the lab has been a masterclass in how to do science – his passion, his incredible ability to consolidate ideas, and his unending optimism and tenacity – are few of the many qualities that I hope to emulate in my work. And I am keenly looking forward to our future endeavors.

I also thank my thesis and ACE committee members, Keith Purpura, Songhai Shi and Glen Prusky for all the advice and inputs along the way. Keith has been lavish with his time to bounce off ideas anywhere anytime, including his office, the lab, the hallways or even on York Avenue. I would also like to express my gratitude to Robert Shapley, Jose Manuel-Alonso, Qasim Zaidi, and Adam Kohn, who have been gracious to review this work.

One person stands out among the people who have contributed substantially to my training here - Mary Conte, a remarkable scientist, who I have been fortunate to call a friend. The list of things I cannot thank her enough for, include the countless project advices, ideas, food, posters, data, abstracts, manuscripts, figures, thoughtful birthday and Christmas gifts, career advice, money for food and coffee, and the list goes on. I owe my sincerest gratitude to Mary for all the advice throughout the past years and I certainly hope to continue asking you for your advice in the future.

I would also like to thank Anita Schmid and Yunguo Yu for teaching me everything that led to me collecting the data that I present in this thesis – including the neurosurgical procedures in macaques, tetrode-loading, histological staining and analyses to name a few.

I would also like to thank the members of Schiff Lab, past and present: Tanya Nauvel, Jon Bardin, Henning Voss, Esteban Fridman, Sudhin Shah, Jon Drover, Jon Baker, Tamar Melman, Peter Forgacs, Jackie Gottshall, Brian Fidali, Zoe Adams, Billy Curley, and Wanda Hyde. A special thanks to Andy Goldfine for getting me started on first projects in the lab.

And I would be remiss if I didn't thank my undergraduate calculus professor, John Velling, who first introduced me to the science happening on the 8th floor of Weill Cornell, during one of our lunch meetings at the Brooklyn College cafe.

None of my projects would have been feasible without the generous support of the Fred Plum Fellowship, and the F31 grant (EY025535) from the NIH National Eye Institute. I express my sincere gratitude to Ms. Susan Plum for continuing the support that has allowed such unparalleled scientific training at Cornell.

Finally, I dedicate this thesis to my parents, Elsy and James, my role models - for the support, love and sacrifices they chose to make, to ensure I could do this. And to my sister Deena and brother(-in-law) Pramod who have been my champions, and have keenly listened to my periodic complaints all through my undergraduate and graduate years. And of course to my 2 favorite people in the whole world, my nephew and niece, Nathanael and Lilianne – seeing the two of them every week has been the light in the often-thick fog of graduate school. Above all, I thank God for His plans for me, and His guidance throughout my academic life, which has culminated in this dissertation.

PREFACE

The time I have spent in graduate school have been the most intellectually exciting and stimulating of my life. Some of the scientific paths I pursued were fruitful and productive leading to publications, and many were not. This thesis consolidates the data, analyses, and computational modeling germane to study of sensory adaptation in the early visual cortex.

Some of the concepts of this thesis have appeared previously in the following conference abstracts (3), and manuscript (1) that is at the time of submission of this thesis under review or in revision:

1. **Thengone, D.J.,** Purpura, K.P., Victor, J.D., *(submitted)* Effects of adaptation on orientation tuning across cell classes in macaque V1 and V2
2. **Thengone, D.J.,** and Victor, J.D (2016) Tuned inhibition model accounts for adaptation-induced tuning shifts in macaque V1 and V2, ***Society for Neuroscience***
3. **Thengone, D.J.,** Yu,Y., and Victor, J.D (2016) Effects of adaptation on excitatory and inhibitory neurons in macaque V1 and V2, ***Vision Sciences Society***
4. **Thengone, D.J.,** Yu,Y., Nitzany, E., and Victor, J.D (2015) Adaptation-induced tuning shifts in excitatory and inhibitory neurons of the primary visual cortex, ***Society for Neuroscience***

Other studies that I was fortunate to undertake during the course of my PhD work have appeared in the following publications:

5. **Thengone, D.J.,** Voss, H.U., Fridman, E.A., and Schiff, N.D. (*2016*) Local changes in network structure contribute to late communication recovery after severe brain injury, ***Science Translational Medicine***
6. **Thengone, D.J.,** Gagnidze, K., Pfaff, D.W., and Proekt, A., (*2016*) Phase-amplitude coupling in mouse spontaneous behavior, ***PloS One***

These projects have been successful due to the considerable support and substantial input of my mentors Dr. Jonathan Victor and Dr. Nicholas Schiff.

TABLE OF CONTENTS

LIST OF FIGURES

LIST OF TABLES

LIST OF ABBREVIATIONS

V1: Visual area V1

V2: Visual area V2

LGN: Lateral geniculate nucleus

Hz: Hertz

F0 response: Mean rate

F1 response: First harmonic response

CI: Confidence Interval

KS Test: Kolomogorov Smirnov test

ms: millisecond

μs: microsecond

KSD: Kernel smoothed density

CHAPTER 1

INTRODUCTION

How we perceive, plan, and act depends on our internal representation of the sensory world. Forming this representation is challenging because it requires analysis and integration of sensory signals from the plethora of inputs that continually bombard the brain. To accomplish this complex task of real-time encoding, sensory systems must have strategies that recalibrate the system to the moment-to-moment environmental fluctuations. One such strategy that is ubiquitous across sensory systems is sensory adaptation – a form of experience-dependent plasticity that influences the response properties of cortical neurons on the basis of recent history, typically by selectively reducing responsiveness (Clifford et al., 2007a; Kohn, 2007; Shapley and Enroth-Cugell, 1984; Webster, 2011). This influence of experience is seen over a wide range of time scales, and affects both perception and neural response properties (Bao et al., 2013; Ghisovan et al., 2009a; Patterson et al., 2013a). In this thesis, I investigate this form of plasticity on a timescale of tens of milliseconds to minutes in the visual cortex of the macaque monkey.

Perceptually, sensory adaptation has been characterized by the distortions of the world it creates, including aftereffects, loss of sensitivity, and perceptual biases (Baccus and Meister, 2002; Clifford et al., 2001a; O'Toole and Wenderoth, 1977a; Wenderoth and Johnstone, 1988a). In the visual system, adaptation to a high-contrast stimulus causes a reduction in the apparent contrast of a test stimulus (Abbonizio et al., 2002; Wenderoth and Johnstone, 1988a). Early work suggested that such loss of sensitivity may have been a result of neuronal fatigue (Barlow, 2012; Carandini and Ferster, 1997). However, recent studies have shown that adaptation effects can be stimulus-specific, and can induce increases in firing rate as well, thus demonstrating that neuronal fatigue alone could not account for adaptation.

Cortical adaptation is also present in motor systems: adaptation affects complex behaviors including reaching, walking, and eye-movements (Bastian, 2008; McDougle et al., 2017; Stavisky et al., 2017; Wei and Kording, 2008). For example motor adaptation has been shown to improve motor calibration, critical for movement-planning and reaching (Wei and Kording, 2008). In this context, adaptation is thought of as a trial-and error process of adjusting movements to changing demands. However as more recent studies demonstrate, the role of adaptation may not be as simplistic as an error-feedback process (Clifford et al., 2007a; Kohn, 2007; Sharpee et al., 2006; Wark et al., 2007). Instead it may calibrate the brain's predictions of how the body will move and takes into account the energy demand, inaccuracy and fatigue associated with the new task. Thus adaptation is a critical process for normal brain function.

Experience-dependent plasticity is also known to occur in instances of reorganization or rehabilitation after severe brain injuries (Marshall, 1984; McDougle et al., 2017). For example, monkeys gradually reacquire sensorimotor skill after focal lesions in the somatosensory hand region along with reemergence of the injured fingertip representation (Xerri et al., 1998). Movement representations are altered in the cortex adjacent to the lesion, but the topographic reorganization depended on the type of post-lesion training experienced by the animal. Importantly, with daily repetitive training after the injury, spared finger representations were retained, suggesting a role for the direct influence of experience on cortical plasticity mechanisms. Similar experience-dependent remodeling of the structure and function of injured brain has been demonstrated with recovery of communication in one patient with severe brain injury as well (Thengone et al., 2016).

In sum, history-dependent plasticity can happen in many sensorimotor domains in normal circumstances, and also in the context of reorganization after injury. There are clear distinctions between the domains, notably the timescale of these processes (Bao et al., 2013; Patterson et al., 2013a; Thengone et al., 2016; Wark et al., 2007). Sensory adaptation may occur in the range of tens of milliseconds to minutes while reorganization after injury may occur on the order of days, months or years. Although each form of plasticity like perceptual learning or reorganization after neurological injuries is likely to involve distinct effects and mechanisms, studying sensory adaptation will contribute to understanding the functional effects of plasticity at the neuronal and population level. Characterizing these effects will provide a linkage between neuronal effects and changes in perception, and further provide insight into the underlying circuitry that govern sensory processing.

WHY STUDY ADAPTATION IN VISION?

In this thesis, we focus on adaptation effects in vision. The visual system is a good model for several reasons. At the most basic level, in order to see how response properties change, one has to be able to measure the response properties of neurons to stimulus ensembles. In the visual system, response properties can be measured along many axes (Bradley et al., 1988; De Valois et al., 1982a, 1982b; Duong and Freeman, 2007) - derived from the statistical properties of the visual environment (Tkacik et al., 2010) - and with a high degree of precision. Secondly, there are existing model frameworks for the circuitry and computations that generate these response properties. So it is possible to ask where and how adaptation exerts its functional effects. Finally, the overall organization of the visual system, into a hierarchy of interconnected cortical areas is typical of other brain systems, thus the principles that emerge from our findings are likely to generalize across the sensory modalities.

To study the effects of cortical adaptation, our initial focus is on the first area of cortical visual computation in mammalian vision: area V1. We study the effects of adaptation on orientation tuning because orientation tuning arises in V1 (Hubel and Wiesel, 1959; Van Essen and Maunsell, 1983), and we can therefore be sure that the observed adapted effects in V1 will relate to cortical circuitry rather than sub-cortical processes. The representations in V1 are then further transformed by downstream regions in the visual cortex (Van Essen and Maunsell, 1983). We will use this aspect of visual processing to study the effects of adaptation in the hierarchy of cortical processing.

Another advantage of studying orientation tuning is that a large number of modeling studies have been focused on the emergence of orientation selectivity, i.e. how does orientation tuning arise in the cortex? (McLaughlin et al., 2000a; Somers et al., 1995a) These studies have proposed several models, and we will utilize them in this study to account for the observed effects of cortical adaptation.

ADAPTATION AND CORTICAL HIERARCHIES

As mentioned above, one of the advantages of the visual system as a model is that it enables us to investigate how adaptation effects cascade across a cortical sensory hierarchy. Although much is known about the hierarchical nature of sensory systems, it remains unclear how a multilevel neural system adapts to changes in the environment. One possibility is that downstream regions simply inherit the effects of adaptation. A second possibility is that they compensate for the adaptation effects, perhaps to maintain a perceptual invariance. A final possibility is that further adaptation occurs in downstream regions. Each of these possibilities would result in different effects on perception.

For subcortical processing, both inherited effects and intrinsic adaptation patterns are known to occur. For example, luminance adaptation takes place primarily in the retina, but contrast adaptation takes place both in the retina and further downstream in the lateral geniculate nucleus (LGN) (and then also subsequently in V1) (Baccus and Meister, 2002; Crowder et al., 2006; Duong and Freeman, 2007). In this thesis, I focus on cortical adaptation, and test whether adaptation acts independently at a single level or it influences multiple cortical regions.

To study effects of cortical adaptation in the sensory hierarchy, I chose to focus on the effects of adaptation to the orientation tuning in area V2. V2 is the largest extrastriate visual area, and in the macaque, the predominant source of input to V2 comes from striate cortex V1. V2 is known to have selectivities to complex features, ie texture features and illusory contours that are not present in V1 (Boynton and Hegdé, 2004; Burkhalter and Van Essen, 1986; Hegdé and Van Essen, 2000, 2003). But, the responses of V2 neurons to oriented gratings are largely similar to the responses of neurons in V1 (Crowder et al., 2006). Directly comparing the effects of adaptation on grating responses in V1 and V2 will enable us to assess whether adaptation is simply inherited from V1, or alternatively that further adaptation (or even compensation) occurs in V2.

EFFECTS OF ADAPTATION ACROSS CELL-TYPES

Another main motivation for this work is to study the effects of adaptation across distinct cell-types in the visual cortex. In many contexts, it has become clear that excitatory and inhibitory neurons play different roles in sensory processing, but whether this applies to adaptation is as yet unknown.

The context in which excitatory and inhibitory cells are known to have different roles generally pertain to modulatory influences. For instance, attention modulates the activity of inhibitory celltypes distinctly from the excitatory cells (Mitchell et al., 2007). Specifically in extrastriate cortex (V4), a subset of narrow spiking inhibitory neurons is known to have a much larger attention-dependent increase in firing rate than the excitatory neurons. Similarly, distinctive role of inhibition has been demonstrated to be important in learning and working memory as well. Furthermore, targeted pharmacological and optogenetic investigations that have elucidated some of the likely mechanisms of attention have highlighted the role of different cell classes and neurotransmitter systems. With regard to learning, inhibitory neurons in the inferior temporal (IT) cortex demonstrate experience-dependent reduction in maximum firing rate, in contrast to the broad-spiking excitatory neurons (Woloszyn and Sheinberg, 2012a). In working memory, in the prefrontal cortex, strong inhibition by reward occurs primarily in fast-spiking inhibitory interneurons (Kim et al., 2016). Furthermore from an anatomic perspective excitatory and inhibitory celltypes are known to be clearly distinct, however it is still unknown whether the distinct cell-types that innervate the laminae differently are involved in distinct processing strategies. With regard to adaptation, prevailing theories hold that adaptation is possibly mediated by inhibitory mechanisms ((Clifford et al., 2007b), (Whitmire and Stanley, 2016)), yet the effects of adaptation on inhibitory celltypes has not yet been characterized. The distinctive effects of excitatory and inhibitory cell-classes thus motivate us to ask whether these classes also play distinctive roles in adaptation.

To determine whether adaptation modulates neuronal responses generically across visual cortical neurons or differs by class, we exploited observations made in anesthetized animals and cortical slices in this study, where different types of neurons can be distinguished on the basis of morphology and protein expression. Intracellular recording studies have found that parvalbumin expressing GABAergic interneurons with the morphology of basket cells and chandelier cells have short duration action potentials, whereas excitatory pyramidal neurons have longer duration action potentials. Neuronal recording studies have found that most pyramidal neurons, which make up 70%– 80% of cortical neurons, have broad action potentials, while the remaining 10%–15% of the neuronal population are fastspiking interneurons with the morphology of basket cells and chandelier cells. This class of GABAergic interneuron is unique in expressing the calcium-binding protein parvalbumin. Its narrow action potentials have been attributed, in part, to high levels of expression of two classes of potassium channels (the Kv3.1 and Kv3.2 channels), which have faster kinetics (Martina and Jonas, 1997). Related experiments, which have combined intra and extracellular recordings, have established that the narrow and broad action potentials observed in intracellular recordings can also be distinguished on the basis of extra cellular recordings. In the set of studies reported here, we utilize this distinction of the extracellular waveshape to classify the cell-types as excitatory (E cells) and inhibitory (I cell), and study their behavior in adaptation.

COMPUTATIONAL MODELING OF ADAPTATION

A final element of this thesis is computational modeling. Here the goal of modeling is to determine what is necessary to account for the range of adaptation-induced changes to the behavior of the tuning curve of visual neurons. As we will show, the feed-forward model originally proposed by Hubel and Wiesel fails to account for adaptive behavior. We will then consider model classes that include intra-cortical interactions with particular emphasis on inhibition, and show that come of these can account for our findings.

The level of modeling is driven by the questions that we intend for the modeling to address. Specifically we are not making detailed biophysical models of neurons but rather focusing on 1) the locus of adaptation, and 2) the connectivity rules between excitatory and inhibitory populations. The simplified models used in this thesis are designed to account for the range of behavior observed in the experimental data, and not to test the plausibility of specific cellular or biophysical mechanisms. Thus, the activity of a single neuron is represented simply by its firing rate, and we don't consider further levels of detail that incorporate spiking statistics, Hodgkin-Huxley dynamics, channels, etc. The chapter on modeling provides further rationale for these and other simplifications, and evidence that the conclusions drawn from the models would hold for more detailed models as well.

In our models, we considered 2 possibilities for the locus of adaptation – post-synaptic or pre-synaptic adaptation. In the post-synaptic adaptation, the reduction in responsiveness is a function of the response of the output neuron, with larger reductions, as the adapter gets closer to the preferred orientation of the cell. This form of adaptation would therefore be expected to act as a gain control mechanism, keeping baseline selectivity intact. In contrast, in pre-synaptic model of adaptation, the inputs themselves are affected by the adapter, and reduce responsiveness accordingly before feeding to the output neuron. Therefore, in this scenario, we expect that the preferred orientation of the output neuron can shift, since the synaptic weights of the inputs are differentially modulated as a function of the degree of adaptation. As we will show, this intuition is borne out by the modeling, and we conclude that presynaptic adaptation must be present.

With regard to the connectivity rules, we also considered 2 possibilities – untuned inhibition or tuned inhibition. The role of inhibition in sculpting orientation tuning has been a topic of much debate, and requires a bit of background.

Historically, the possibility that inhibition was relevant to orientation tuning arose following the recognition that solely feed-forward models alone could not account for the strength and selectivity of cortical neurons (McLaughlin et al., 2000a; Somers et al., 1995a). To account for the observed degree of tuning, alternative model architectures were proposed that included a prominent role for intra-cortical interactions. A subset of models specified a role for cortical inhibition in these interactions – but inhibition played two kinds of roles. In some of these models, inhibition acted to maintain cortical activity levels and avoid runaway excitation, but did not make specific contributions to shaping the tuning curve. Evidence for this form of untuned inhibition came from early pharmacological experiments in the cat that showed that blocking cortical inhibition (with a $GABA_A$ agonist) increased overall firing rates but did not change tuning. Moreover, optogenetic studies in the mouse have suggested that inhibitory cells nonspecifically pool inputs from their neighborhood, and thus, they might not even be expected to have orientation tuning. In contrast, in other models, inhibition is postulated to play a substantial role in sculpting cortical tuning. Initial support for this idea comes from intracellular studies in the cat that showed that V1 cells were suppressed by a grating that was orthogonal to their preferred orientation (Sillito, 1979). More recent 2-photon imaging studies of parvalbumin and somatostatin cells in the ferret have shown that V1 inhibitory cells can be as sharply tuned as the excitatory cells (Wilson et al., 2017). Given the conflicting evidence about the role of inhibition, we constructed models with either form – untuned inhibition and tuned inhibition – and characterize their behavior with respect to adaptation.

As we will show, pre-synaptic adaptation in untuned and tuned model classes makes qualitatively distinct predictions. Specifically, pre-synaptic adaptation in the untuned inhibition model can result in selective suppression of responses near the adapter, inducing the baseline tuning preferences to shift away from the adapting orientation. In contrast, when tuned inhibition is present, adaptation at a non-preferred orientation can cause the baseline tuning to shift towards the adapting orientation. This phenomenon is essentially a kind of disinhibition, in which adaptation reduces the tuned inhibitory signals, which at baseline were dominating the responses at non-preferred orientations.

Overview of thesis chapters

In this thesis, I describe not only new experimental results, but also methodological advances and modeling. Therefore it is organized as follows: Chapter 2 describes the standard methods employed common to all the results chapters. The next two chapters describe the methodological advances: spike width classification of tetrode data (Chapter 3) and physiological characterization of tetrode recording locations into pinwheel centers or isoorientation domains, which are characteristic components of the V1 orientation map (Chapter 4). Note that although we introduce these new methods in the context of studying adaptation, they are applicable to any tetrode recordings in general (Chapter 3), or dense multichannel recording in V1 (chapter 4). Chapter 5 describes the experimental data concerning adaptation in visual area V1. Chapter 6 describes the effects of adaptation in extrastriate visual area V2. Chapter 7 describes the models that account for the adaptation-induced effects. Finally, these experimental chapters will be followed by a discussion chapter (Chapter 8), in which I consider the implications of these results and potential future directions.

CHAPTER 2

STANDARD EXPERIMENTAL METHODS

This chapter describes the main procedures common to all experiments. Physiologic methods (anesthesia, surgery, and maintenance under anesthesia) are standard for the laboratory. Neurophysiologic methods (tetrode recordings, unit isolation, measurements of tuning functions) are also standard. The protocols used for studying adaptation are modified from the paradigms of (Patterson et al., 2013a). In addition, this work made use of two new methodologic innovations enabled by tetrode recordings, and these are described in chapter 3 (extracellular waveform classification) and chapter 4 (pinwheel vs iso-orientation domain classification). All procedures performed comply with the guidelines provided by the US NIH and the Institutional Animal Care and Use Committee at Weill Cornell Medical College.

Text and figures in this chapter are adapted from the methods sections of Thengone et al (submitted). Figures 2.4, 2.5 and 2.6 are added to this chapter to provide additional detail and explanation.

Physiologic methods

We used standard techniques to prepare 6 adult macaques for acute extracellular recordings from areas V1 and V2. After initial sedation with ketamine, anesthesia with isoflurane, and topical bupivacaine, endotracheal tube placement and catheterization of one femoral artery, both femoral veins and the urethra were performed. During the experiments, anesthesia and analgesia levels were maintained with propofol and sufentanil, respectively, hydration was provided with Normosol and dextrose, and neuromuscular blockade (to minimize eye movements) was maintained with rocuronium bromide. The electrocardiogram, arterial blood pressure, body temperature, end-tidal CO_2 partial pressure, arterial oxygen saturation, electroencephalogram, urine output, and urine specific gravity were monitored during the entire course of the experiment. The monkey was ventilated artificially so as to keep end-tidal CO2 near 33 – 35mmHg (4.4% - 4.6%). The EEG, ECG, end-tidal CO2, and blood pressure were monitored continuously, and at any sign of the anesthesia becoming less effective, the dose of sufentanil citrate was increased. Temperature was monitored with a rectal probe and kept near 37°C with a heating blanket. Topical atropine was used to dilate the pupil, the eyelids were elevated with 6-0 silk sutures, and gas-permeable contact lenses were placed to protect the corneas . Supplementary lenses (with power determined by ophthalmoscopy) were used to focus the eyes at a distance of 114 cm. At the beginning of the experiment, and at regular intervals afterward, the positions of the foveae were hand-mapped.

Each fovea is directed to one half of the display monitor with the aid of a laser pointer optically configured to lie at the pupil. Animal maintenance also included administration of penicillin and dexamethasone at the start of the experiment, periodic infiltration of accessible wound sites with bupivacaine, gentamicin for evidence of systemic infection, topical flurbiprofen to prevent ocular inflammation, and periodic cleaning of the contact lenses.

Following the craniotomy (10-15 mm diameter), a small incision was made in the dura, and the 6 guide tubes containing an electrode each (quartz-platinum–tungsten microelectrodes; 1–5 MΩ; Thomas Recordings, Marburg, Germany) were positioned over the opening (3 mm diameter) just above the cortical surface.

NEUROPHYSIOLOGIC METHODS

Visual stimulation and characterization

Once visually-drivable units are encountered, a multiunit receptive field from each active tetrode is hand-mapped and then reflected onto the display of a ViewSonic G225f 21” monitor. Then tuning properties of the multiunit activity are determined with 8 (4-6 sec) presentations of drifting sinusoidal gratings using the following range of parameters: 16 orientations 22.5^0 apart, with spatial and temporal frequencies chosen from the hand mapping; 8

spatial frequencies 0.125 cyc/^{0} to 8 cyc/^{0} at the optimal orientation for one or more clusters determined by online quantitative analysis, 7 temporal frequencies, 0.5 Hz to 25 Hz, at the optimal orientation and spatial frequency determined by the online quantitative analysis; and 6 contrast levels (0.06 to 1.0) at the optimal orientation, spatial frequency, and temporal frequency, again determined by the online quantitative analysis for one or more clusters. Stimulus size was chosen by handmapping the receptive fields of the target tetrodes.

ONLINE ANALYSIS OF MULTIUNIT DATA

In order to measure tuning of the multi-unit activity recorded at the tetrodes, the responses were measured to drifting sinusoidal gratings (Figure 2.1).

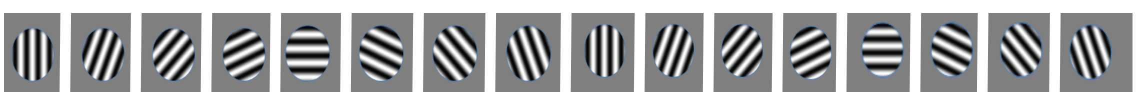

Figure 2.1 Standard stimuli for measuring orientation tuning - Orientation tuning of cortical cells in V1 and V2 were measured using sinusoidal gratings at 8 orientations drifting at 2 directions each.

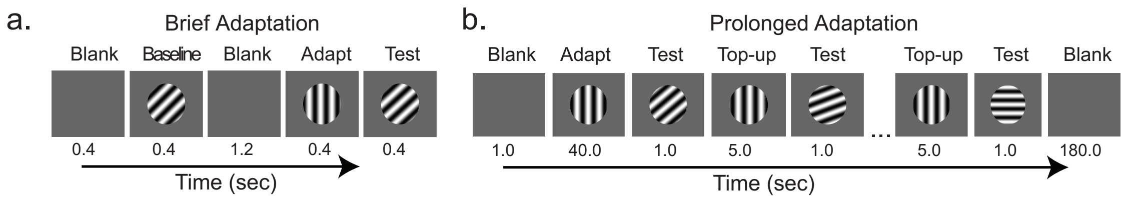

Figure 2.2 Brief and prolonged adaptation paradigm

Brief adaptation paradigm: drifting gratings were presented for 400 ms (baseline) and then immediately following a 400 ms adapting stimulus (test).

Prolonged adaptation paradigm: test stimuli were presented for 1 sec following an initial 40 sec presentation of the adapting stimulus, and then following 5-sec "top-up" presentations of the adapting stimulus. In both paradigms, each of 16 test orientations was presented at least 8 times, in randomized blocks.

ADAPTATION PARADIGMS

Once the optimal orientations are identified from the baseline tuning and online analysis, the adaptation paradigms are performed. Our design were modeled after the short (0.4 sec) and long (40 sec) adaptation paradigms of (Patterson et al., 2013a). Whenever possible, both paradigms were carried out at each site, in random order. The orientation of the adapter was chosen based on an online analysis of the baseline tuning response of the multiunit activity, which allowed us to identify two (or more) target tetrodes at which the multiunit activity had similar orientation preferences and robust tuning curves (Figure 2.3). We used gratings at the preferred orientations of these tetrodes as adapting stimuli, selecting a spatial frequency and temporal frequency that was at or near peak as well, and a contrast of 1.0. If recordings remained stable after the short and long adaptation paradigms, we then selected other tetrodes as target. Thus, our recordings consisted both of neurons that were adapted with stimuli near their peak orientation, and neurons, recorded in parallel from other tetrodes, that were adapted with stimuli that were far from their peak orientation.

For the 0.4 sec adaptation experiment, each of the 16 kinds of trials (one for each orientation) consisted of a blank interval, a baseline test stimulus, blank stimulus, the adapting stimulus, and then the test stimulus again (Figure 2.2). After the final trial, we waited a 3 min interval to allow recovery prior to the next experiment. For 40s adaptation we use an adapt-test- top-up paradigm, with 1 s test stimuli and 5 s top- up presentations of the adapter (times which has been shown to have strong adaptive effects, Patterson 2013) (Figure 2.2). A standard tuning run was performed at the end of each long-adaptation run (Figure 2.1), and we only analyzed neurons for which this final run indicated a return to baseline tuning. For both short and long adaptation runs, the order of the test stimuli was randomized within each block of 16 trials.

SELECTION OF TETRODE FOR ADAPTATION PARADIGM

Since we are recording at 6 tetrodes simultaneously, we obviously can't expect to choose a single orientation that is at or near the peak for all neurons. But although this might at first appear to be a serious drawback, it isn't. Even if the 6 recording sites have peak preferences that are randomly distributed among the 16 that we measure, there is a 98.6% chance probability that 2 or more of them are within one step of a common orientation and direction, and a 35.7% chance that 3 or more of them will be similarly related. This counterintuitive result is similar to the "birthday paradox" phenomenon, and our recordings typically show such commonality. So, as illustrated in Figure 2.3, we first use an adapting grating that is at or near the common peak orientation and direction for two or more tetrodes (providing peak- and near-peak adaptation data for these neurons, and off-peak adaptation data for the others), and then test up to 2 other adapting orientations, as time permitted.

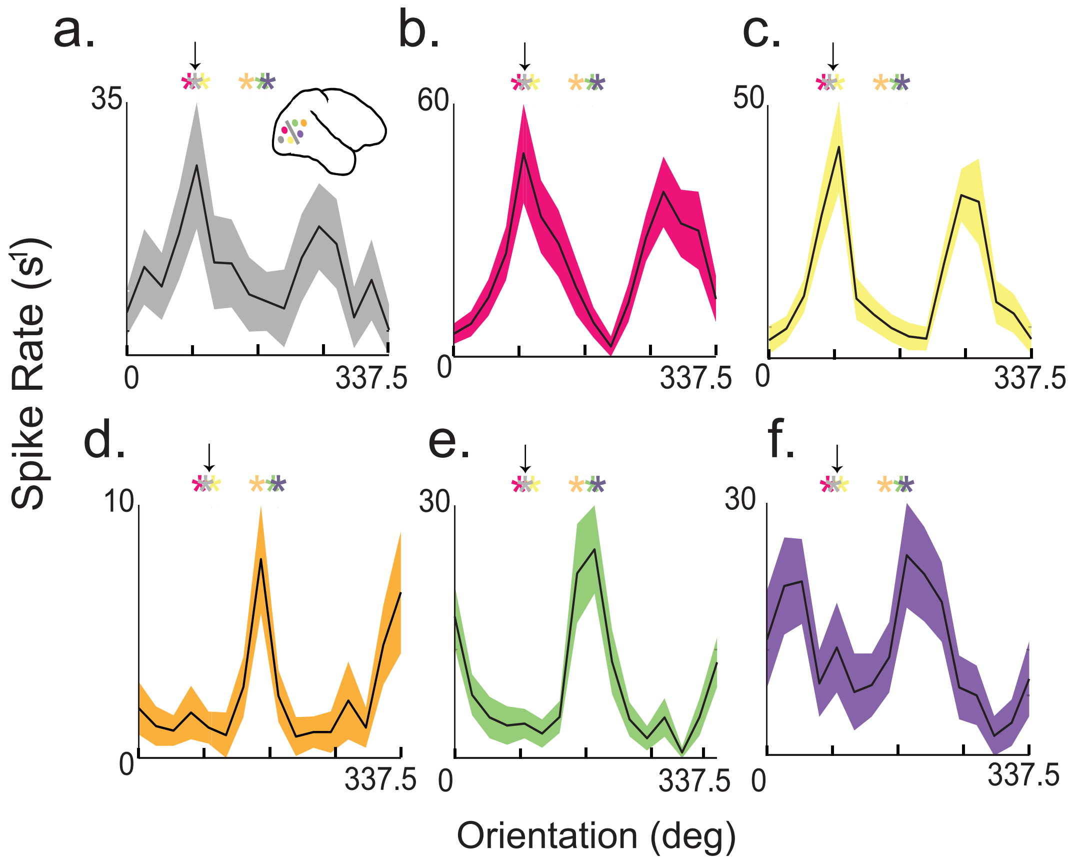

Figure 2.3 Selection of tetrode for adaptation paradigm

Setup of adaptation experiments based on online analysis of tuning. Tetrodes A, B, and C are in V1; D, E, and F are in V2. Activity at 3 of 6 tetrodes have peaks within 22.5 degrees of a common direction. The arrows(at 90^0 and 112.5^0) are therefore selected for adaptation experiments. Across the two experiments, neurons at 3 tetrodes are adapted at on-axis orientations and neurons at all 6 tetrodes are adapted at off- axis orientations.

HISTOLOGY

An electrolytic lesion is made at the end of each penetration, and further lesions are made at irregular intervals during withdrawal of the electrode. At the end of the experiment the monkey is perfused through the heart with 0.9% saline in neutral phosphate buffer, followed by a solution of 10% paraformaldehyde, then 10% sucrose in phosphate buffer. The brain is blocked and sunk in 30% sucrose, after which it is frozen and cut in 50μm sections and alternate ones are stained for Nissl substance and cytochrome oxidase. Locations of recorded neurons are recovered from reconstructed electrode tracks.

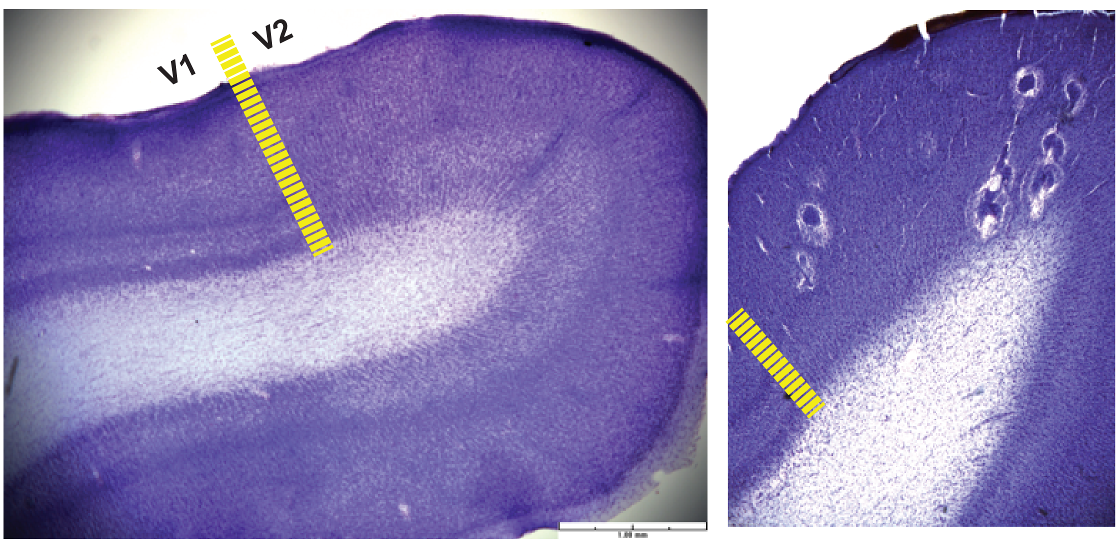

Figure 2.4 Histological staining to identify cortical regions – Nissl staining of cortical slides showing the lesion sites used for identification of V1 and V2 lamina. Yellow bar indicated the boundary of V1 and V2

Offline Data Analysis

Spike sorting

This procedure was carried out offline, based on spike waveforms recorded during the experiment. These spike waveforms consisted of 32 samples at 33 kHz of bandpass-filtered (300-6000 Hz) recordings on each of the four tetrode channels; the eighth sample was at the time that a voltage criterion was first reached on any channel. The recorded extracellular action potential waveforms were preprocessed offline for further analysis. No neurons were recorded simultaneously on more than one tetrode, so each tetrode's data were handled independently. The first stage was semiautomated spike sorting. This was carried out separately at each stepped position. Using KlustaKwik (Rossant et al., 2016) (http://klusta.readthedocs.io/en/latest/), we clustered the extracellular waveforms based on 17 features: the peaks and troughs of the waveforms across 4 channels (8 features), the first eight principal components (8 features) and time (1 feature). The initial automated selection of candidate spike clusters was conservative (tending to create multiple clusters from spikes from the same source rather than a single cluster of spikes from different sources) and yielded more clusters than were eventually accepted as single units.

To create final clusters (Figure 2.5), the candidate clusters were manually fused, and noisy clusters (those that violated the refractory periods) were eliminated. Any two clusters were manually combined if 1) the corresponding waveforms were scaled versions of similarly shaped spikes, and 2) the projections of the waveforms into feature space, particularly time, were continuous, and could be traced through all tetrode steps. Finally, to obtain the waveforms used for classification, waveform samples were interpolated (cubic spline), aligned to peak time, and averaged separately for each cluster at each recording site.

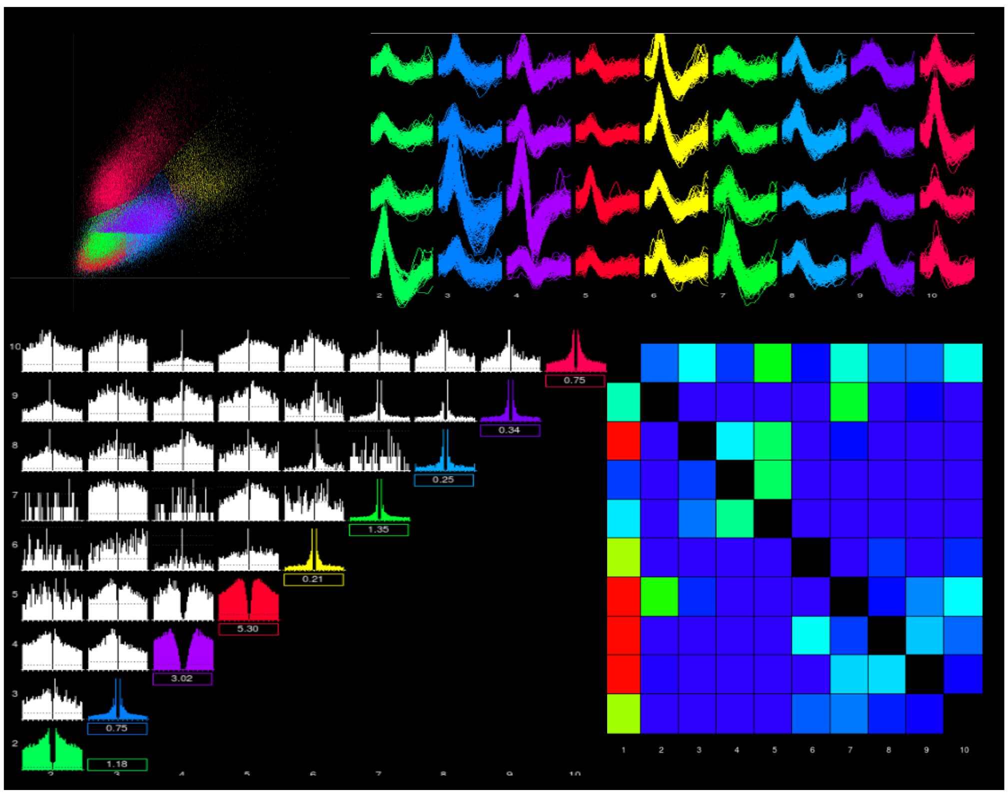

Figure 2.5 Spike Sorting – Following the automated clustering step, the output clusters are then manually merged to get the following 9 single-unit clusters (Cluster ID: 2 – 10) and 1 multi-unit cluster (Cluster ID: 1). The multi-unit cluster is labeled cluster 1 (column 1).

QUANTIFICATION OF RESPONSE PROPERTIES

Orientation tuning curves were measured from the DC response (F0), and fundamental modulated response (F1) of the spike train to the drifting oriented gratings. Tuning curves were fit with a non-parametric polynomial, so as not to assert a particular shape for the tuning curve. The preferred orientation was taken to be the position of the peak of this smoother tuning curve, the maximum response amplitude was taken to be its height, and the half bandwidth was taken to be half of the difference between the flanks of the curve at 1/√2 as used in (Ringach et al., 2002a). 95% confidence intervals for response amplitudes, and tuning parameters were determined via a parametric bootstrap procedure. Specifically, 500 surrogate datasets were generated based on Poisson statistics, and the observed spike counts at each orientation, and the above analyses were applied to each surrogate dataset.

For modeling (see below), orientation tuning curves were fit to a von Mises function

$$R(\varphi) = B_j + M_j e^{\beta_j \cos(2(\varphi-\mu))-1} \qquad \text{Eq.1}$$

with baseline firing rate B_j, amplitude M_j , concentration parameter β_j that determines the bandwidth of tuning, and preferred orientation μ_j .these parameters were determined via maximum likelihood fit to the firing rates measured at each orientation, assuming Poisson statistics, using Matlab's fminsearch.m

Except as otherwise noted, all analyses were carried out in Matlab using existing laboratory code for the online analyses and custom-developed software for the offline analyses.

$$\text{Circular Variance} = 1 - \left| \frac{\sum_k r_k e^{i2\theta k}}{\sum_k r_k} \right|$$

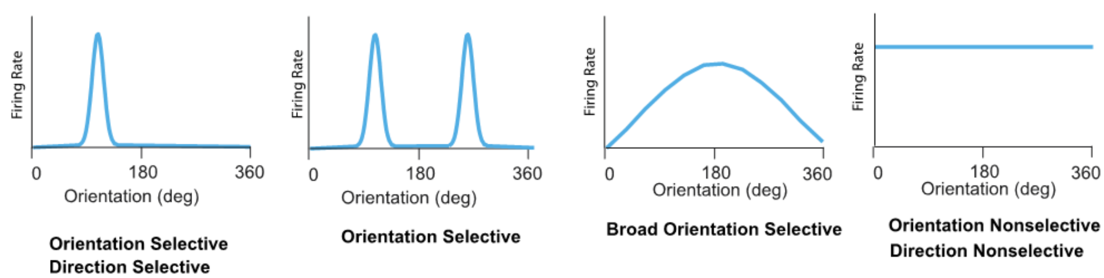

Figure 2.6 Quantifying selectivity of orientation tuning – Orientation selectivity is measured using circular variance using the equation shown here. Schematic shows the definition of tuned and untuned tuning of orientation curves.

CHAPTER 3:

SPIKE WAVESHAPE ANALYSIS FOR TETRODE RECORDINGS: METHODS DEVELOPMENT AND TUNING PROPERTIES

The balance of excitation and inhibition is a critical aspect of cortical function and circuitry. In the context of neuromodulatory phenomena like attention, learning and working memory, inhibitory cells have been shown to operate distinctly within the circuits compared to their excitatory counterparts.

While the most accurate ways to distinguish excitatory and inhibitory neurons require intracellular recordings, it has been shown that these cell classes can also be distinguished on the basis of action potential waveform recorded extracellularly (Kaufman et al., 2010a; Mitchell et al., 2007; Woloszyn and Sheinberg, 2012b). Until now this method has only been applied to standard microelectrode recordings. Here we extend this method to tetrode data. Our approach is to establish a robust strategy to reduce the dimensionality of multi-channel tetrode recordings, so that established methods of classification based on the extracellular waveshape can be applied. The results from this classification are used in chapters 4 and 5.

In brief, the biophysical rationale for the use of the extracellular waveshape for cell-type classification is based on the kinetics of the ion channels that are known to be distinctly expressed in excitatory and inhibitory cell-types (Bartho, 2004). Specifically, the narrower action potentials of parvalbumin-expressing GABAergic interneurons are the result of high levels of the potassium channels Kv3.1 and Kv3.2 that have faster kinetics (Bean, 2007; Du et al., 1996; Rudy and McBain, 2001). The finding that duration of the extracellular spike waveform is directly related to the duration of the intracellular waveform has made it possible to distinguish fast-spiking inhibitory interneurons from pyramidal neurons in extracellular recordings in many cortical regions, including prefrontal cortex (Kaufman et al., 2010a), primary visual cortex (Mitchell et al., 2007; Yu et al., 2015), and somatosensory cortex in both the macaque and human cortex (Peyrache et al., 2012). In the set of studies reported in this chapter, we show that action potential widths derived from tetrode data are distributed bimodally in visual areas V1 and V2. We then use this distinction of the extracellular waveshape to classify the cell-types as excitatory (E cells) and inhibitory (I cell) and characterize their tuning properties. In later chapters, we apply this distinction to the study of adaptation.

The critical step in these analyses is to deal with the issue of reducing the dimensionality of multi-channel tetrode data prior to making any measurements of the waveforms. Specifically, we establish an objective strategy of estimating waveform shape when four recording channels are present.

Figures 3.2 is from the manuscript (Thengone et al), where the methods are briefly described. This chapter presents the method in full, and its rationale.

METHOD

WAVE SHAPE CLASSIFICATION

Following the manual spike-sorting step (described in Chapter 2), the resulting waveforms are further processed to reduce the dimensionality of tetrode data. For each semi-automated cluster, all recorded action potentials are aligned by their troughs (because it was generally the sharpest feature of the waveform).

To isolate a single estimate of the tetrode data (4 channels) that could be used for the spike-width duration, we performed a variety of ways of measuring the width from the following reduced dimensions of the tetrode data:

1) mean waveform across the 4 channels,

2) mean of the 4 channels,

3) median waveform across the 4 channels,

4) width of the channel with the largest signal:noise ratio (SNR).

5) width of the first principal component of the 4 channels, and

6) width of the channel with the largest amplitude,

In order to test for reliability and consistency of the width estimates, measurements of waveform width were made for each cluster using a block analysis of the clusters. Specifically, the data from each cluster was analyzed both from the individual waveforms, as well as after averaging the waveforms in blocks of 10, 100 and 1000. The averaged waveforms were interpolated by a spline to give a precision of 2.5 μs (chosen based on the typical width of waveforms in microelectrode recordings (Kaufman et al., 2010a)). To identify the most reliable and consistent width measurement for our tetrode recordings, this analysis was performed on 100 independent clusters from 81 recordings sites in the laboratory database, and repeated on the 50 clusters collected and used in this thesis.

RESULTS

REDUCING THE DIMENSIONALITY OF MULTI-CHANNEL TETRODE RECORDING

The first analysis was aimed at reducing the dimensionality of the tetrode data to attain a single estimate of the waveform widths. For most clusters, the 6 different approaches yielded similar results: estimates of waveform width were narrow and approximately Gaussian distributed. However in clusters where recording SNR was relatively poor, the widths measured from the median waveform, channel with the largest amplitude and first principal component performed better. Outliers were more frequent in the methods using mean waveform and mean latency of the waveforms. I (Fig 3.1). In a few case, the max SNR was significantly better, and so we settled on this measurement. This analysis was performed separately on the data that I collected for this thesis and the historical laboratory database, and these findings were consistent.

WAVESHAPE DISTRIBUTIONS

Having determined that the channel with the max SNR is the most reliable way to reduce the multi-channel recordings to a single waveform, we next used this approach to measure the width of all the waveform clusters collected for this thesis. We consider two parameters of waveform widths: the peak-trough width, and the half-peak width. Distribution of the widths measured from the spline-interpolated (Figure 3.2) waveforms were bimodal (Hartigan dip test).

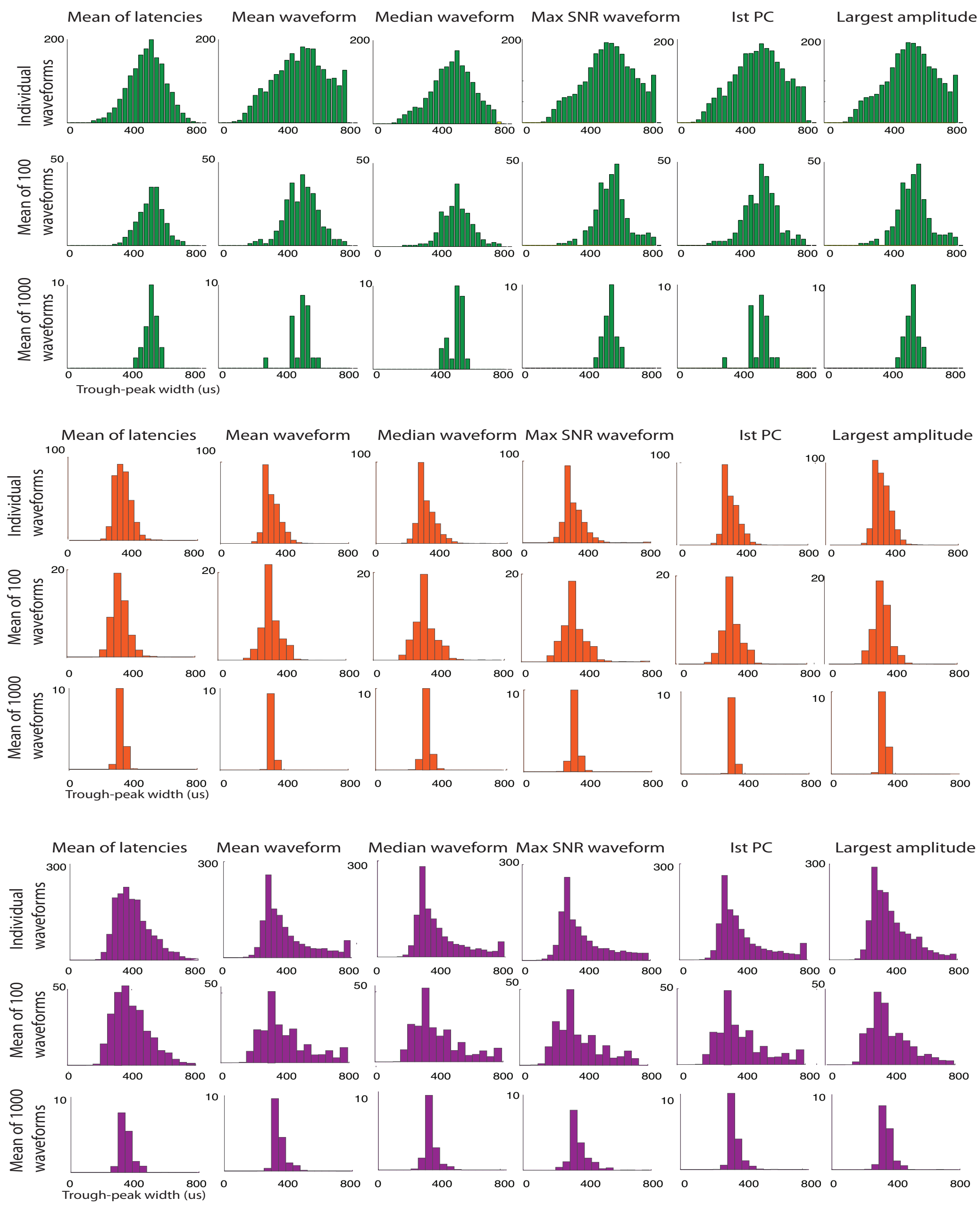

Figure 3.1 Reducing dimensionality of multi-channel tetrode recordings in 3 example cells – The durations of trough-peak widths were measured using one of the 6 ways of reducing the multi-channel recordings for 3 different clusters shown in green, orange and purple respectively.

We therefore classified clusters into subgroups based on the notch in the histogram. The notch (minimum) in the bimodal histograms was identified using the first derivative of its kernel smoothed density estimate, and clusters within +/- 5 percentiles of this point were labeled unclassified. Waveforms whose spike widths were 5%-ile or more below the notch were designated as narrow-spiking neurons, and waveforms whose spike widths were 5%-ile or more above the notch were designated as broad-spiking neurons. The classification based on the two kinds of measurements (the peak-trough width and the half-peak width) yielded similar cluster assignments. (Figure 3.3). This was not surprising because these 2 measurements are closely correlated. (Figure 3.3). So we arbitrarily chose trough-to-peak width measure for subsequent analyses. Using this choice, narrow-spiking cells are those with a trough-to-peak interval less than 390μs, and broad-spiking neurons are those whose trough-to-peak interval was higher than 425μs.

As a further check on the robustness of this approach, we also classified the averaged extracellular waveforms using k-means clustering, which resulted in 2 clusters. The classification based on trough to peak width was in close correspondence to the k-means analysis: the narrow-spiking neurons mapped to one cluster, and the broad-spiking neurons mapped to the second cluster, and the unclassified neurons were divided between the clusters. (Figure 3.3 panel C and D).

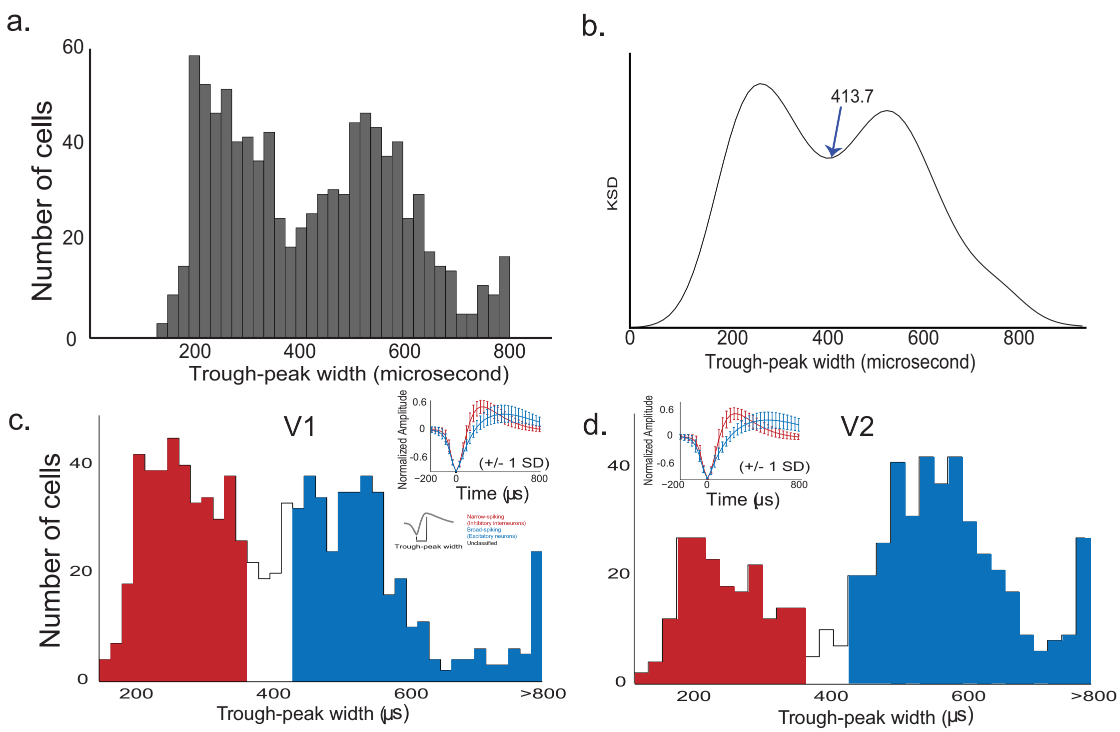

Figure 3.2 Extracellular waveshape widths. – Distribution of trough-to-peak widths measured from the spline-interpolated waveforms across the population (V1 and V2) show in A. The first derivative of the KSD of the histogram was used to identify the notch in the distribution (B). C and D shows the distribution of E and I cells in V1 and V2.

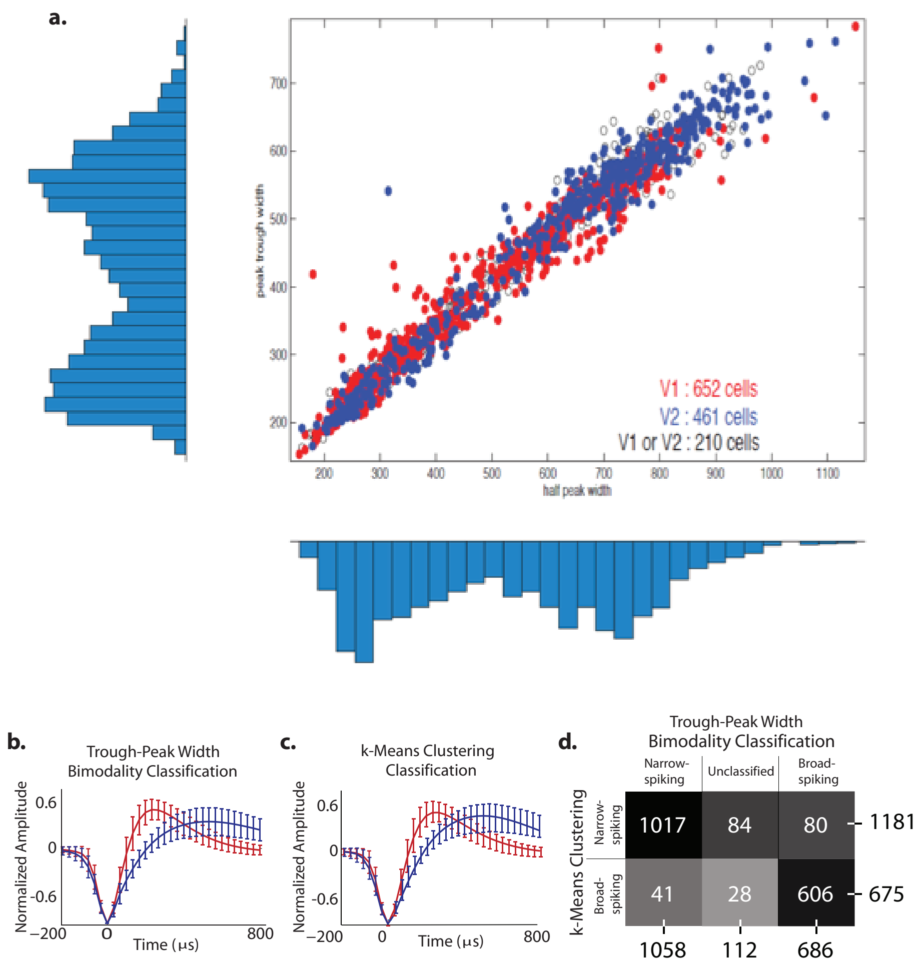

Figure 3.3 Robustness of extracellular waveshape measurement -

(A) Trough-to peak widths of the extracellular waveforms were correlated with the half-peak widths of the same waveforms. Extracellular waveform classification performed using **(B)** the bimodality of the peak-trough width distribution (blue: E cells, red: I cells) and **(C)** k-means clustering of the averaged waveforms. Error bars in B and C indicate the 1 standard deviation of the corresponding sub-population. **(D)** Confusion matrix shows the correspondence of findings from the 2 classification methods. There are three columns in the confusion matrix, because in the bimodality method, the 10% of cells nearest the trough of the distribution were not classified.

PHYSIOLOGICAL PROPERTIES OF NARROW-SPIKING AND BROAD-SPIKING NEURONS

In V1, overall, although there is a broad range of physiological properties at the level of individual neurons, we found the expected differences between the broad-spiking and narrow-spiking populations. Cells in the narrow-spiking cluster had more untuned cells (CV values close to 1) compared to the broad-spiking E cells.(Figure 3.5)Cells in the narrow-spiking cluster showed higher baseline firing rates compared to the broad-spiking cluster. (Figure 3.6).

In V2, the bimodality seen across laminae and these physiological differences between the two cell-types were present as well. (Figure 3.5, 3.6)

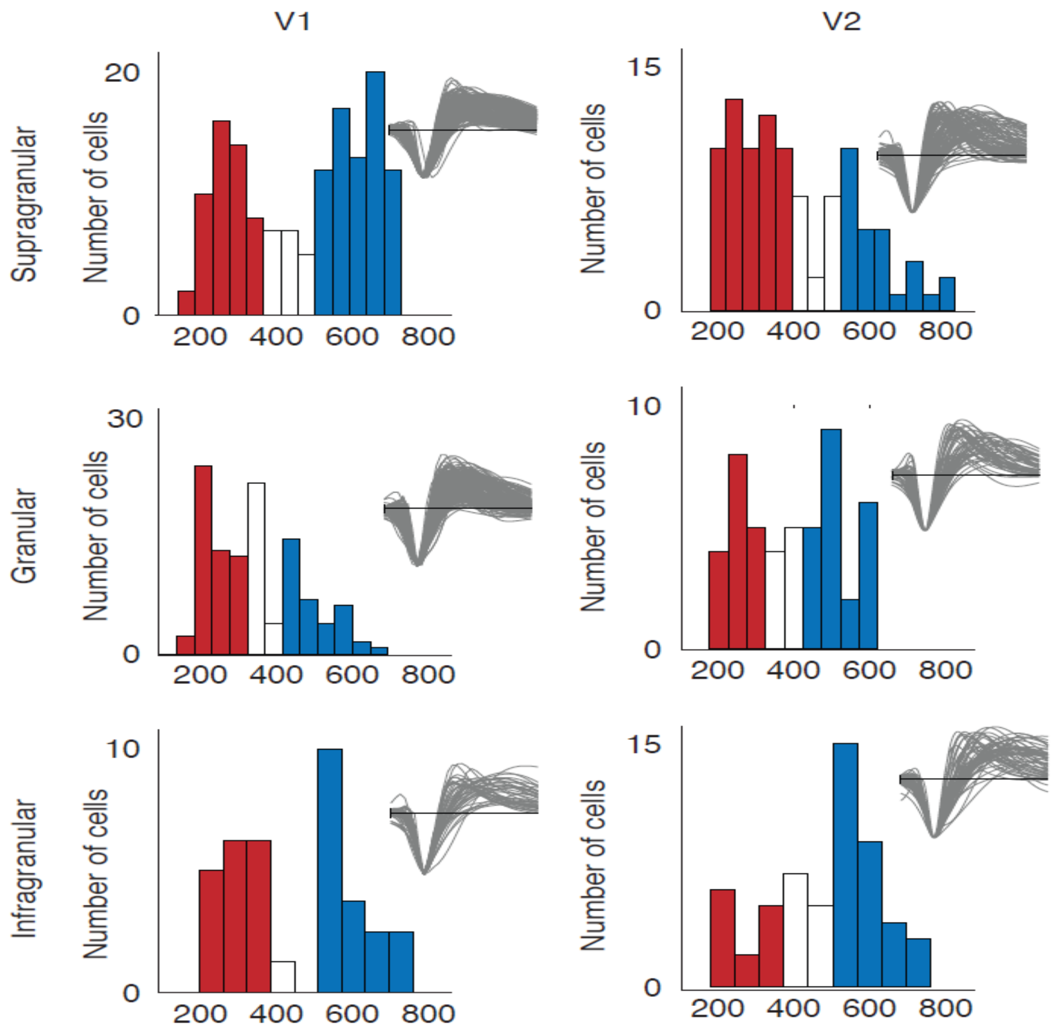

Figure 3.4 Waveshape distribution in V1 and V2 lamina – Distribution of waveforms across the supragranular, granular and infragranular layers in V1 and V2 show similar bimodaility

a.

V1

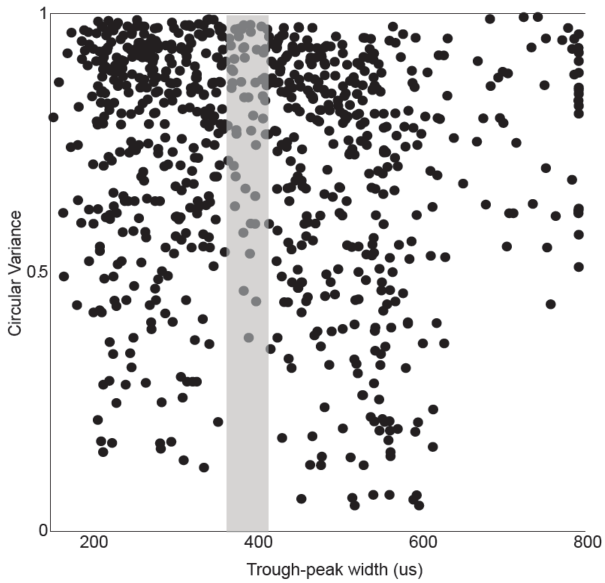

b.

V2

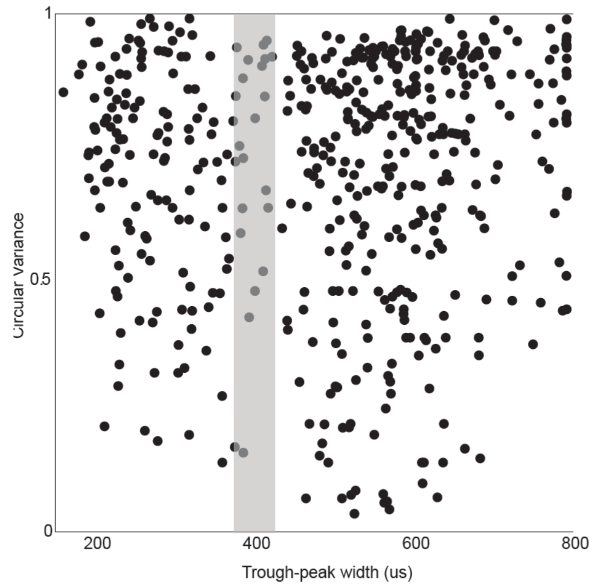

Figure 3.5 Orientation Selectivity across celltypes in V1 and V2 - Selectivity of cells, measured using circular variance show that narrow-spiking cells were more untuned (CV close to 1) than cells in the broad-spiking clusters. This is true for both V1 **(A)** and V2 **(B)**. The gray bar indicates the cells that were labeled unclassified using the bimodality cutoff.

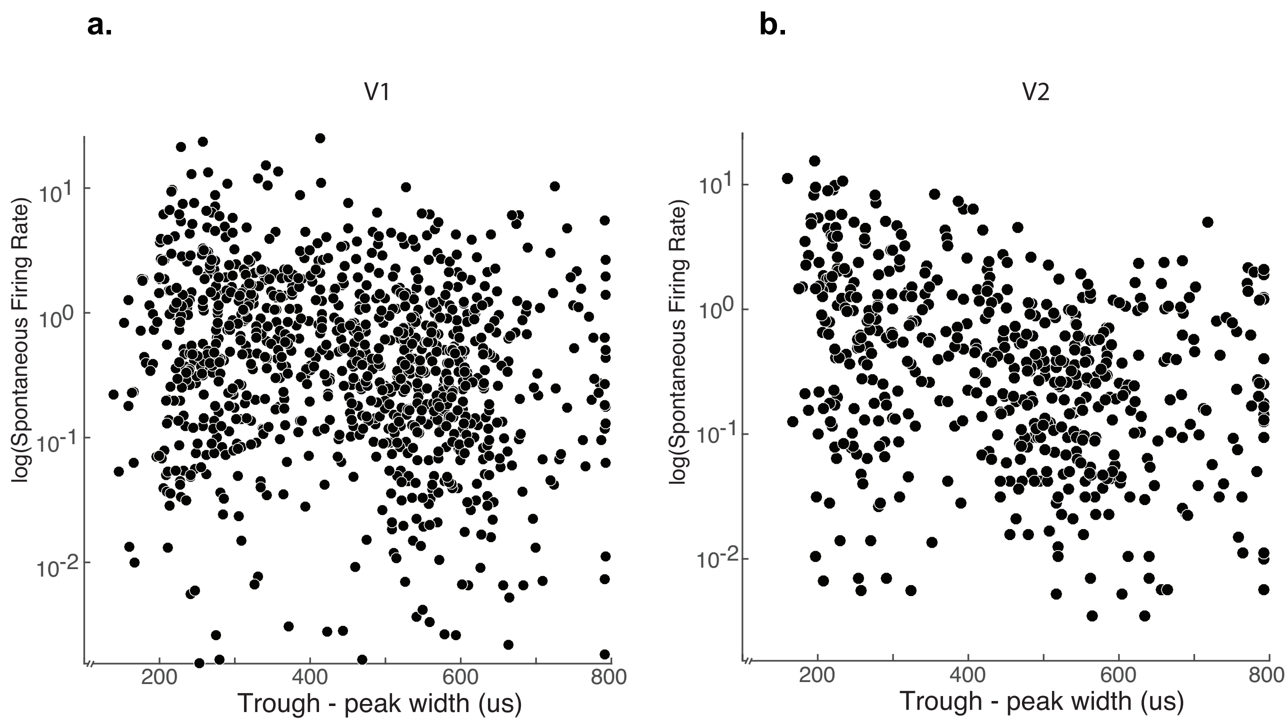

Figure 3.6 Spontaneous firing rates of narrow-and broad-spiking cells in V1 and V2. In both V1 **(A)** and V2 **(B)**, cells in the narrow-spiking cluster (i.e. putative inhibitory cells) (trough-peak width < 390μs) showed higher mean firing rates than the cells in the broad-spiking cluster (i.e putative excitatory cells) (trough-peak width > 410 μs).

DISCUSSION

The present results show that tetrode recordings can be used to classify neurons in macaque area V1 and V2 into two subgroups based on their extracellular action potential widths. The bimodality in the waveform widths measured from the tetrode channel with the largest SNR coincide with findings in subpopulations of neurons in visual cortex (Mitchell et al., 2007) and other cortical areas ((Kaufman et al., 2010b)). Corroborating this classification, we find that other physiological properties of the cells differed systematically between groups. The narrow-spiking neurons exhibited higher firing rate than did the broad-spiking neurons. This is consistent with intracellular studies that have shown that narrow-spiking inhibitory interneurons were more active (ie high firing rates than broad-spiking excitatory neurons when stimulated by current injection (McCormick et al., 1985) as well as with visual stimuli (Contreras and Palmer, 2003). We also find that the narrow-spiking cluster had more cells that were untuned than cells in the broad-spiking cluster. This is consistent with the findings that inhibitory cells may be involved in more non-selective pooling of local inputs, compared to the highly selective excitatory cells.

Despite the consistency of the findings from our tetrode recordings with known properties of inhibitory and excitatory celtypes, there are a few caveats to consider in the interpretation of the findings. Since cortical celltypes can be grouped into subsets based on similarities of binding proteins, ionic channels, morphology, neurotransmitters and connectivity profiles, it is likely that the narrow-spiking and broad-spiking clusters identified from the tetrode recordings are also composed of multiple subclasses (Bartho, 2004; Bean, 2007; Bock et al., 2011). Moreover, the correspondence between waveshape and neurochemical features that we assume for the macaque is largely based on an extrapolation from mouse (Du et al., 1996). Thus the analysis of extracellular waveform shape is an inexact way to classify neurons as excitatory and inhibitory. Nevertheless this approach has been shown to identify subpopulations of neurons with markedly different functional properties – in visual and sensorimotor cortices (Mitchell et al., 2007). Moreover our finding of systematic differences between celltypes, consistent with the literature, supports the use of this approach for the study of adaptation in the visual cortex.

CHAPTER 4

DEVELOPMENT OF ORIENTATION DOMAIN CHARACTERIZATION OF TETRODE DATA

In mammalian striate cortex, neuronal orientation preferences are mapped across the columnar architecture to form a mosaic of “iso-orientation domains” and “pinwheel centers”. In iso-orientation domains, neighboring neurons have similar orientation preferences; in pinwheel centers, the assorted orientation preferences of several iso-orientation domains converge (Bonhoeffer and Grinvald, 1991; Maldonado et al., 1997; Ohki et al., 2006). The gold standard for identifying iso-orientation domains and pinwheel centers across the cortical surface uses optical imaging methods (Weliky et al., 1996). Here we demonstrate a method for distinguishing these domains based on tetrode recordings.

The rationale for this approach is based on the fact that neurons in iso-orientation domains have a narrow range of orientation preferences compared to neurons situated near pinwheel centers. Our strategy for distinguishing the two types of domains is to leverage the capability of simultaneously recording from multiple single-unit neurons with a single tetrode. We expect that since cells in pinwheel centers have diverse orientation preferences, tetrode recordings near pinwheel centers should isolate cells with correspondingly diverse orientation tunings. Conversely, since neighboring neurons located in iso-orientation domains have similar orientation tunings, tetrode recordings from these sites should yield cells that have a narrow range of orientation preferences. This approach makes sense because our tetrodes (Thomas Recording) have a recording radius of approximately 100μ - 130μ, and this is comparable to the scale of iso-orientation domains.

As we show in this chapter, the distribution of the range of orientation preferences in individual tetrode recordings suggests the presence of two such modes, and we use this range to assign recordings to iso-orientation domains, and pinwheel centers. We then show that the tuning properties of cells from these putative subpopulations have the expected differences that match the findings based on standard optical imaging and microelectrode recordings.

METHOD

To classify the recording sites as pinwheel centers vs iso-orientaion domains based on a physiological criterion, we first considered only those recording sites with at least 4 oriented neurons isolated at a single tetrode. Then, for each site, we assessed the range in orientation preferences across the single-unit clusters. Specifically, we define the orientation range at each location as the smallest arc containing all orientation preferences across the multiple isolated single unit neurons. This measurement of the orientation range was restricted to include only tuned cells to avoid contamination of this measurement by assigning random orientations to untuned or poorly tuned neurons. The distribution of orientation ranges was then utilized to establish a cut-off for classifying the recording sites as iso-orientation domains or pinwheel centers.

RESULT

Across the 142 recording sites, 72 sites had at least 4 well-isolated single unit clusters, which were then used for subsequent analyses.

The distribution of orientation ranges measured at these sites (Fig 4.1) suggests bimodality. The notch in the kernel smoothed density estimate of the histogram was used to establish as the cut-off point, which is at 83^0. We therefore assigned sites with a range of orientations $<83^0$ to the "iso-orientation" subset, and those with a greater range of orientations to the “pinwheel” subset. Note that, by this procedure, each site with at least four recorded neurons was considered either entirely “pinwheel” or “iso-orientation”, based on the collective properties of the recorded neurons.

To corroborate this assignment, we measured the orientation bandwidth of individual cells in the subsets assigned to pinwheel centers and iso-orientation domains. As expected (Maldonado et al., 1997; Ohki et al., 2006), differences in the orientation ranges between cells in iso-orientation domains and pinwheel centers, the range of tuning profiles across the neurons were also distinct between them, consistent with our expectation.

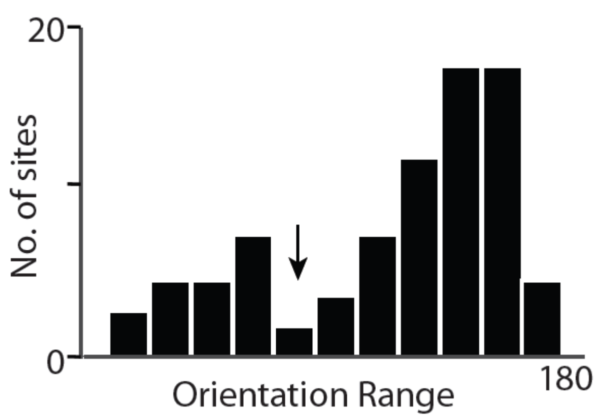

Figure 4.1 Distribution of orientation ranges across tetrode recording sites – The orientation range, defined as the smallest arc that contains the orientation preferences across the cells at a recording site was measured for all the sites.

As expected, cells in the iso-roentaion domain were more sharply tuned with narrow bandwidths (Figure 4.2), and cells in regions classified as pinwheel centers had more broadly selective tuning. Figure 4.4 shows an example site that was labeled as iso-orientation domain (orientation range = 24.6^0). As expected, the cells recorded in this domain are tuned to similar orientations with narrow bandwidths. To ensure that the 4 tuning curves were distinct clusters on the basis of the 17 features used for spike sorting (see Chapter 2), we retrospectively inspected the tetrode channels corresponding to the 4 isolated single-units for additional validation. Figure 4.5 shows an example site labeled as pinwheel center based on our orientation range criterion (orientation range = 87.2^0). As expected, the five neurons recorded from this pinwheel center are indeed tuned to widely different orientations and include both broadly tuned and sharply tuned cells.

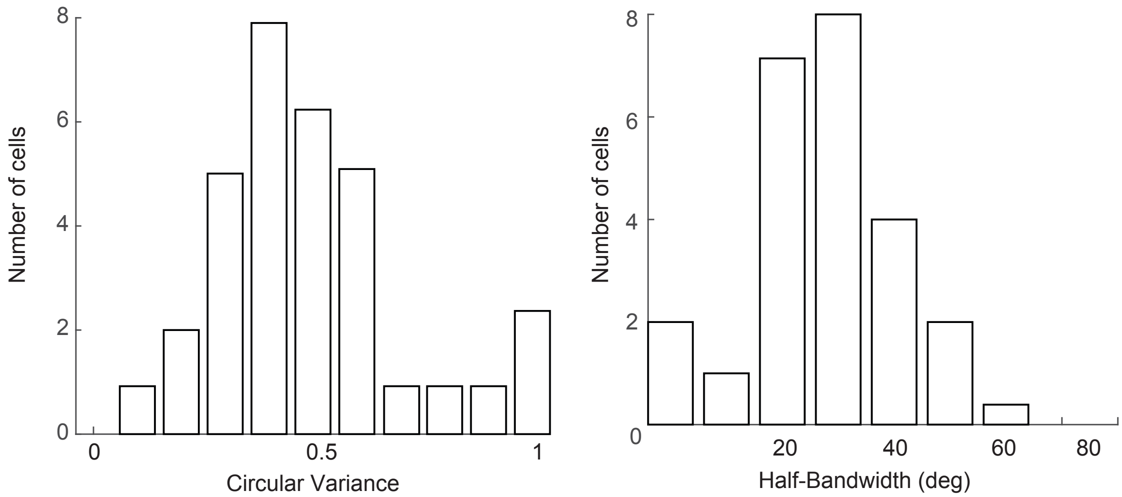

Figure 4.2 Histogram of half-bandwidths of orientation tuning in iso-orientation domains

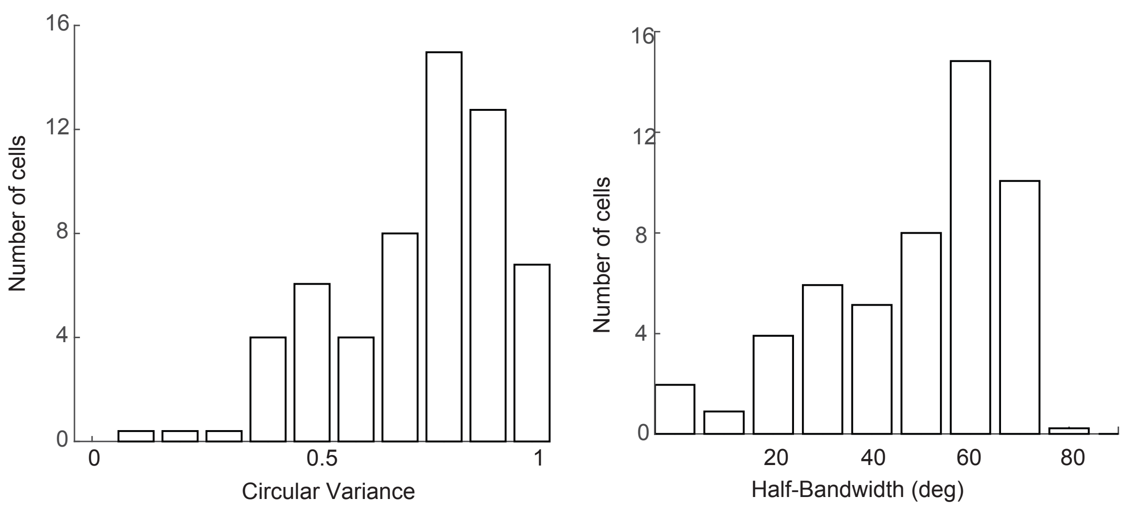

Figure 4.3 Histogram of half-bandwidths of orientation tuning in pinwheel centers

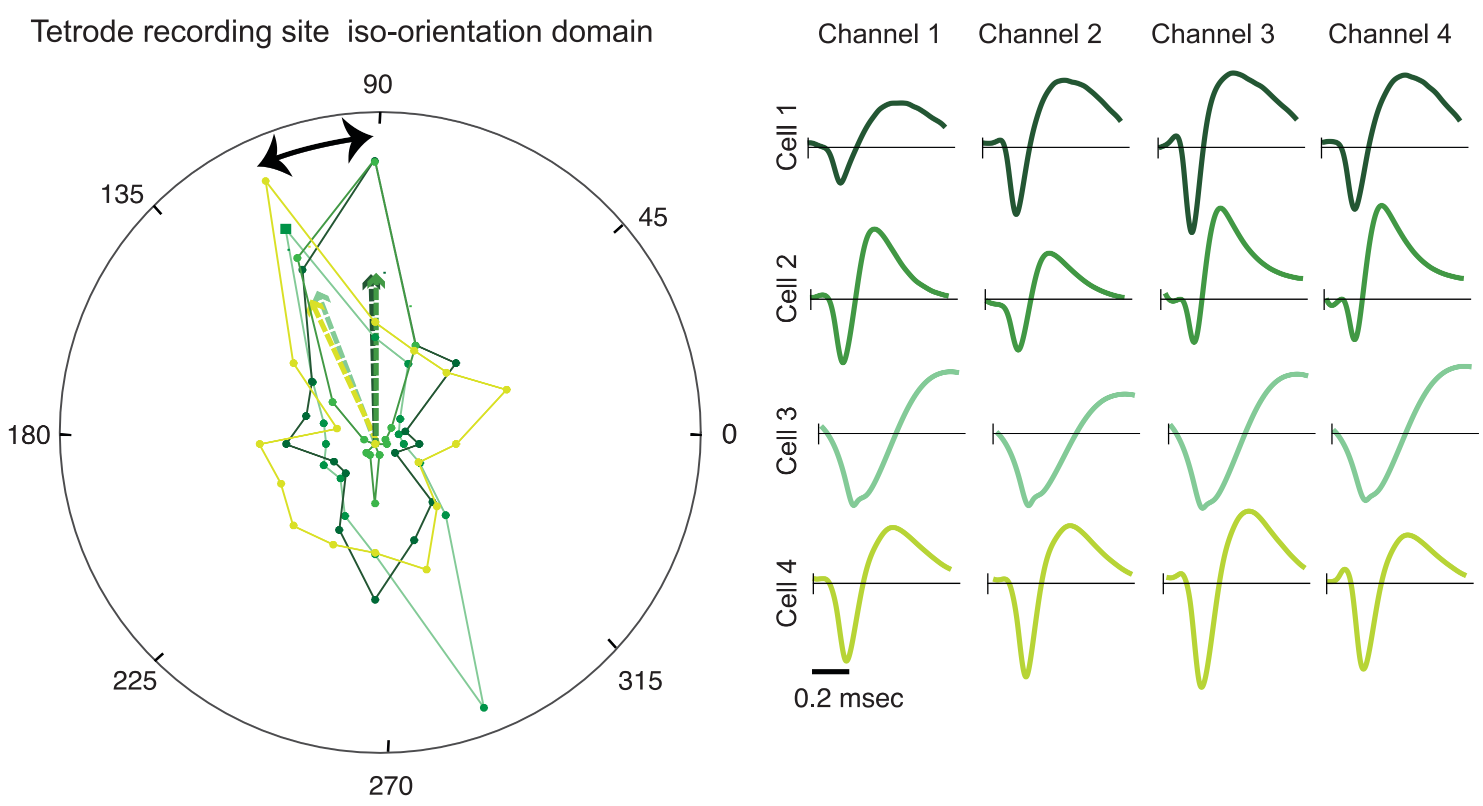

Figure 4.4 Example iso-orientaion domain

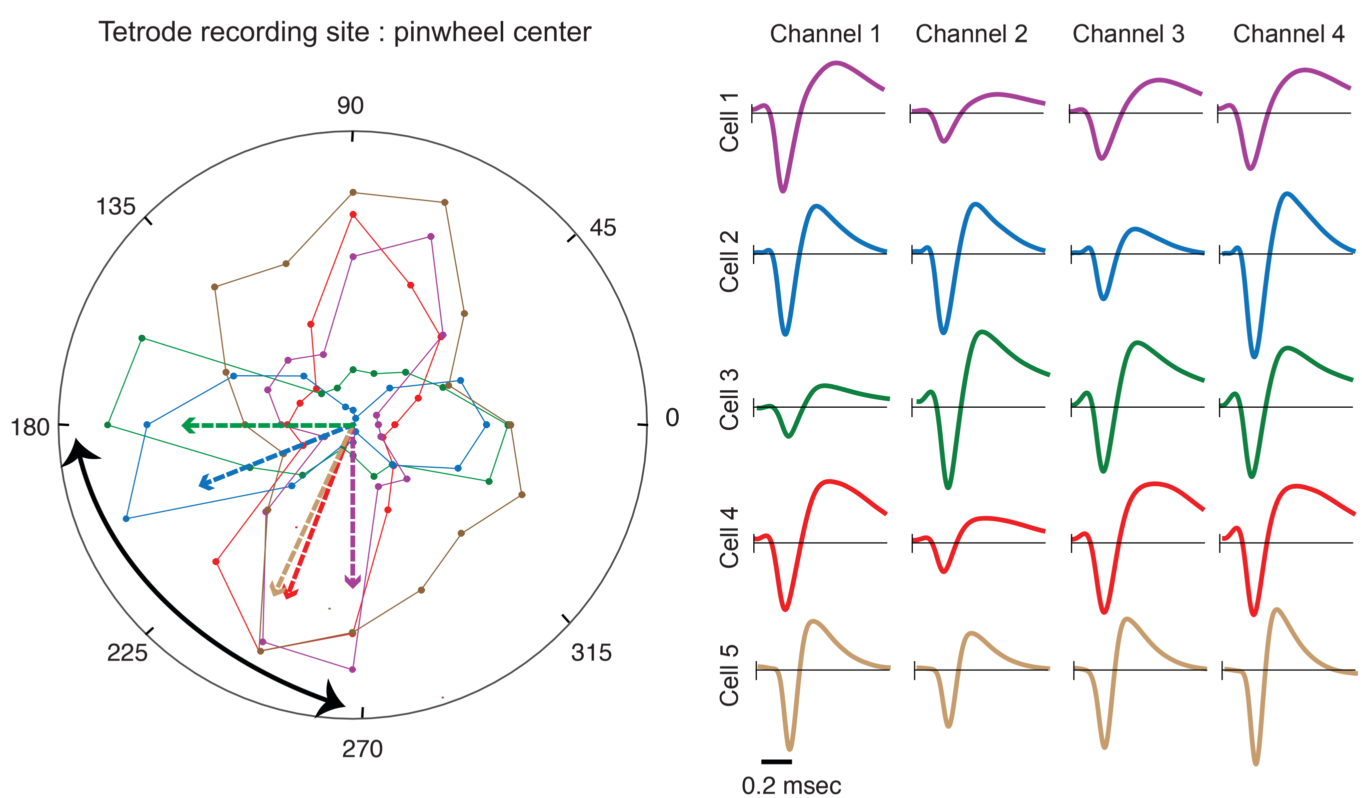

Figure 4.5 Example pinwheel center

DISCUSSION

Using a physiologically motivated criterion – the range of orientation preferences present in distinct domains of the orientation map – our results show that it is possible to identify iso-orientation domains and pinwheel centers with tetrode recordings. Consistent with our expectations based on the literature, we find that the orientation ranges in our recording sites indeed fall into 2 modes. In our data, the cut-off for separating the two mode was 83^0. Further inspection of the individual recording sites revealed that neurons in iso-orientation domains had narrower bandwidths, than neurons in pinwheel centers.

While we did not demonstrate a direct correspondence between orientation range and pinwheel vs iso-oreintation domain distinction, this correspondence is known to be present. Specifically (Maldonado et al., 1997) made targeted recording of pinwheel centers and iso-orientation domains identified by optical imaging. These authors found a cutoff of 42^0. Most likely our larger cutoff is due to our larger recording volumes of tetrodes.

In Chapter 5, we utilize the method developed here to study how the tuning of cells in these distinct domains of the orientation map is altered by adaptation.

CHAPTER 5

ADAPTATION IN VISUAL AREA V1

Sensory adaptation influences both neuronal response properties ((Kohn and Movshon, 2004a)), and perception ((Gibson and Radner, 1937),(Clifford et al., 2001b),(O'Toole and Wenderoth, 1977b),(Wenderoth and Johnstone, 1988b)). In area V1, adapting to an oriented stimulus can cause shifts in neural tuning, including changes in gain, bandwidth, and orientation preference ((Dragoi et al., 2000a),(Patterson et al., 2013b),(Bachatene et al., 2012)). In addition, perceptual studies show that adapting to an oriented stimulus shifts the apparent orientation of subsequent stimuli, a phenomenon referred to as the tilt after-effect ((Gibson and Radner, 1937),(Wenderoth and Johnstone, 1988b)). However these studies focused on the average behavior of V1 and it is well known that V1 neurons are diverse in many ways. Here we will test whether the effects of adaptation covary with functionally significant cell characteristics such as their response properties and their anatomic locations.

Specifically, we considered the effects of adaptation in these subpopulations of V1.These classifications include : 1) their functional characteristics: excitatory vs inhibitory, 2) their response profile: simple vs complex, 3) their anatomic location: supragranular layer vs granular layer, and 4) their functional location on the orientation map: iso-orientaion domain vs pinwheel centers.

We find that adaptation induces a wide diversity of changes in orientation tuning in excitatory and inhibitory neurons, including both attractive and repulsive tuning shifts and bandwidth changes. Population responses reveal that the diversity of tuning shifts increase with the distance of the adapting stimulus to the preferred orientation of the cells, with repulsive shifts dominating within 45^0 of the preferred orientation, and predominantly attractive shifts in tuning when the adapter is 75^0 to 90^0 away. In addition, we find a subset of neurons – including inhibitory cells -- that are untuned under baseline conditions and become tuned after adaptation.

A portion of this chapter is adapted from the text and the figures from the submitted manuscript, Thengone et al. This is augmented by further analyses of the effects of adaptation on response size and on combinations of tuning indices.

METHODS

The physiological preparations and experimental paradigms are detailed in chapter 2. The criteria for classifying cells into excitatory and inhibitory subtypes are described in chapter 3, and the method to classifying cells into pinwheel and iso-orientation domains are described in chapter 4.

All the comparisons are made from the indices measured from the non-adapted tuning curve and the adapted tuning curves for the brief and prolonged adaptation paradigms separately. (Chapter 2). Briefly, the main comparisons concern the tuning peaks, and selectivity of the tuning curves before and after adaptation (included in the submitted manuscript). In addition here we analyze the effect of adaptation on the response amplitudes, and the joint distribution of selected combinations of indices: amplitude and bandwidth, and amplitude and peak shift.

RESULTS

We performed simultaneous recordings with up to 6 tetrodes in V1 (granular and supragranular layers) in 6 macaques; in 3 of these 6 preparations, one or more of the tetrodes also sampled V2. At all recording sites, brief (400 ms) and prolonged (40 s) adaptation paradigms were studied. The adapting orientation was chosen to be near the preferred orientation of one or more of the recorded clusters, based on online analysis of orientation tuning runs (see Fig 2.2 and Methods). Along with these recordings that captured effects of adaptation to a near-preferred stimulus, our dataset also includes parallel recordings at the other tetrodes, which captured effects of adaptation to a stimulus whose orientation is far (45^0 to 90^0) from the tuning peak. When recording stability permitted, we repeated the adaptation experiment at a second orientation, so that some cells were studied both with near-peak and far-from-peak adapting stimuli.

Only spike-sorted single units with peak firing rates over 8Hz, and stable tuning curves (baseline compared to a second baseline following the prolonged-adaptation runs) were analyzed. This dataset totaled 173 units in V1 (112 sites along 21 penetrations), and 95 units in V2 (28 sites along 6 penetrations, analyzed in Chapter 6). From these totals 44 units in V1 passed the selection criteria for both brief and prolonged adaptation paradigms; 87 were only analyzed for the brief paradigm, and 42 for the prolonged paradigm.

We use standard orientation tuning measurements ((Shapley et al., 2003),(Skottun et al., 1991),(Carandini and Ringach, 1997)) to characterize how recent stimulus history affects response properties. We focus on the diversity of behavior and comparisons between putative excitatory (E) and putative inhibitory (I) cells, classified by spike-shape (Figure 3.2, Methods). The data show that a diversity of adaptive effects is present across cell types and cortical regions – a level of diversity that goes beyond what might be expected from the average behavior across the population -- and within this diversity, differences between the behaviors of E and I cells, and between V1

The results are organized as follows: We begin with example neurons, and the population results across the distinct characteristics in V1 comparing the effects of adaptation to individual features of the tuning curve. We then considered whether changes in response amplitudes and bandwidths are associated with the shifts in tuning preferences. Finally, we describe the effects of adaptation that were not expected, with regards to the tuning of the cells. Computational modeling results are described in chapter 8

ADAPTATION EFFECTS IN E AND I CELLS IN V1

We begin with an analysis of adaptation effects in well-tuned cortical V1 neurons, as these are readily quantified by changes in selectivity and orientation preference. We used two measures of selectivity: circular variance (CV) (Ringach et al., 2002b) and tuning bandwidth (half height at half-width) (Sompolinsky and Shapley, 1997a); the former is a more global measure of orientation selectivity and the latter focuses on responses near the preferred orientation. To quantify orientation preference, we fit responses with a von Mises function. To ensure that there was a well-defined peak in the tuning function, we restricted this analysis to neurons whose baseline CV was <0.6).

EXAMPLE TUNED NEURONS

Figure 5.1 shows the effects of brief and prolonged adaptation on the tuning curves of representative E units (A - D) and I units (E - H). In some units, adaptation induces increases in tuning bandwidth (Figure 5.1 A – C, H); in others, it induces decreases (Figure 5.1 E and H). Tuning shifts, when present, could be either repulsive (i.e., away from the adapting orientation), as seen in panels C,D,E,F, or attractive, as seen in panels A and G. Independently, the maximum firing rate could either increase or decrease. Decreases in overall gain are much more common. However, as a result of peak shifts and bandwidth changes, responses to specific orientations near the peak often increase even though overall gain decreases. Note that a broadly similar range of phenomena is seen in E units and I units.

At the level of individual neurons, brief and prolonged adaptation sometimes have similar effects (Figure 5.1), but often the effects are different. For instance, brief adaptation of the neuron modestly reduces overall gain, while prolonged adaptation in this neuron leads to almost complete suppression of the peak response.

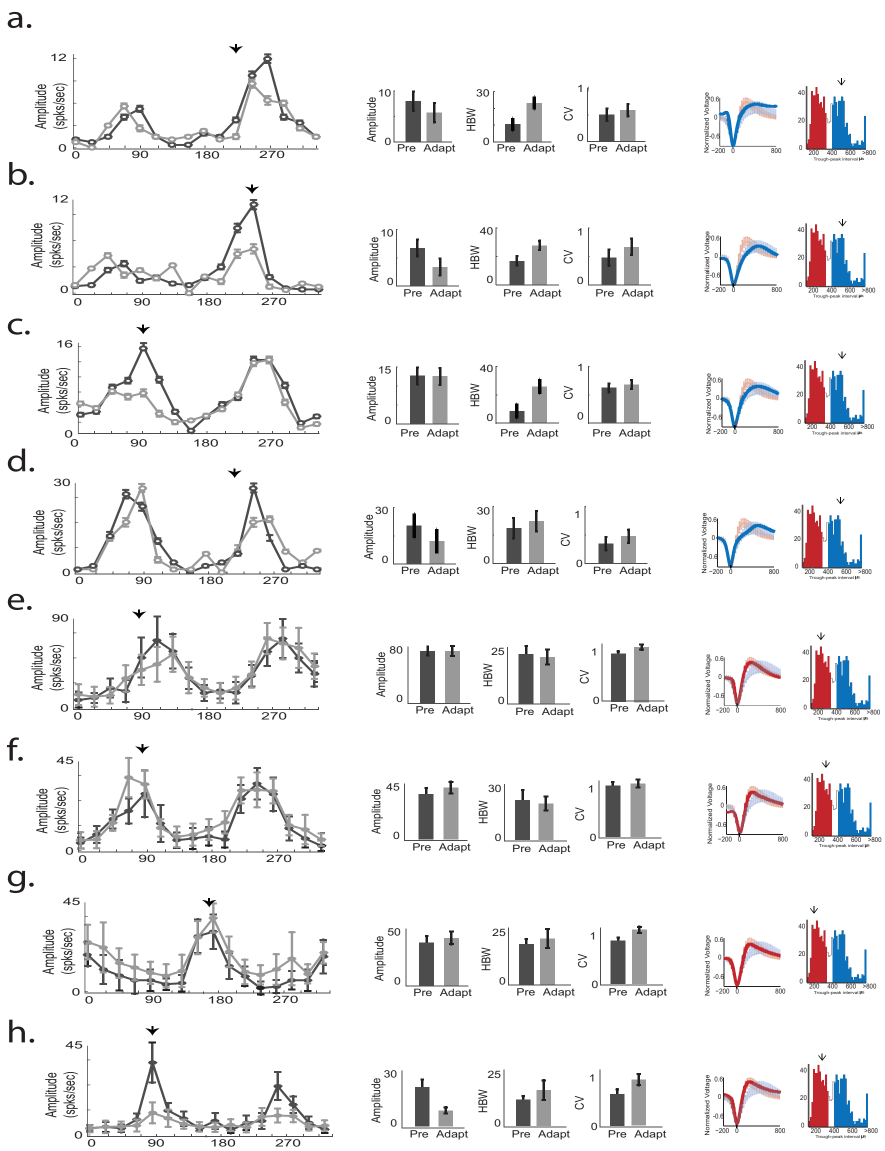

Figure 5.1 Adaptation-induced peak shifts and bandwidth changes :Example units Each row shows: tuning curve under baseline conditions (black) and following adaptations (gray) to selected orientations (black arrows), three tuning parameters (von Mises amplitude parameter, the half bandwidth(HBW), and circular variance (CV)), and the extraceullular waveshape and peak width, overlaid on the laboratory database. Error bars indicate 95% confidence limits for tuning curves and indices.

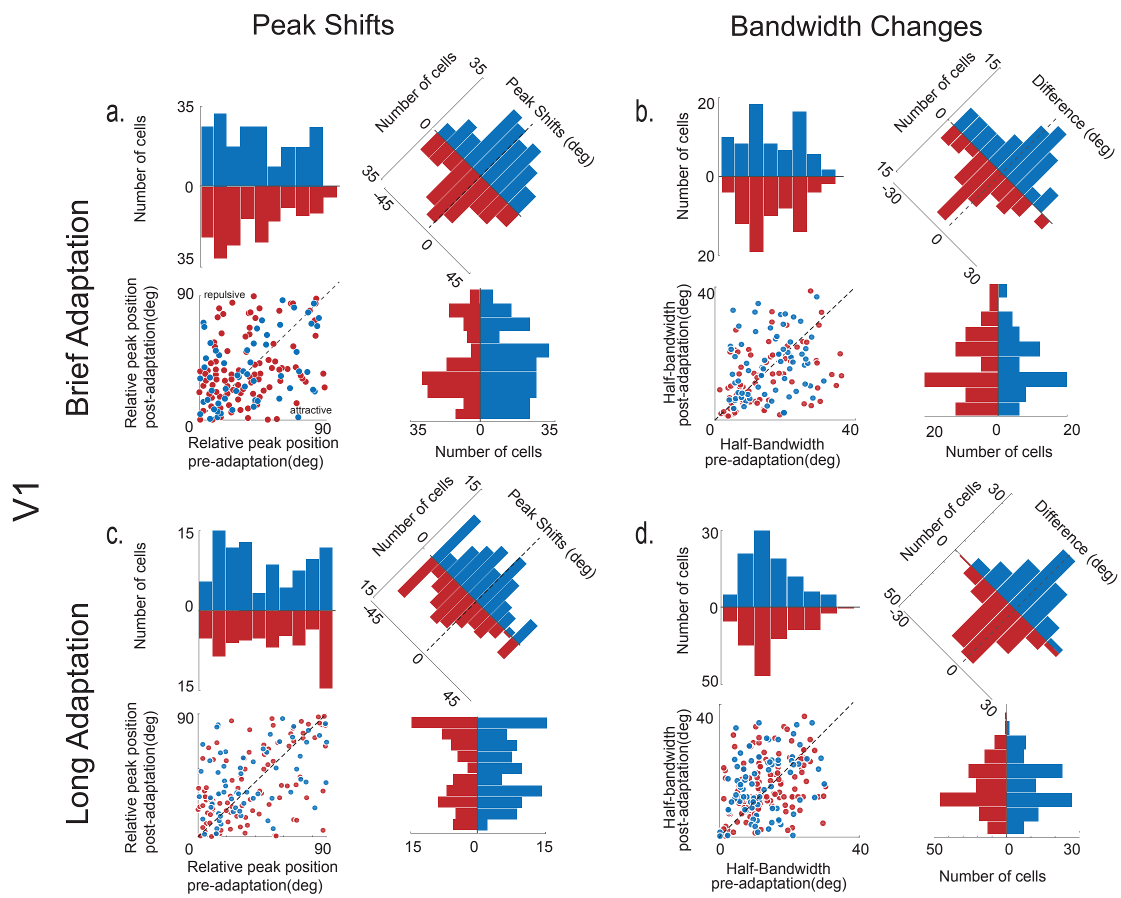

Figure 5.2 Population summary of adaptive changes of tuned E and I cells in V1 - Tuning curves are summarized by two parameters: orientation preference relative to the adapter (left column: A, C), and bandwidth (right column: B, D). Blue indicates E cells, red indicates I cells. V1 data shown in panels A-D (brief adaptation: A and B, prolonged adaptation: Within each panel, the scattergram shows the joint distribution of a parameter before and after adaptation; its projections onto the coordinate axes show the parameter's value before and after adaptation, and its projection onto the oblique axis shows the adaptation-induced change. For the scattergrams of peak shifts, points above the diagonal indicate repulsive shifts; points below the diagonal indicate attractive shifts. For the scattergrams of tuning widths, points above the diagonal indicate broadening; points below the diagonal indicate narrowing.

Although we are not focusing on direction selectivity, we note that adaptation-induced direction selectivity also occurs among the tuned cells.

Population behavior

The vast majority (68% of cells) of our sample had a lower spike rate after adaptation, regardless of where they were adapted. There was a significant decrease in spike rate for both the peak and baseline spike rates in many neurons at the single-unit level. However there were many cells, in which the maximum spike rate increased after adaptation. Past studies of orientation adaptation have not commonly reported increases in tuning curve amplitude, but a few studies have observed this effect following flank adaptation ((Dragoi et al., 2000b; Kohn and Movshon, 2004a; Patterson et al., 2013a)). Nevertheless this shows that adaptation is not simply “fatigue” because in a substantial number of neurons firing rate increases.

Adaptation induced changes in the bandwidth of the tuning as well. The mean half-bandwidth in our sample was 33.2° before adaptation and 29.2° after adaptation. The histogram in Figure 5.2 shows bandwidth change, with on-peak and off-peak adaptation. In our sample, 62 tuning curves narrowed,

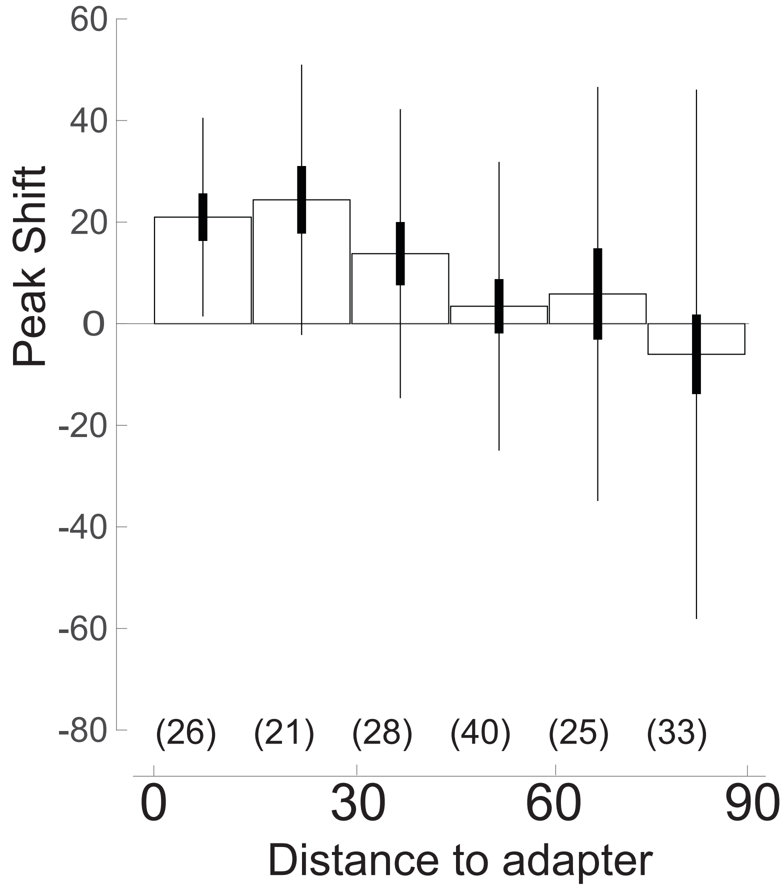

Figure 5.3 Shifts in orientation tuning as a function of distance of the adapting orientation to the preferred orientation. Population tuning shifts as a function of distance between adapter and preferred orientation. Bar heights indicate population average, heavy line indicates 1 SEM, and thin line indicates 1 SD.

41 broadened, and 12 flank adapted neuron had no change in bandwidth (<1°). Mean bandwidth changes for peak and off-peak adapted were 12.2 deg and 26.4 deg respectively. However, bandwidth changes were not consistent enough to produce a statistically significant effect at the population level ($p>0.05$). With regard to tuning bandwidth (brief adaptation, Figure 5.2C, prolonged adaptation, Figure 5.2D), both narrowing and broadening are seen, without an obvious dependence on the relationship between the adapter and the cell's tuning preference. Although the timescales of adaptation (400 ms vs 40 sec) often have distinct effects on individual cells' tuning bandwidths, there was little difference in the distribution of bandwidth changes across the population (KS Test p= 0.5, Wilcoxon test p=0.8 for 40 ms vs 400 ms).

Figure 5.2 summarizes the effects of adaptation across the recorded V1 population (A-D), and shows that the wide range of adaptation effects are similar in E and I cells. With regard to tuning shift (brief adaptation, Figure 5.2A; prolonged adaptation, Figure 5.2C), both repulsive and attractive shifts are present. The phenomenon of attractive adapting shifts is well-recognized ((Kohn and Movshon, 2004a),(Patterson et al., 2013b),(Ghisovan et al., 2009b)), and here we show that it is present in both cell types. For adapting stimuli within 45^0 of the tuning peak, there is a bias towards repulsive shifts, as seen by the greater number of cells above the diagonal. For adapting stimuli further away from the tuning peak, there is no such bias. Further, as the distance between the adapting stimulus and tuning peak increases, the diversity of tuning shifts also increases. These trends are summarized in Figure 5.3.

As mentioned in the introductory chapter, adaptation was originally considered to be a kind of “fatigue”. In this simple scenario, adaptation would be expected to reduce firing rates. Since this reduction would be greatest at the adapting orientation, the peak of the tuning curve would be shifted away from the adapter (ie, a repulsive shift), and the tuning curve would also be narrowed. But we found many instances of adaptation-induced increases in firing rates, attractive shifts, and broadening of the tuning curve. So we next asked if these paradoxical changes in the tuning curves occur in cells that increase their firing rate with adaptation.

We find that this is the case for peak shifts, but only in the inhibitory cells during prolonged adaptation. (Figure 5.4, Table 5.1). Specifically, there is a strong correlation between the response amplitude and the peak shifts. (Pearson correlation coefficient = -0.3791, $p<0.005$) (Figure 5.4, Table 5.1). However, there was no clear correlation between firing rate changes and tuning bandwidth in the inhibitory neurons. There was also no correlation between firing rate and any other parameter in the excitatory cells, or in the inhibitory subpopulation during brief adaptation. We will return to these points in Chapter 7 where we discuss the model.

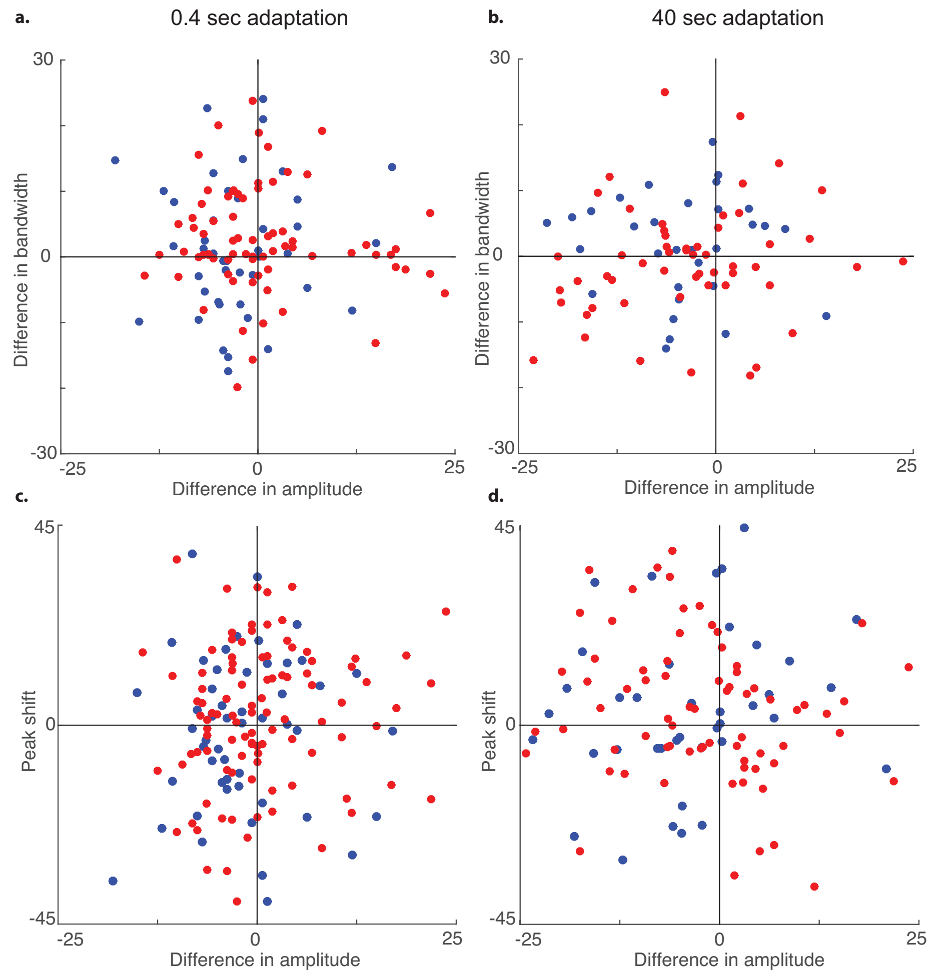

Figure 5.4 Joint distributions of adaptation-induced amplitude changes to peak shifts and bandwidth changes Adaptation-induced tuning shifts are correlated with amplitude changes in the inhibitory cells during prolonged adaptation (See Table 5.1)

Table 5.1 Correlation of amplitude changes to peak shifts and bandwidth changes. r: Pearson's correlation is noted for both brief and prolonged adaptation. * p<0.05; ** p<0.005

	Brief	Prolonged
Excitatory Cells		
Peak shifts and Amplitude Changes (r)	0.0487	-0.1582
Bandwidth Changes and Amplitude Changes (r)	0.0477	-0.1573
Inhibitory Cells		
Peak shifts and Amplitude Changes (r)	0.1706	-0.3791**
Bandwidth Changes and Amplitude Changes (r)	-0.0962	0.0285
All Cells		
Peak shifts and Amplitude Changes (r)	0.1384	-0.1964*
Bandwidth Changes and Amplitude Changes (r)	-0.0549	-0.0384

CONTRIBUTIONS TO DIVERSITY IN THE POPULATION

One of the prominent features of our data was the diversity of the effects of adaptation. (Figure 5.2) We next consider several potential contributors to this diversity, including the simple/complex distinction, laminar differences ((Ringach et al., 2002b)), and the pinwheel architecture (Koch et al., 2016).

ADAPTATION IN SIMPLE AND COMPLEX CELLS

To determine the contribution of the simple/complex distinction, we determined the dependence of adaptation-induced changes in tuning properties on the cell's modulation ratio (F1/F0), a standard measure of the linearity of cell's response ((Skottun et al., 1991),(Shapley et al., 2003),(Mechler and Ringach, 2002)). While this distinction captures much of the variation of neurons' temporal response patterns ((De Valois et al., 1982c)), it does not appear to contribute to the diversity of adaptive effects. Specifically, there is no dependence of the adaptation-induced change in tuning shift (Fig. 5.5A) and bandwidth (Fig.5.5B) on the F1/F0 ratio. This conclusion holds whether the F1/F0 ratio is treated as a dichotomous variable (either with cutpoints at 1 ((Skottun et al., 1991)) or 0.8, the notch in our F1/F0 distribution), or as a continuum, and whether tuning parameters are treated dichotomously (attractive vs. repulsive, bandwidth increase vs. decrease), or as a continuum. Statistics for dichotomous treatment of F1/F0 are as follows: for dichotomous tuning parameters, chi-squared p>0.05; for continuous tuning parameters: KS-test,p>0.05. Statistics for continuous treatment of F1/F0: regression of orientation shift or bandwidth change on this ratio yield a regression coefficient which is not significantly different from 0 (p>0.05). These findings hold for the brief-adaptation and prolonged-adaptation paradigm.

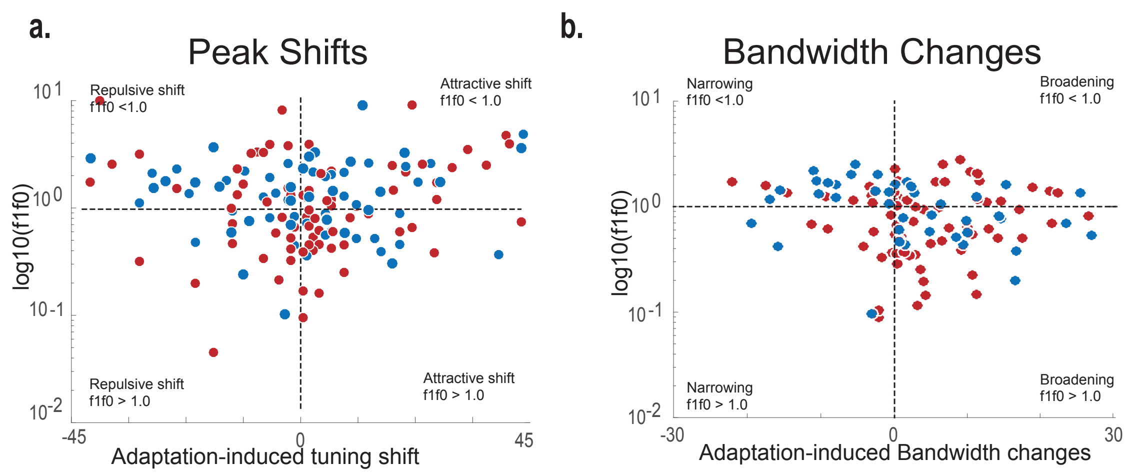

Figure 5.5 Adaptation effects in simple and complex cells – Adaptation-induced tuning shifts are present in both simple and complex cells. This classification did not appear to explain the diversity of repulsive and attractive shifts. No correlations were seen in either brief or prolonged adaptation.

ADAPTATION IN SUPRAGRANULAR AND GRANULAR LAYERS

The contribution of laminar position (supragranular layer vs granular layer) to adaptive shifts is minor. Orientation tuning shifts (Figure 5.6 A and C, Figure 5.7 A and C), and bandwidth changes (Figure 5.6 B and D, Figure 5.7 B and D) occur in either direction, in either layer, with either brief or prolonged adaptation. When E and I cells are considered together, there is no difference between the distribution of shifts in the input layer vs. the supragranular layers (KS tests, $p>0.05$). However, there appears to be a difference in behavior between E and I cells in the input layer, for the brief adaptation paradigm (Fig. 5.7 D): I cells tend to increase their bandwidth, while E cells tend to decrease their bandwidth ($p< 0.05$ KS test)

ADAPTATION IN PINWHEEL CENTERS AND ISO-ORIENTATION DOMAINS

We hypothesized that proximity to pinwheel centers would contribute to the observed population diversity. Specifically, since neurons in pinwheel centers are located in close proximity to neurons of all orientations, they are therefore more likely to be connected to neurons with a broader range of orientations than neurons in iso-orientation domains. Thus pinwheel center neurons might be expected to have a wider range of shifts in tuning after adaptation.

Using the method of Chapter 3 to classify tetrode recordings into iso-orientation domains and pinwheel centers, we indeed find that the units that have large orientation shifts are primarily found in pinwheel centers (Fig 5.8 A-C (brief adaptation) and 5.8 D-F (prolonged adaptation)). Restricting consideration to datasets in which the adapting stimulus and the peak stimulus

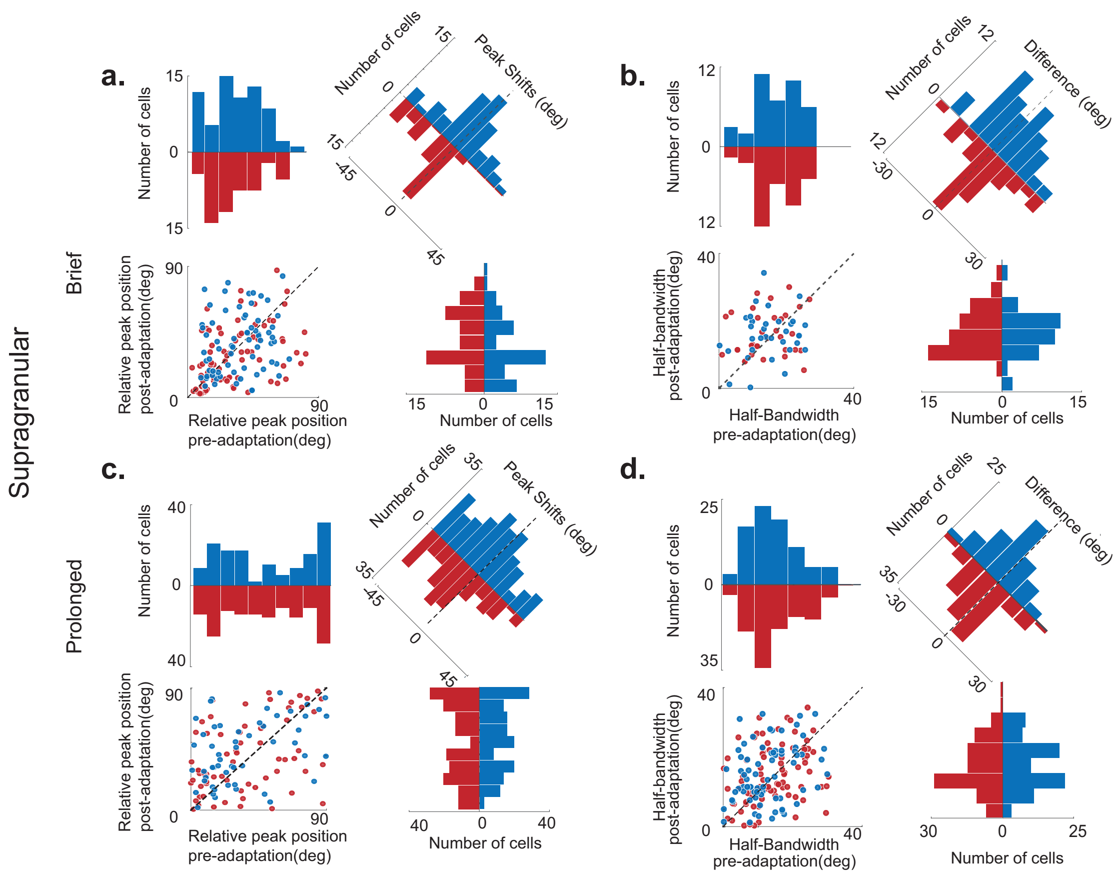

Figure 5.6 Adaptation effects in supragranular layer – Both attraction and repulsive shifts are present in the supragranular layer. The scatterplot shows the peak position (left column) and bandwidth changes (right column) before (abscissa) and after adaptation (ordinate axis). Blue refers to E cells, and red refers to I cells.

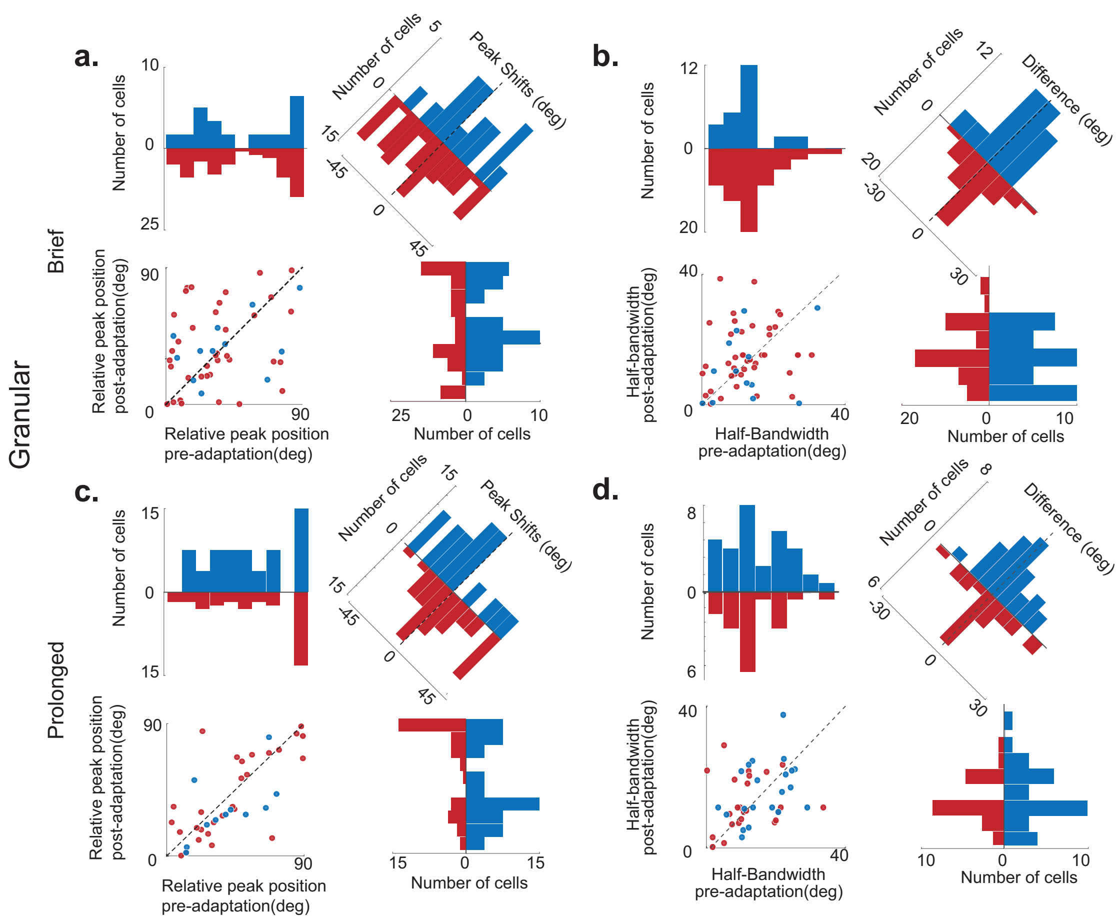

Figure 5.7 Adaptation effects in granular layer - Both attraction and repulsive shifts are present in the granular layer. The scatterplot shows the peak position (left column) and bandwidth changes (right column) before (abscissa) and after adaptation (ordinate axis). Blue refers to E cells, and red refers to I cells.

differ by more than 22.5^0 (i.e those datasets in which overall population diversity is large, Fig 4A), this difference is significant for either brief or prolonged adaptation paradigms (KS-test on the magnitude of the peak shifts $p<0.005$). The same trend is present in both brief and prolonged adaptation when all datasets are considered, but is only significant for the prolonged adaptation paradigm. Tuning shifts in iso-orientation domains do not exceed 44^0, while neurons at pinwheel centers have larger shifts in tuning up to 78^0.

For bandwidth changes, a parallel analysis did not reveal a dependence on location with respect to pinwheel vs iso-orientation domains.

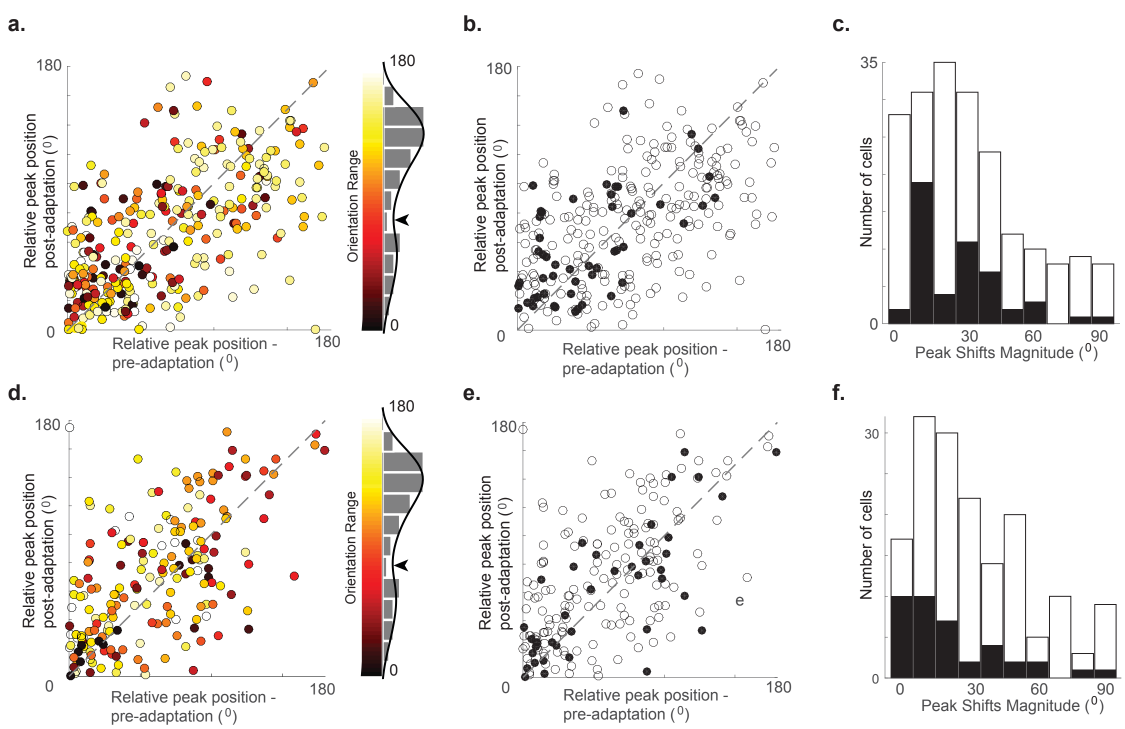

Figure 5.8 Adaptation effects in pinwheel centers and iso-orientation domains - Scatterplot of tuning shifts for brief adaptation with symbols colored according to the range of orientations encountered at the recording site. The plot is restricted to recordings with at least 4 neurons at the same tetrode. The distribution of orientation ranges is shown to the right. B. As in A, but with dichotomous coloring: filled, orientation range $<83^0$; open: orientation range $> 83^0$. C: Histogram of prevalence of peak shifts. Among the cells with large tuning shifts, a disproportionate fraction is from recordings with a large orientation range at the recording site. D, E, and F: as in A, B, and C, but for prolonged adaptation. Larger adaptation-induced tuning shifts are more prominent near pinwheel centers

UNTUNED NEURONS CAN GAIN SHARPER TUNING WITH ADAPTATION

Until this point we have focused on neurons that had clear-cut orientation tuning prior to adaptation. These neurons constitute approximately 80% of the population. However, adaptation-induced changes in orientation tuning were not restricted to this subset, and in fact, many cells that were untuned under baseline conditions became tuned after adaptation (examples). Of the 80 neurons that were untuned (95% confidence limits for $CV > 0.6$) under baseline conditions, 31 became tuned (95% confidence limits for $CV < 0.6$) after adaptation by this criterion. These shifts occurred in 12 out of a total of 56 untuned E cells and 19 of 24 untuned I cells. This phenomenon was present in both brief and prolonged adaptation in V1. Across the population, there was a slight tendency of the adaptation-induced tuning peak to be aligned with the adapter (circular variance = 0.91, $p<0.05$).

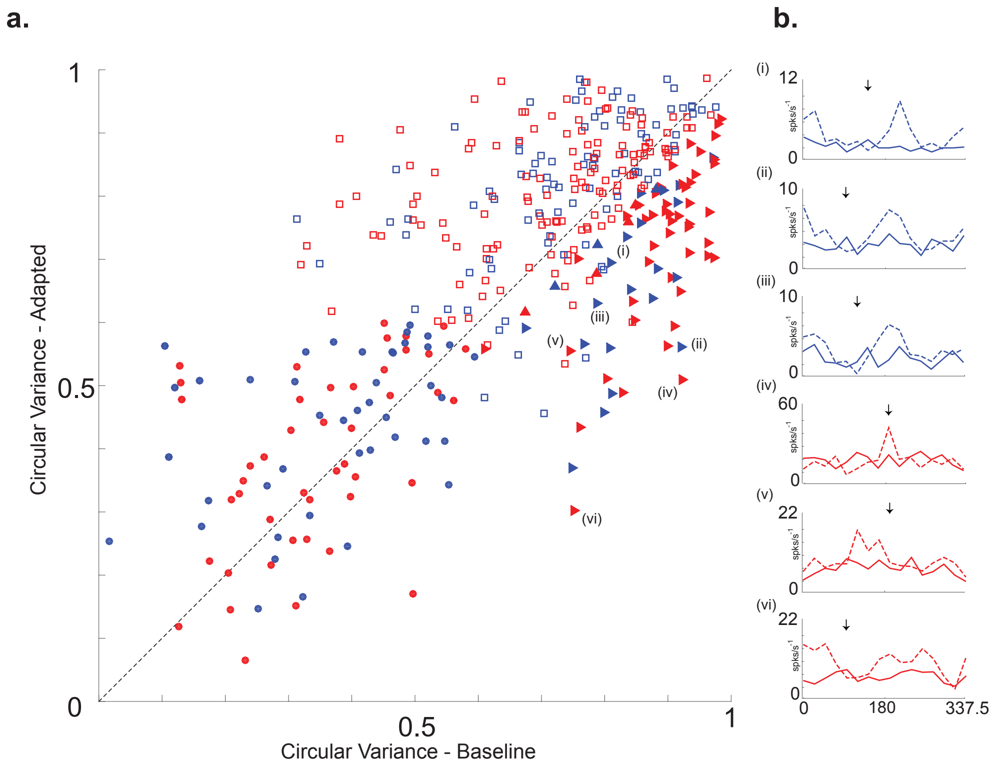

Figure 5.9 Untuned cells can become tuned after adaptation
Scatterplot of the circular variances (CV), before and after brief adaptation in V1. Blue indicates E cells, red indicates I cells. Filled triangles: units that were untuned (CV 95% confidence range entirely >0.6) under baseline conditions, but tuned (CV 95% confidence range entirely <0.6) after adaptation. Filled circles: units tuned before and after adaptation, and analyzed in Figures 3-5); open squares: all other units. Symbols identified by letters correspond to the example tuning curves shown in Panel B (baseline: solid, after adaptation: dashed).

Discussion

Here we examined the effects of adaptation on the orientation tuning of excitatory and inhibitory neurons (distinguished by their extracellular action potential widths: E and I cells) in area V1 of the primate visual pathway. We find that adaptation influences the responses of both E and I cells in V1, and a difference in adaptation effects emerges during prolonged adaptation. The population responses reveal a striking diversity of adaptation-induced effects in both cell types in the form of gain changes, bandwidth changes, and orientation tuning shifts (repulsive shifts and attractive shifts). The correlated increases in firing rates and attractive shifts in orientation tuning are consistent with the notion of disinhibition in the cortex. Adding to this diversity is the finding some untuned V1 cells acquired orientation tuning after adaptation. We considered the sources of this diversity, and showed the pinwheel vs iso-orientation domain contributed to it.

Tuned inhibitory cells

One notable result from our analysis is the presence of inhibitory cells that are sharply tuned. In fact, the fraction of inhibitory cells that were untuned were similar to the fraction of excitatory cells that were untuned. Both brief and prolonged adaptation induced changes to the tuning of these tuned inhibitory cells. Adaptation-induced gain changes, tuning shifts and bandwidth changes were comparable to the excitatory population. (Fig 5.2) Our finding of tuned inhibitory cells adds credence to the model classes that have included tuned inhibitory signals that contribute to shaping the tuning of cortical cells.

One notable distinction between E and I cells was observed during prolonged adaptation. Specifically, we found that the in inhibitory cells (but not in excitatory cells), attractive shifts in tuning were accompanied by increases in the response amplitude (Figure 5.4). This is consistent with the notion that adaptation induces disinhibition near the adapted orientation. Specifically, if adaptation at non-preferred orientations suppressed the tuned inhibitory inputs to the cell, then the cell's new preferred orientation would shift towards the adapting orientation, as a consequence of the loss of tuned inhibition at these orientations. As we show in Figure 5.4, amplitude increases accompanied attractive shifts, and conversely amplitude decreases accompanied repulsive shifts. This coupling was not present in the brief adaptation.

DIVERSITY

The relatively modest effects of adaptation on average across the population (Figure 5.3) give little hint to the diversity of behavior at the single-cell level. This diversity is found not only for the size of the peak shift, but also for the firing rate changes and tuning bandwidths. While the average effects were similar across brief and prolonged adaptation, there were noted differences across the cell-types on the population level.

While this diversity does not appear to be related to the division between E vs I cells, or to a difference between input and output layers, or the simple vs complex cell classification, in V1 it is at least partially related to the location of the cells in the orientation map. Specifically, cells whose neighbors varied substantially in orientation preference have larger peak shifts than cells whose neighbors have similar orientation preferences (Figure 5.8). This dependence is a predictable consequence of the notion that a neuron's orientation tuning is heavily dependent on the tuning properties of its neighbors, and is supported by our modeling in Chapter 7. The functional importance of orientation tuning in the local neighborhood (Wilson et al., 2016) is also supported by recent modeling efforts which show that cells situated near pinwheels have greater cross-orientation suppression than cells in iso-orientation domains (Koch et al., 2016).

Another new finding was that some untuned V1 cells became tuned with adaptation. Orientation selectivity is generally considered a fundamental property of V1 neurons, and many previous studies have taken the view that tuned and untuned cells have different functional roles ((Xing et al., 2011),(Shapley et al., 2003)). Our finding that untuned neurons can acquire tuning with adaptation strongly suggests that this distinction is not fixed, but rather depends on cortical dynamics and stimulus history. While this finding might appear surprising, adaptation-induced orientation tuning could also a predictable consequence of the notion that a cortical neuron's tuning properties depend on those of its local cortical inputs. That is, a neuron that is untuned under baseline conditions is a neuron that receives oriented inputs that happen to be balanced across orientations. Adaptation leads to orientation tuning by altering the balance of these local inputs, either excitatory or inhibitory or both. Our finding also raises the possibility that the adaptation-induced emergence of direction selectivity that has been in V4 is an analogous downstream consequence of adaptive changes in V1. (Tolias et al., 2005a).

In sum, adaptation induced a diversity of changes to the tuning of both E and I cells in V1. This diversity of effects was not simply a consequence of differences in the functional characteristics, their response profile, or the differences in the laminar location. However, the diversity of tuning shifts was partly accounted by the cell's functional location on the orientation map. At the population level, the average shift in tuning selectivity was repulsive when the adapter was within 45^0 away from the preferred orientation, and attractive when the adapting orientation was closer to orthogonal to the preferred orientation of the cell.

CHAPTER 6

ADAPTATION IN AREA V2

Sensory processing in primates is hierarchical, with a sequence of areas that transform the sensory inputs into neural signals that guide perception. While much is known about these distinct areas, it is still unknown whether these distinct stages of processing adapt independently. This issue is the focus of the present chapter.

Given that adaptation alters the representations in early sensory coding, we consider two contrasting scenarios for how adaptation behaves in the sensory cortical hierarchy. One scenario is that sensory inputs adapt at an early stage of processing, resulting in an altered representation that is inherited by downstream areas, where no further adaptation occurs. The obvious alternative is that there is an independent effect of adaptation on the downstream areas, and therefore the adapted representations from the early processing areas are further modified by a second stage of adaptation. The net effect could either enhance or compensate for the effects of adaptation in the earlier regions.

In the visual system, considered as a whole, there is strong evidence for both scenarios. For instance, both inherited effects and intrinsic adaptation patterns are known to occur in the peripheral visual system. In the retina, adaptation to mean luminance is an intrinsic property, and not present in the retinal-recipient cells of the lateral geniculate nucleus (LGN) of the thalamus (Shapley and Enroth-Cugell, 1984). On the other hand, adaptation to contrast takes place initially in the retina (Shapley and Victor, 1978), and then again in the LGN(Solomon et al., 2004), and then additionally in cortical area V1(Reich et al., 2001). However the rules of adaptation within the cortical hierarchy are relatively unknown.

To test the hypotheses concerning the roles of adaptation in altering responses in the sensory hierarchy, we chose to compare adaptation in V1 to adaptation in V2. V2 receives bulk of its inputs from area V1, and is selective for complex features like textures and illusory contours, which are not salient to V1 (Burkhalter and Van Essen, 1986). According to the classical hierarchical view, higher extra-striate areas like V2 integrate inputs from V1 to encode these complex features of the visual input (Van Essen and Maunsell, 1983). Despite the differences in selectivities across regions for complex features, the responses of V2 neurons to oriented gratings are largely similar to the responses of neurons in V1 (Crowder et al., 2006). Thus by directly comparing the effects of adaptation on grating responses in V1 and V2, we will assess whether adaptation is simply inherited from its upstream source V1, or alternatively that further adaptation occurs in V2. If there is no intrinsic adaptation in V2, then adaptation-induced changes in tuning curves in V2 will mirror those in V1. However we found that certain aspects of adaptation, specifically attractive tuning shifts, are more prominent in V2 than in V1, indicating intrinsic adaptation in V2 that builds on the adaptive changes initiated in V1.

METHODS

The experimental procedures used in this chapter are idential to those used in Chapter 5; the only difference is that we analyze the parallel recordings in V2. In this analysis, from 3 animals and 16 sites, a total of 12 units in V1 passed the selection criteria for both brief and prolonged adaptation paradigms; 52 were only analyzed for the brief paradigm, and 31 for the prolonged paradigm.

RESULTS

To compare the effects of adaptation in V2 with the effects observed in V1 (Chapter 5), we examine the results from V2 obtained with these paradigms. Figure 6.1 shows example E and I cells after brief (Figure 6.1 A, B, D, E) and prolonged adaptation (Fig 6.1 E and F). The range of behavior is generally similar to what is seen in V1 (Fig 5.1). Notably, both attractive and repulsive shifts are present in E and I cells (Fig 6.2 A and C). The dependence of the direction of shifts on the relationship to the adapter is similar in V1 and V2. (Fig 6.3).

However, there are substantial quantitative differences in the nature of peak shifts seen in V2, compared to V1. The magnitude of peak shifts are larger in V2 than in V1 (medians: 31^0 in V2, 21^0 in V1, KS $p = 0.004$, Wilcoxon $p < 0.001$). In V2, the direction of peak shift is strongly biased towards the adapter, while in V1, there is a small bias away from the adapter (median: 11^0 of attraction in V2, 1^0 of repulsion in V1, KS $p = 0.02$, WRS $p = 0.09$). Along with the overall bias towards attraction, the magnitude of attractive shifts is larger in V2 than in V1 (median: 33^0 in V2, 21^0 in V1, KS $p = 0.04$ WRS $p = 0.005$). But even in the cells that show repulsive shifts, the magnitude of peak shifts is larger in V2, than in V1 (medians: 28^0 in V2, 20^0 in V1, KS $p = 0.05$, WRS $p = 0.01$).

The difference between V2 and V1 is greatest when the adapting orientation was nearly orthogonal to the preferred orientation. Specifically, when the adapting orientation was at least 60^0 away from the preferred orientation, the median behavior was a 38^0 attractive shift in V2, but only a 5^0 shift in V1 (KS $p = 0.03$, Wilcoxon $p = 0.02$.)

As in V1, some cells increased their firing rates with adaptation as well as some that decreased. For prolonged adaptation, these firing rate increases were correlated with attractive tuning shifts in V1 inhibitory neurons, suggesting a disinhibitory process. The same relationship is present in V2.

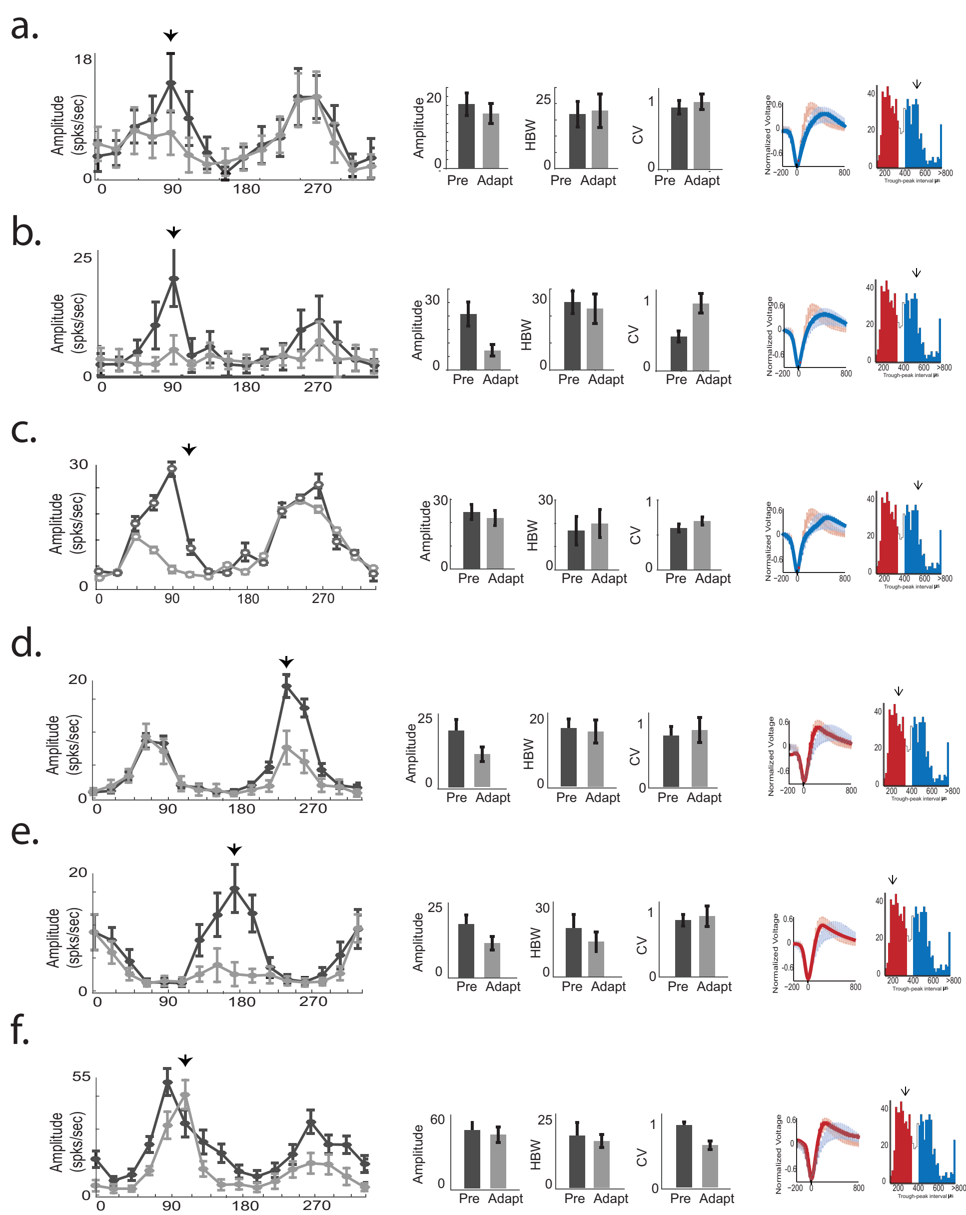

Figure 6.1 Adaptation-induced peak shifts and bandwidth changes :Example units Each row shows: tuning curve under baseline conditions (black) and following adaptations (gray) to selected orientations (black arrows), three tuning parameters (von Mises amplitude parameter, the half bandwidth(HBW), and circular variance (CV)), and the extraceullular waveshape and peak width, overlaid on the laboratory database. Error bars indicate 95% confidence limits for tuning curves and indices.

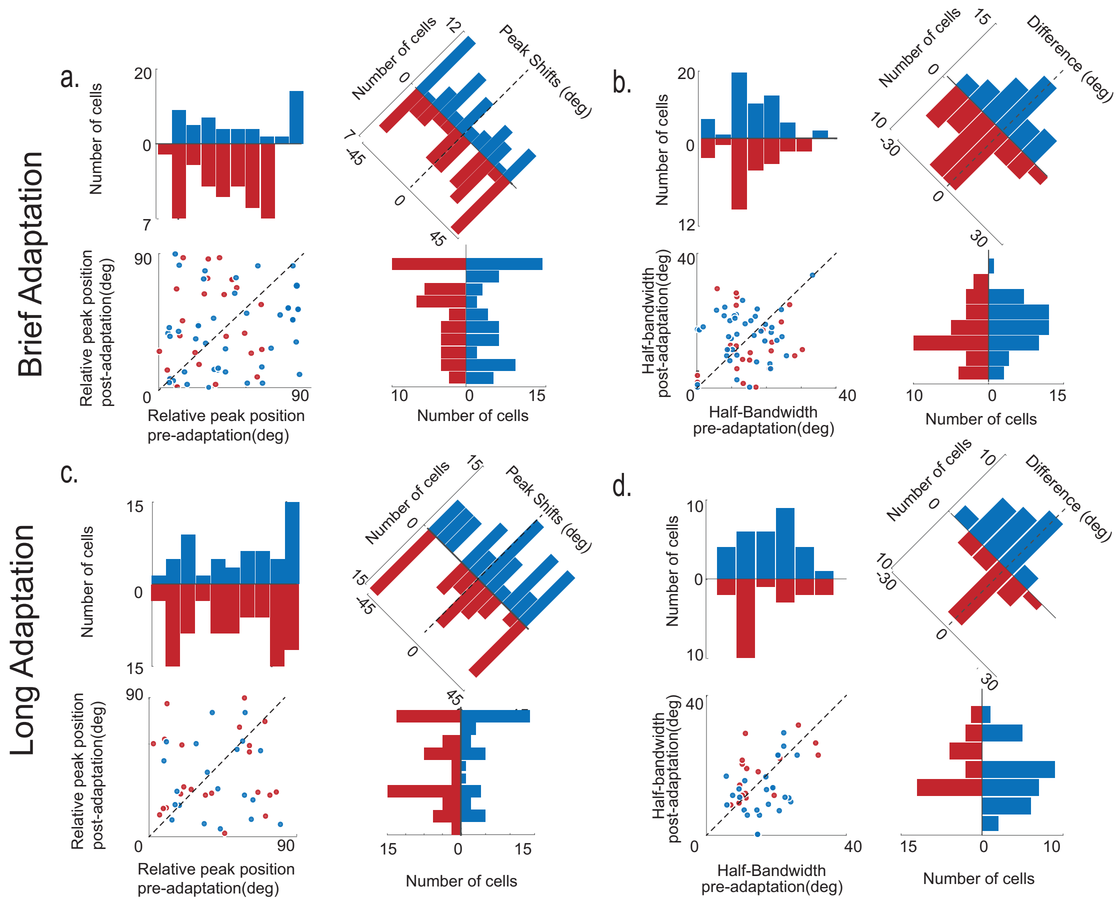

Figure 6.2 Population summary of adaptive changes of tuned E and I cells in V2 Tuning curves are summarized by two parameters: orientation preference relative to the adapter, and bandwidth. Blue indicates E cells, red indicates I cells. Within each panel, the scattergram shows the joint distribution of a parameter before and after adaptation; its projections onto the coordinate axes show the parameter's value before and after adaptation, and its projection onto the oblique axis shows the adaptation-induced change. For the scattergrams of peak shifts, points above the diagonal indicate repulsive shifts; points below the diagonal indicate attractive shifts. For the scattergrams of tuning widths, points above the diagonal indicate broadening; points below the diagonal indicate narrowing.

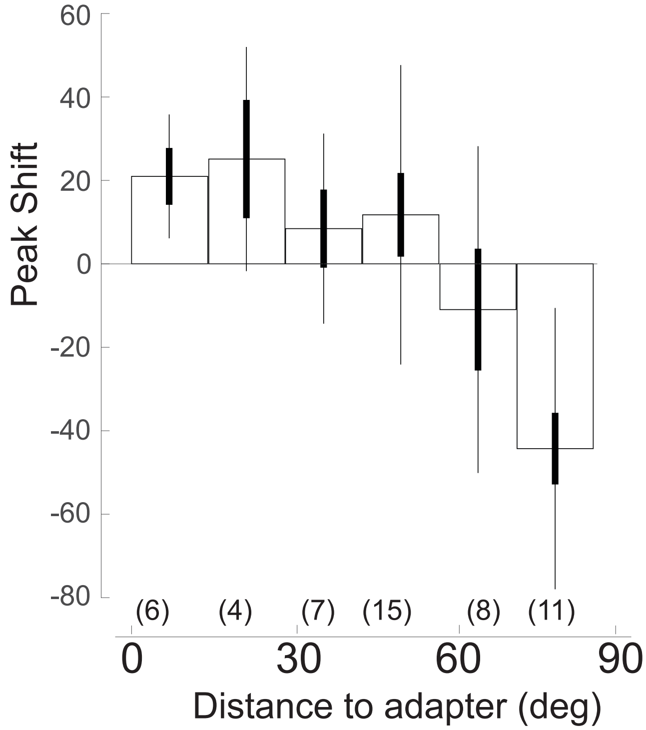

Figure 6.3 Shifts in orientation tuning as a function of distance of the adapting orientation to the preferred orientation. Population tuning shifts as a function of distance between adapter and preferred orientation. Bar heights indicate population average, heavy line indicates 1 SEM, and thin line indicates 1 SD. Repulsive shifts dominate near the adapter, and attractive shifts dominate orthogonal to the adapter, especially in V2.

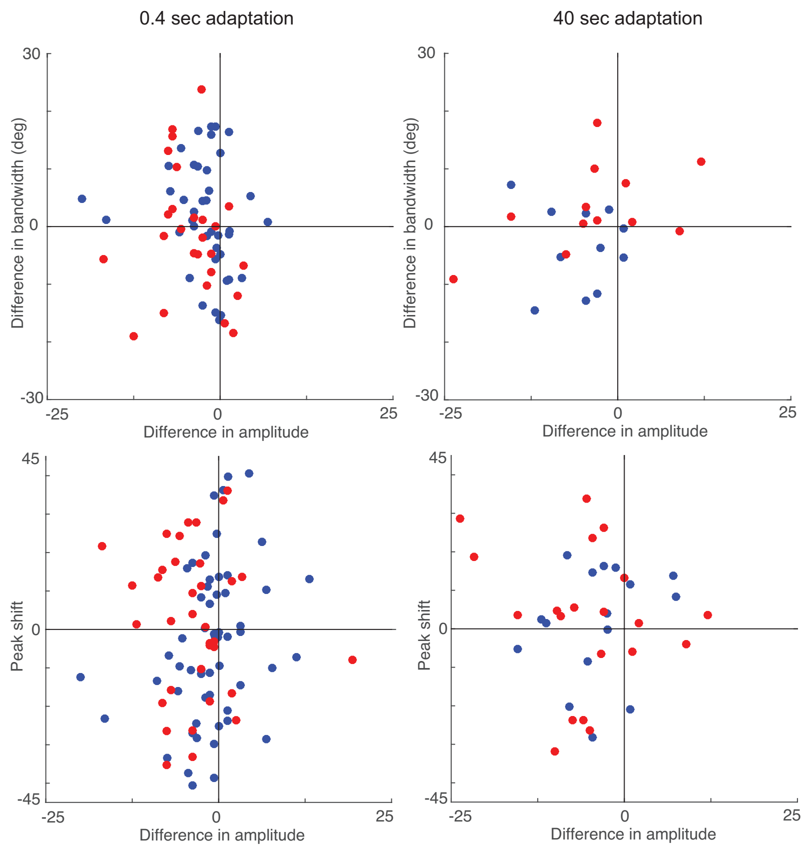

Figure 6.4 Joint distribution of adaptation-induced amplitude changes to peak shifts and bandwidth changes. Adaptation-induced tuning shifts are correlated with amplitude changes in the inhibitory cells during prolonged adaptation (See Table 6.1)

Table 6.1 Correlation of amplitude changes to peak shifts and bandwidth changes in V2. r: Pearson's correlation is noted for both brief and prolonged adaptation. * p<0.05; ** p<0.005

	Brief	Prolonged
Excitatory Cells		
Peak shifts and Amplitude Changes (r)	0.1923	0.0006
Bandwidth Changes and Amplitude Changes (r)	–0.1067	0.1136
Inhibitory Cells		
Peak shifts and Amplitude Changes (r)	-0.1247	-0.5062*
Bandwidth Changes and Amplitude Changes (r)	–0.1603	0.3327
All Cells		
Peak shifts and Amplitude Changes (r)	0.0485	0.0127*
Bandwidth Changes and Amplitude Changes (r)	–0.1049	0.2283

Discussion

Our results show that adaptation in area V2 leads to larger adaptation-induced shifts in orientation preference than in area V1. Moreover, V2 has an overall bias towards the attractive direction, and this bias is driven by the neurons whose preferred orientation is far from the adapter (Figure 6.3). These findings likely reflect local processing within V2, and imply effects of adaptation beyond those inherited from V1.

A sensory system could adapt by modifying the transformations it carries out at each processing stage (Shapley et al., 2003), or alternatively it could adapt early in the processing stream and this adapted representation could be passed on to further downstream regions, whose intrinsic computations do not change. Our findings reveal that for orientation, the visual system uses the first approach. Specifically, orientation adaptation in V2 involves intrinsic changes as well as effects inherited from upstream sources, i.e. V1. This is unlike luminance adaptation, for instance, which occurs largely in the retina (Enroth-Cugell et al, 1973).

Perceptual correlates

Perceptual aftereffects are widely considered to be a functional consequence of adaptation, and this study provides further links. The consensus of many studies is that in V1, repulsive shifts dominate for neurons whose preferred orientation is near the adapter, and this correlates with repulsive orientation aftereffects. However, the effects of adaptation on neurons whose tuning is far from the preferred orientation have received much less attention, even though such neurons predominate in the cortical population under natural viewing.

Because of the multiple tetrode recording approach, our population included many cells whose orientation preferences covered the gamut of distances from the adapter. We found that the balance shifted from repulsive shifts to attractive shifts as the distance between the adapter and the preferred orientation increased, with V1 and V2 both showing predominantly attractive shifts for orthogonal orientations. This likely corresponds to the “indirect aftereffect”, namely the attractive perceptual aftereffect for probe stimuli orthogonal to the adapter (Gibson and Radner, 1937), (Wenderoth and Johnstone, 1988b). Wenderoth and Johnstone (1988) investigated the indirect aftereffect in detail, and found that it was distinguished from the “direct aftereffect” in that the former occurred over a wider extent of the visual field. Based on this they postulated that the indirect aftereffect likely reflected adaptation in extrastriate cortex. Our data supports this notion : the balance of shifts that move from repulsive to attractive as the distance between the adapter and the preferred orientation increased, were significantly larger in V2 than in V1.

However there are caveats in assuming a simple correspondence between neurophysiology and perception, i.e. repulsive shifts in tuning correspond to repulsive perceptual aftereffects. Theoretical analyses indicate that such a simple relationship may not always hold: gain changes and bandwidth changes -- which are both seen in our data -- , as well as peak shifts may be relevant to decoding (Seriès et al., 2009). For example, in a study of direction selectivity in MT, mild attractive shifts were present but gain changes dominated, and modeling showed that repulsive aftereffects may result (Kohn and Movshon, 2004a). A corollary is that the magnitude of physiological findings in macaque cannot be directly linked to the magnitude of perceived shifts seen in perceptual studies in humans ((Clifford et al., 2001b),(O'Toole and Wenderoth, 1977b)). Thus, while caution is necessary in drawing a direct connection between psychophysical studies and our findings of attractive adaptation effects and their greater prominence in V2, our data clearly show that there are effects of adaptation on processing in V2 that go beyond effects inherited from V1.

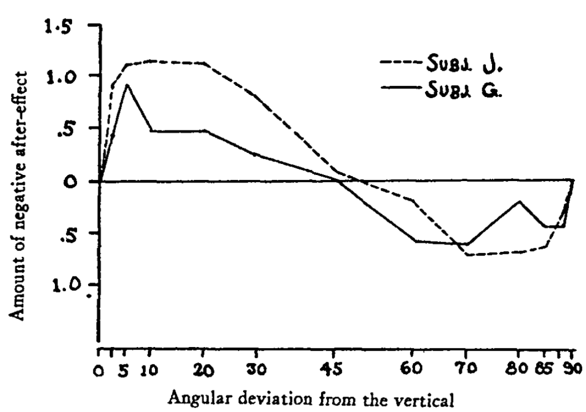

Figure 6.5 Reproduced figure from Gibson and Radner 1937. Negative after-effect in degrees on the vertical axis as a function of the objective deviation from that axis of the inspected line. Points above the abscissa indicate a shift of the subjective vertical towards the inspected line (Direct After-effect); points below indicate a shift in the opposite direction (Indirect After-effect).

CHAPTER 7

MODELING ADAPTATION EFFECTS ON ORIENTATION TUNING

The goal of modeling in this thesis is to determine the characteristics of cortical circuitry needed to account for the effects of adaptation on the orientation tuning of cortical neurons observed in visual areas V1 and V2. The main features that we will focus on are: the presence, magnitude and diversity of attractive and repulsive tuning shifts observed in the data. A critical aspect of this diversity that we intend to account for is the differences across V1 and V2 population in the nature and size of their adaptation-induced tuning shifts.

In order to simulate the effects of adaptation, we begin with established classes of models for cortical selectivity. In broad terms, models of orientation selectivity fall into 2 categories: models that include cortical sharpening by tuned inhibition, and models that do not consider inhibition to contribute to the tuning (Harris and Mrsic-Flogel, 2013; Sompolinsky and Shapley, 1997b) . This distinction can be formalized by the structure of the model’s connectivity rules between the excitatory and inhibitory cells. We consider both these categories in our model framework.

Although these two kinds of orientation tuning models are fairly mature, their behavior in the context of adaptation has not yet been considered. Nevertheless, they serve as a useful starting point. To each kind of model, we will add one parameter to describe adaptation, and track how it influences the behavior of model cells.

To include adaptation in either orientation tuning models, we considered two possibilities for its locus ie, whether adaptation acts solely at the post-synaptic level, or if it acts at the pre-synaptic level. For post-synaptic adaptation, we reduce the effective connectivity of two neurons based on the firing of the output neuron. This form of adaptation can result in gain changes in proportion to their sensitivity to the stimulus or to particular range within their selectivity. Yet the tuning preferences of the cells are not expected to be altered.

Because tuning shifts are a prominent feature of the data, we also considered the possibility that adaptation acts at the pre-synaptic level. To simulate pre-synaptic adaptation, we reduce the effective connectivity based on the firing of the input neuron. In this scenario, the simulated reduction in responsiveness can shift the value of the encoded stimulus parameters away from those to which the system had been exposed. If only excitatory inputs contribute to tuning, only repulsive shifts should be observed, but if inhibitory inputs contribute as well, attractive shifts may result.

For building the models, we chose to represent neuronal activity as a rate, and, at the model output, we convert this rate to a Poisson firing pattern. Clearly this choice makes many simplifications: for example, we forgo a more realistic model of neuronal dynamics (e.g., an integrate-and-fire neuron, a Hodgkin-Huxley neuron, or even a neuron with compartments and channels). Note, though recent work has suggested that the model simulations that included multiple layers of neurons show similar results to model simulations that included a single layer of neurons with more parameters for biophysical compartments and ionic membrane potentials (Yamins et al, 2016).

We also simplify at the level of network architecture: we primarily consider only two levels of neurons (an input population and an output population), rather than the full multilayered structure of cortex. We also only consider a feedforward architecture, although extending the model to a third level (and thus approximating the effects of feedback) yields essentially the same behavior. Finally, this model is agnostic to how orientation tuning emerges in the cortex, although this has been an area of great interest: whether this arises primarily via the pattern of thalamocortical activity or intracortical connections. Here we simply assume that the inputs come from thalamic inputs, and there are intracortical connections. Overall, while there are many ways that the model could be made more realistic, we leave them for future work, as they do not appear necessary to address the key questions of interest, and would add a large number of free parameters and computational complexity.

METHOD

Orientation Tuning Function

For the input population (Population 1), orientation tuning was modeled by von Mises functions, with parameters drawn from the data (see above). Specifically, the firing rate of neuron j in response to a grating at orientation φ_{stim} is given by

$$R_{input}(\varphi_{stim}, j) = B_j + M_j e^{\beta_j \cos(2(\varphi_{stim} - \mu_j)) - 1)}. \qquad \text{Eq.1}$$

The firing rate B_j, amplitude M_j, and concentration parameter β_j are drawn from a randomly-selected neuron in the dataset, and the preferred orientation μ_j is chosen uniformly across all orientations.

Responses of neurons in the output population were modeled as a weighted sum of responses in the input population,

$$R_{output}(\varphi_{stim}, k) = \sum_{j \in input} C(j,k) A(j,k) R_{input}(\varphi_{stim}, j), \qquad \text{Eq. 2}$$

where $C(j,k)$ is determined by the connectivity rule and $A(j,k)$ is determined by the adaptation state and site.

Connectivity rules

In the model, excitatory connections are strongest among the cells with the same preferred orientation, and they drop off with increasing difference between the preferred orientations of the cells. In accordance with the observed range of tuning bandwidths for both excitatory and inhibitory cell types in collected data, laboratory database and the and the evidence in the literature, we allowed a wide range of selectivity for both these cell categories in our models

To determine the excitatory inputs to neuron k, we first randomly choose its preferred orientation, μ_k. The probability that neuron j in Population 1 is connected to this neuron is then given by:

$$P_E(j,k) \propto e^{-(\mu_j-\mu_k)^2/2\sigma_E{}^2}, \qquad \text{Eq. 3}$$

where σ_E denotes the width of the connectivity rule (here, 22.5^0, see Table 7.1), and the proportionality constant is chosen so that, on average, there are 750 excitatory connections. The connectivity coefficient $C(j,k)$ is then set to 1 with probability $P_E(j,k)$, and 0 otherwise. Thus the excitatory connections in the model are strongest among the cells with the same preferred orientation, and they drop off with increasing difference between the preferred orientations of the cells.

As the nature of inhibitory connectivity is debated (,(Bonds, 1989),(Somers et al., 1995b),(Sompolinsky and Shapley, 1997a), (Phillips and Hasenstaub, 2016)) , we built two kinds of models that consider the two varieties: one with untuned inhibition and one with tuned inhibition. For untuned inhibition, a random subset of, on average, 250 Population 1 neurons were chosen to be connected to output neuron k, and for these neurons, $C(j,k)$=-1. For tuned inhibition, we specified the connection probability as

$$P_{I_{tuned}}(j,k) = \frac{1}{K}\left(e^{-(\mu_j-(\mu_k-\sigma_I/2))^2/2\sigma_I^2} + e^{-(\mu_j-(\mu_k+\sigma_I/2))^2/2\sigma_I^2}\right), \qquad \text{Eq. 4}$$

where $\mu_k \pm \sigma_I/2$ are the peaks of side-lobes, where inhibitory inputs are maximal. To keep the number of free parameters small, we set $\sigma_I = \sigma_E$. The connectivity coefficient $C(j,k)$ was set to -1 with probability $P_{I_{tuned}}(j,k)$, and 0 otherwise.

Post- and pre-synaptic adaptation

To model post-synaptic adaptation, we reduced the connection strength of all inputs by a factor A_{adapt}= $\alpha\left(\frac{r_k - r_{k_{min}}}{r_{k_{max}} - r_{k_{min}}}\right)$, where r_k denotes the unadapted response at the adapting orientation, $r_{k_{max}}$ is the peak unadapted response, and $r_{k_{min}}$ is the minimum unadapted response. α is the adaptation strength; a value of α = 1 leads to complete attenuation of the response when the adapting orientation is the preferred orientation, while α = 0 corresponds to no adaptation. Membrane hyperpolarization is a likely contributor to this mechanism of adaptation, which can be activated by both brief and prolonged adapting stimuli, in both excitatory and inhibitory neurons.

To model presynaptic adaptation, we reduced the strength of individual inputs by the above factor Aadapt, but calculated and applied it separately for each input. Since this form of adaptation is input-specific, synaptic depression may underlie it. Assuming (as we find) that inhibitory neurons adapt, the modeled effects of adaptation depend on whether or not the inhibitory inputs are tuned. In the untuned case (Figure 7.1, row 3), adaptation can lead to bandwidth narrowing. Off-axis adaptation can lead to tuning shifts, they are predicted to always be repulsive (i.e., away from the adapting orientation). So, presynaptic adaptation, along with untuned inhibition, can account for the findings that neurons demonstrate repulsive shifts when adapted at nonpreferred stimuli. However, presynaptic adaptation in the tuned inhibition model (Figure 7.1 row 4) can account for the attractive shifts

In all of the above mentioned model classes, adaptation was captured by the coefficient $A(j,k)$. In the unadapted state, $A(j,k)$=1; in the adapted state, it depended either on the pre- or the post-synaptic neuron, depending on the site of adaptation that was being modeled:

$$A(j,k) = 1 \textit{ before adaptation}$$
$$A(j,k) = f(\varphi_{adapt}, j) \textit{ for pre-synaptic adaptation}$$
$$A(j,k) = f(\varphi_{adapt}, k) \textit{ for post-synaptic adaptation}$$

The adaptation function f was based on a comparison between the neuron's response to the adapting orientation, and its response range:

$$f(\varphi_{adapt}, j) = 1 - \alpha\left(\frac{R(\varphi_{adapt}, j) - R_{min}(j)}{R_{max}(j) - R_{min}(j)}\right) \qquad \text{Eq. 6}$$

Where $R_{min}(j)$ indicates the minimal unadapted response of neuron j, $R_{max}(j)$ indicates its maximal unadapted response, and $R(\varphi_{adapt})$ indicates its response at the adapting orientation. The adaptation strength is determined by model parameter α : α = 1 yields complete attenuation of the response when the adapting orientation is the preferred orientation, while α = 0 corresponds to no adaptation.

RESULTS

To determine aspects of cortical circuitry that are necessary to account for our findings, we constructed simple models of orientation adaptation based on variants of the ring model framework ((McLaughlin et al., 2000b)). The model classes we considered are distinguished by the locus of adaptation (i.e. post-synaptic vs pre-synaptic) and the connectivity rules (i.e., untuned vs tuned inhibition). Thus we considered four model classes: 1) post-synaptic adaptation with untuned inhibition (Fig 7.1 row 1); 2) post-synaptic adaptation with tuned inhibition (Fig 7.1 row 2); 3) pre-synaptic adaptation with untuned inhibition (Fig 7.1 row 3); and 4) pre-synaptic adaptation with tuned inhibition (Fig 7.1 row 4).

From a qualitative perspective, we anticipate that only the fourth model class can produce attractive shifts, a prominent aspect of our findings. (Fig 7.1 row 4) The logic is as follows: any change in the orientation bandwidth or peak preference can only result from the adaptation of a neuron's inputs, so model classes 1 and 2 cannot account for those effects as only their outputs are influenced by adaptation. With regard to the presynaptic model classes (3 and 4), adaptation in model class 3 acts to reduce excitatory drive near the adapting orientation, leading to repulsive shifts. However, tuned disinhibition can occur in model class 4, leading to attractive shifts.

To test the above predictions and consistency with neuroanatomic parameters, we formulated the above models using physiological parameters drawn from our data (the tuning curves) and the literature at large (other parameters of Table 7.1 and 7.2). Each model consisted of two populations: an input population with fixed tuning (Population 1), connected to an output population (Population 2) via connections whose strengths could adapt. Neurons were considered to have Poisson firing rates, and their inputs combined by simple summation (See Methods). We present the results of simulations using the parameters of Table 7.1 below. We also varied the key model parameters (number of inputs, E/I ratio, adaptation strength, connectivity rule) over a wide range, and present the results of these simulations. (Table 7.2) Unless otherwise noted, these yielded similar results.

As expected (Figure 7.1), simulations of the post-synaptic models show minimal changes in orientation tuning, both in terms of preferred orientation and bandwidth. (Model classes 1 and 2). Presynaptic adaptation with untuned inhibition leads to changes in bandwidth comparable to what we observe, but only repulsive shifts in tuning (Model 3). Only model class 4 (presynaptic adaptation with tuned inhibition) leads to a mixture of repulsive and attractive shifts, along with changes in tuning bandwidth.

ACCOUNTING FOR THE DIVERSITY OF ADAPTATION EFFECTS

Although this was not a primary goal of the modeling, we found that the model accounted for the observed diversity, ie, the diversity of effects of adaptation of neurons within each model was comparable to what we observed experimentally (Figure 5.2 in V1; Figure 6.2 in V2). This holds for most of the parameter ranges tested, but not for some extreme values (Figure 7.4 – Figure 7.8).

Importantly, the dependence of the adapter to the preferred orientation observed in V1 and V2 were captured by the model (Figure 7.2). Notably, the larger effect sizes seen in V2 compared to V1 could be captured by increasing the fraction of inhibitory neurons from 0.2 to 0.35 and increasing the orientation range for inhibitory connectivity from 15^0 to 40^0. (Figure 7.2D). We speculate how modulating the E/I balance could cause such effects below.

Table 7-1 Model parameters

			Percentiles		
	Symbol	**Mean**	**25^{th}**	**50^{th}**	**75^{th}**
Excitatory Input Neurons					
Half-Bandwidth (deg)	n/a	26.3	20.5	24.5	50.2
Concentration	β_j	1.9	2.6	2.4	0.5
Peak Firing Rate (s^{-1})	M_j	11.5	6.2	8.2	29.2
Baseline Firing Rate (s^{-1})	B_j	9.5	3.2	9.5	12.2
Inhibitory Input Neurons					
Half-Bandwidth (deg)	n/a	32.3	18.6	35.5	60.2
Concentration	β_j	1.1	2.8	0.8	0.2
Peak Firing Rate (s^{-1})	M_j	12.2	8.4	14.2	35.8
Baseline Firing Rate (s^{-1})	B_j	12.4	7.6	8.5	12.5

Table 7-2 Network parameters

			Range Explored	
Network Parameters		**Typical**	**Min**	**Max**
Average number of inputs	n/a	1000	100	10,000
Fraction of inhibitory inputs	n/a	0.2	0.1	0.4
Connectivity Rule width (deg)	σ	20	5	60
Adaptation strength	α	0.9	0.2	1

ACCOUNTING FOR CORRELATION OF CHANGES IN TUNING PARAMETERS

Another noteworthy finding was the correlation between the response amplitude and the peak shifts in the inhibitory celltypes during prolonged adaptation. While our model as mentioned earlier does not include dynamics or distinguish cell-types, we asked if these paradoxical effects are accounted by this model architecture. When considered as a whole, we indeed find a similar correlation between the response peak and the direction of the tuning shift in the model population. This effect was most prominent when the E/I balance of the network was shifted towards more inhibition. (Figure7.3)

To determine the robustness of this conclusion, we examined its behavior over a range of model parameters.

MODEL SIMULATION: INTRACORTICAL INPUTS

Figure 7.4 shows the effect of modifying the number of intracortical inputs from 100 to 10,000. Across this range, our basic finding held: tuned inhibition and presynaptic adaptation are both required to generate attractive shifts. However, when the number of inputs is set at an unphysiologically-low level, the diversity of tuning shifts is less than what was found experimentally.

MODEL SIMULATION: FRACTION OF INHIBITORY INPUTS

Figure 7.5 shows that a similar conclusion holds for the fraction of inhibitory neurons: across a broad range of values for this fraction (10% to

40%), only models with tuned inhibition and presynaptic adaptation produce attractive shifts. For fractions below this range, there is a preponderance of repulsive shifts, inconsistent with the experimental findings.

MODEL SIMULATION: CONNECTIVITY RULE

Figure 7.6 shows that the requirement for both tuned inhibition and presynaptic adaptation also holds across variations in the connectivity rule. In the middle column of the Figure, we replace the standard inhibitory connectivity rule (a sum of Gaussians in relative orientation) with an inverted Gaussian; this provides stronger inhibition from non-preferred directions.

Recurrence - an important aspect of cortical networks (Chariker et al., 2016), is not taken into account by any of these models However, we can gain an understanding of whether inclusion of recurrence would alter our conclusions by adding a third population of neurons that receives its input from the second population described above including a second stage of presynaptic adaptation. In effect, the output of this population shows the behavior of signals that make two loops through a recurrent adapting network: one loop is approximated by the transformation between population 1 and population 2, and the second loop is approximated by the transformation between population 2 and population 3. We implement this feature by adding a third population that receives input from the output population of the standard model. Thus the output of the third population corresponds to signals that make two loops through a recurrent network: one loop is the transformation between population 1 and population 2, and the second loop is the transformation between population 2 and population 3 – output of recurrence. We find that the behavior of population 3 is very similar to that of population 2, indicating that our conclusions are likely to hold even after more loops through this network (Figure 7.6 right column).

Model simulation: adaptation strength

The first three columns of Figure 7.7 show that the model behavior is maintained across a broad range of values of the adaptation strength, from α = 0.2 (first column) to α = 0.9 (third column). As expected, for more extreme values, model behavior changes: for α = 0 there is no adaptation at all (not shown), and for α = 1 (right column), there is near-complete suppression of off-peak responses, so tuning shifts are diminished below the range seen in the data.

Accounting for the difference between V2 and V1

Figure 7.8 column 3 shows how model parameters can be modified to account for the greater prominence of attractive shifts seen in V2. Increasing the amount of inhibitory inputs from 0.2 (the standard value) to 0.35, and broadening the connectivity rule (give new and standard parameter) induces a preponderance of attractive shifts with adaptation. The preponderance of attractive shifts seen in V2 is not found if only one of these parameters are changed: Figure 7.5 shows the effect of just increasing the fraction of inhibitory cells, and the middle column of this figure shows the effect of just broadening the connectivity rule.

In sum, simulations in simplified models of orientation selectivity demonstrate that presynaptic adaptation and tuned inhibitory inputs are necessary to account for the attractive shifts that we observe. Moreover, for physiologically reasonable parameters, models reproduce the range of adaptation effects seen experimentally.

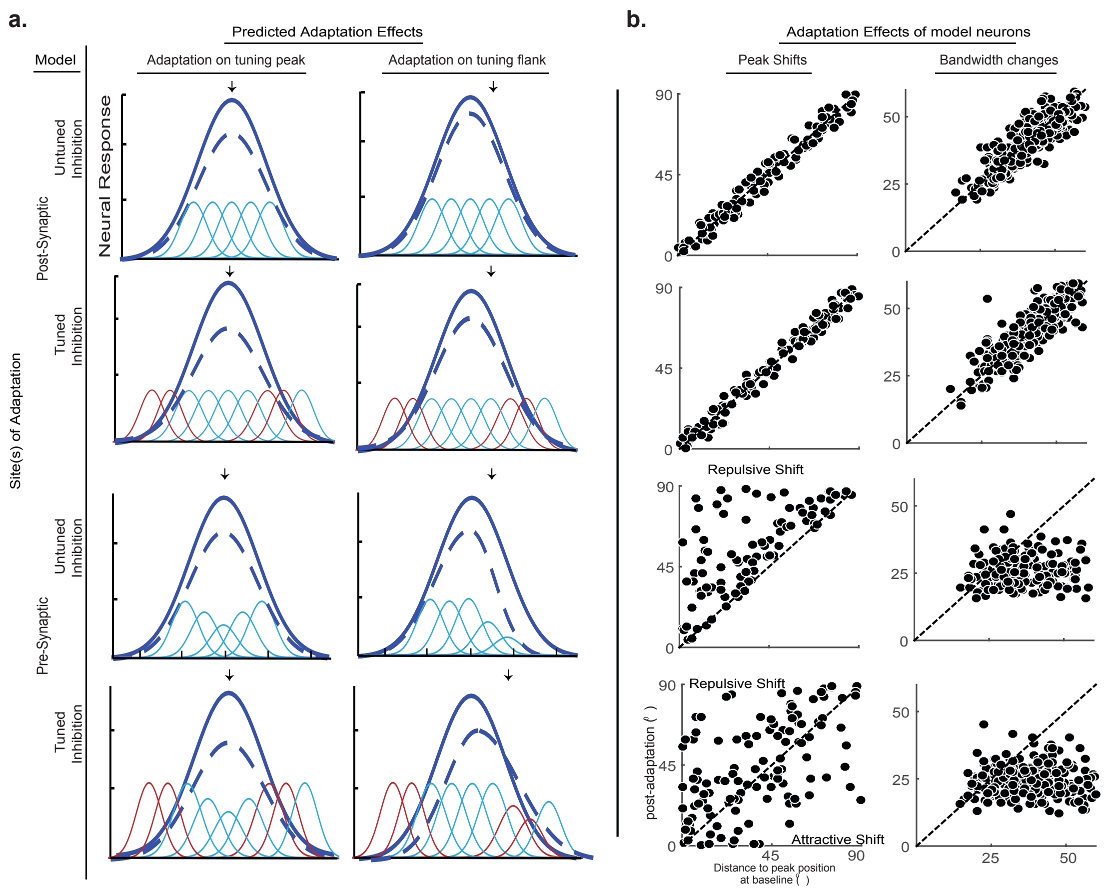

Figure 7.1 Attractive tuning shifts require pre-synaptic adaptation and tuned inhibition. A. Models are distinguished by site of adaptation (postsynaptic, upper two rows; presynaptic, lower two rows) and the nature of inhibitory inputs (untuned are in rows 1 and 3, tuned in rows 2 and 4). The thin lines indicate the tuning curves of input neurons (blue: excitatory, red: inhibitory); the heavy lines indicate the tuning curves of the output neuron (solid curve: baseline, dashed curve: after adaptation). Adapting orientation indicated by arrow. B. Simulation results. Scattergrams plotted as in Figure 5.2. See Methods and Table 1 for detailed description and model parameters. The bottom two scattergrams for ‘peak shift’ and ‘bandwidth change’ bear striking resemblance to scattergrams for the E cells (blue dots) in Figs. 5.2E and 5.2F, respectively.

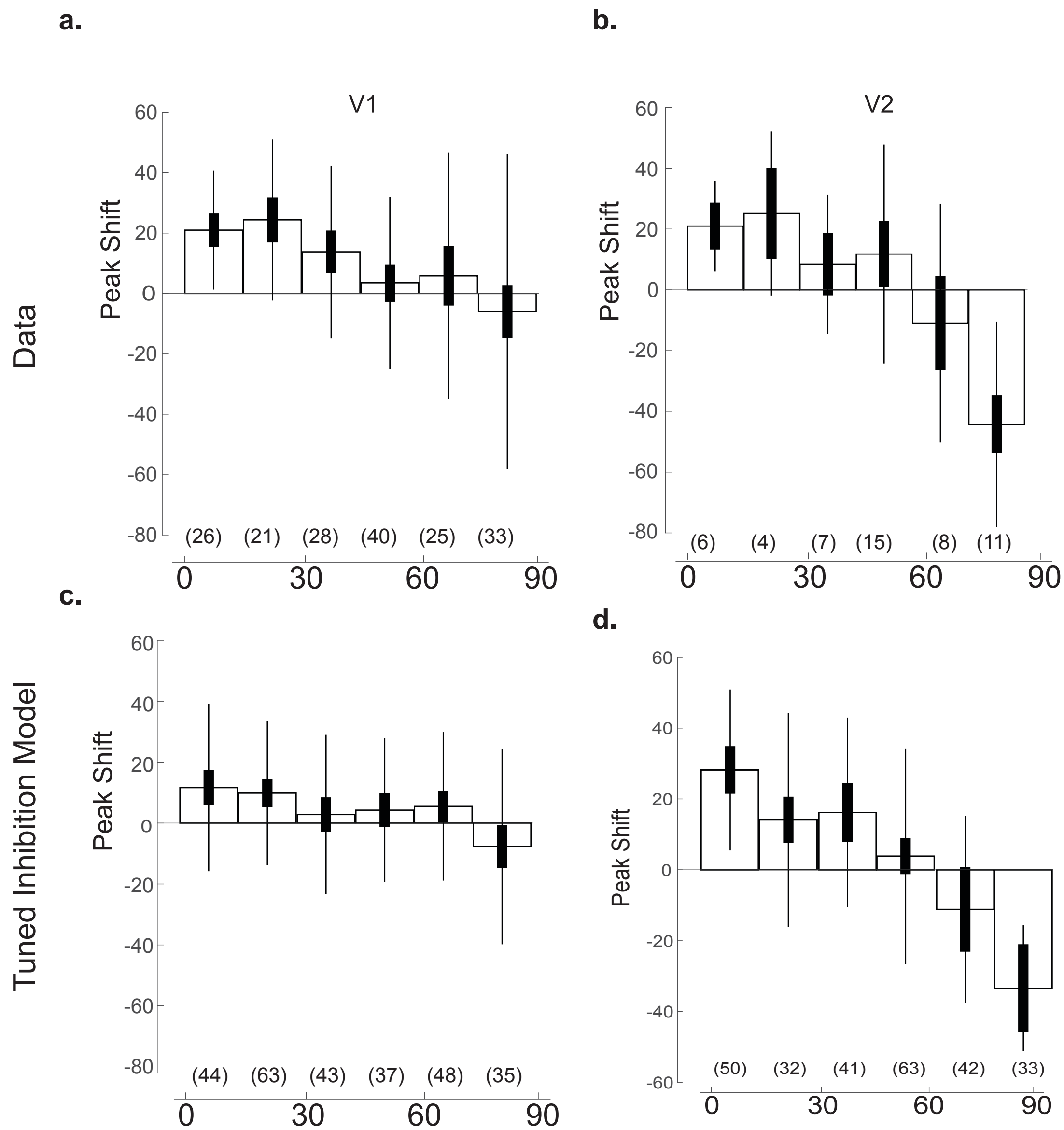

Figure 7.2 Model captures tuning shifts seen in V1 and V2 Repulsive shifts dominate near the adapter, and attractive shifts dominate orthogonal to the adapter, especially in V2.
Population tuning shifts as a function of distance between adapter and preferred orientation. (A): V1, (B): V2, (C): model with presynaptic adaptation and tuned inhibition, see also row 4 of Figure 7.1. Bar heights indicate population average, heavy line indicates 1 SEM, and thin line indicates 1 SD.

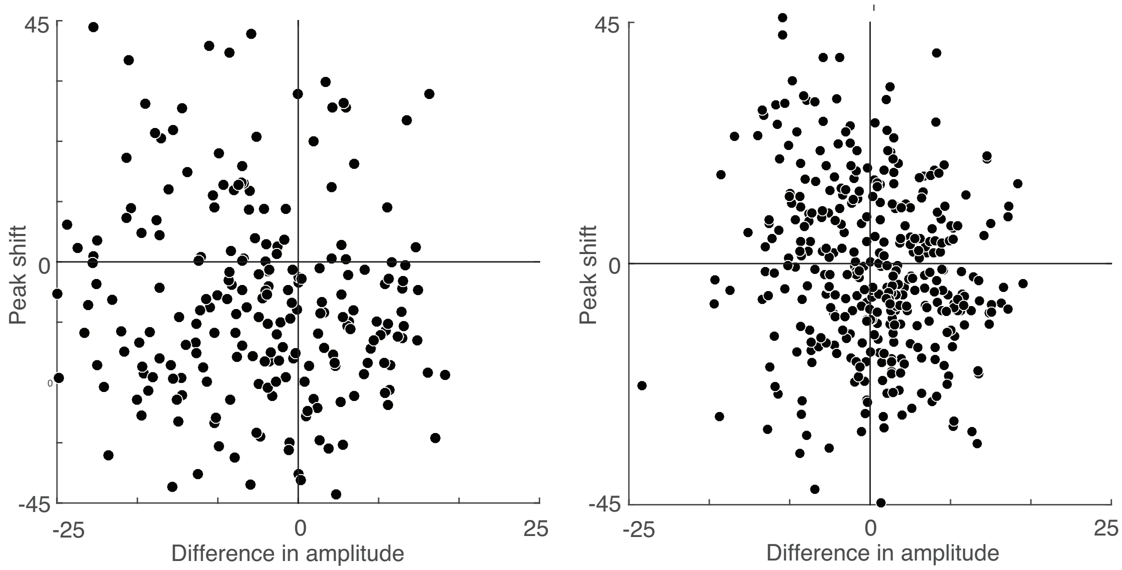

Figure 7.3 Joint distribution of amplitude changes and peak shifts – Peak shifts were correlated to the amplitude changes in the standard model, similar to the effects seen in the inhibitory cells during prolonged adaptation. This negative correlation was stronger in the V2 model ($r = 0.151$, $p<0.005$) in which the net inhibition was larger, than in the standard model ($r = 0.122$, $p<0.05$).

Figure 7.4. Model Simulations: Impact of the number of intracortical inputs

For the four model classes considered in the main text (pre- vs. post- synaptic adaptation, untuned vs. tuned inhibition), we varied the average number of intracortical inputs from 100 (left column) to 10,000 (right column); middle column, reproducing Figure 8 of the main text for comparison, shows the simulations for 1000 inputs. Upper panels show changes in orientation tuning bandwidth; lower panels show changes in preferred orientation relative to the adapter. Other model parameters taken from Table 1.

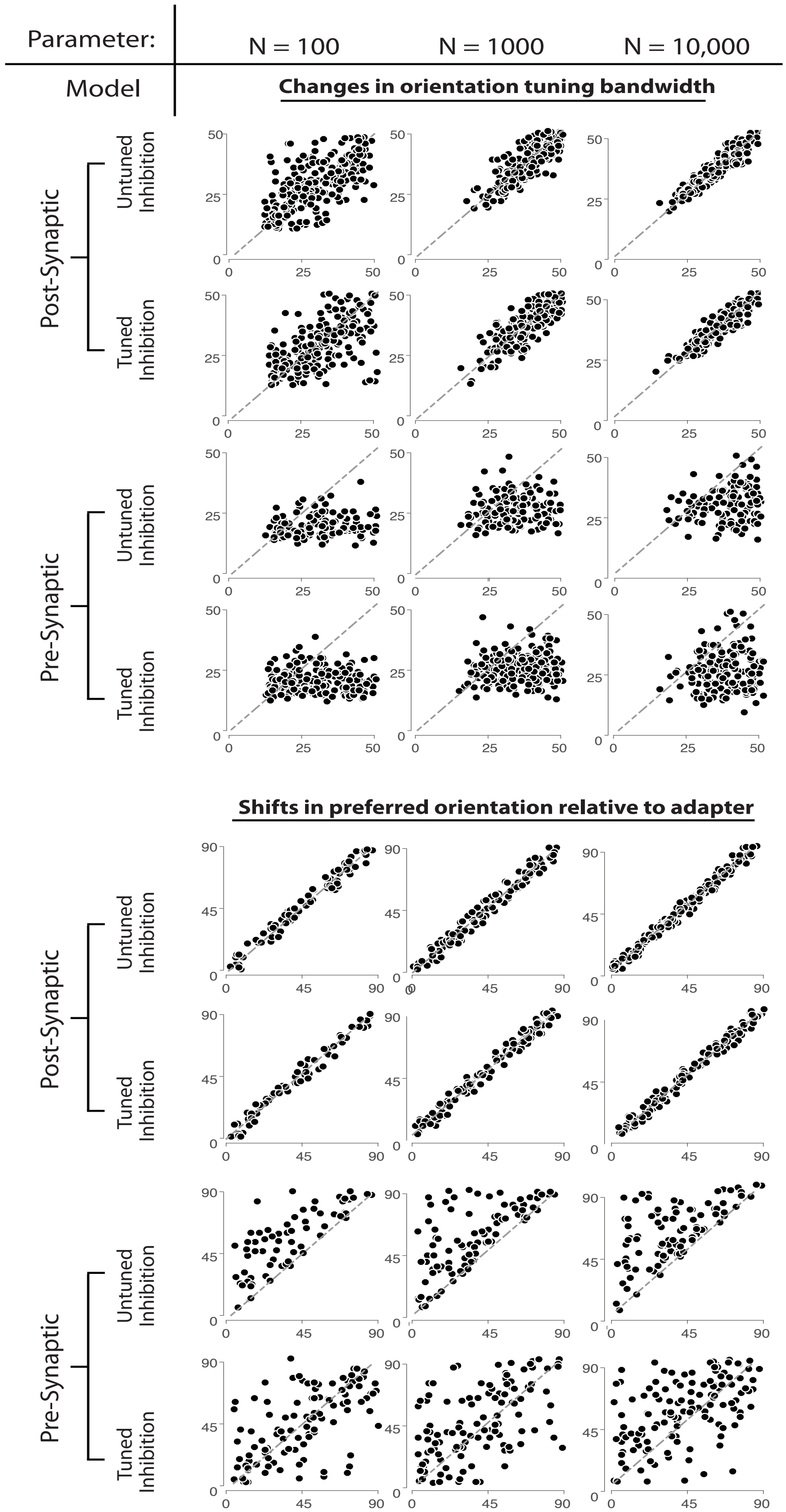
Parameter:
N = 100
N = 1000
N = 10,000
Model
Changes in orientation tuning bandwidth
Post-Synaptic
Untuned Inhibition
Tuned Inhibition
Pre-Synaptic
Untuned Inhibition
Tuned Inhibition
Shifts in preferred orientation relative to adapter
Post-Synaptic
Untuned Inhibition
Tuned Inhibition
Pre-Synaptic
Untuned Inhibition
Tuned Inhibition

Figure 7.5. Model Simulations: Impact of Fraction of Inhibitory Inputs

For the four model classes considered in the main text, we varied the fraction of inhibitory inputs from 10% (left column) to 40% (right column); middle column, reproducing Figure 8 of the main text for comparison, shows the simulations for 20% inhibitory inputs. Other details as in Figure 7.1.

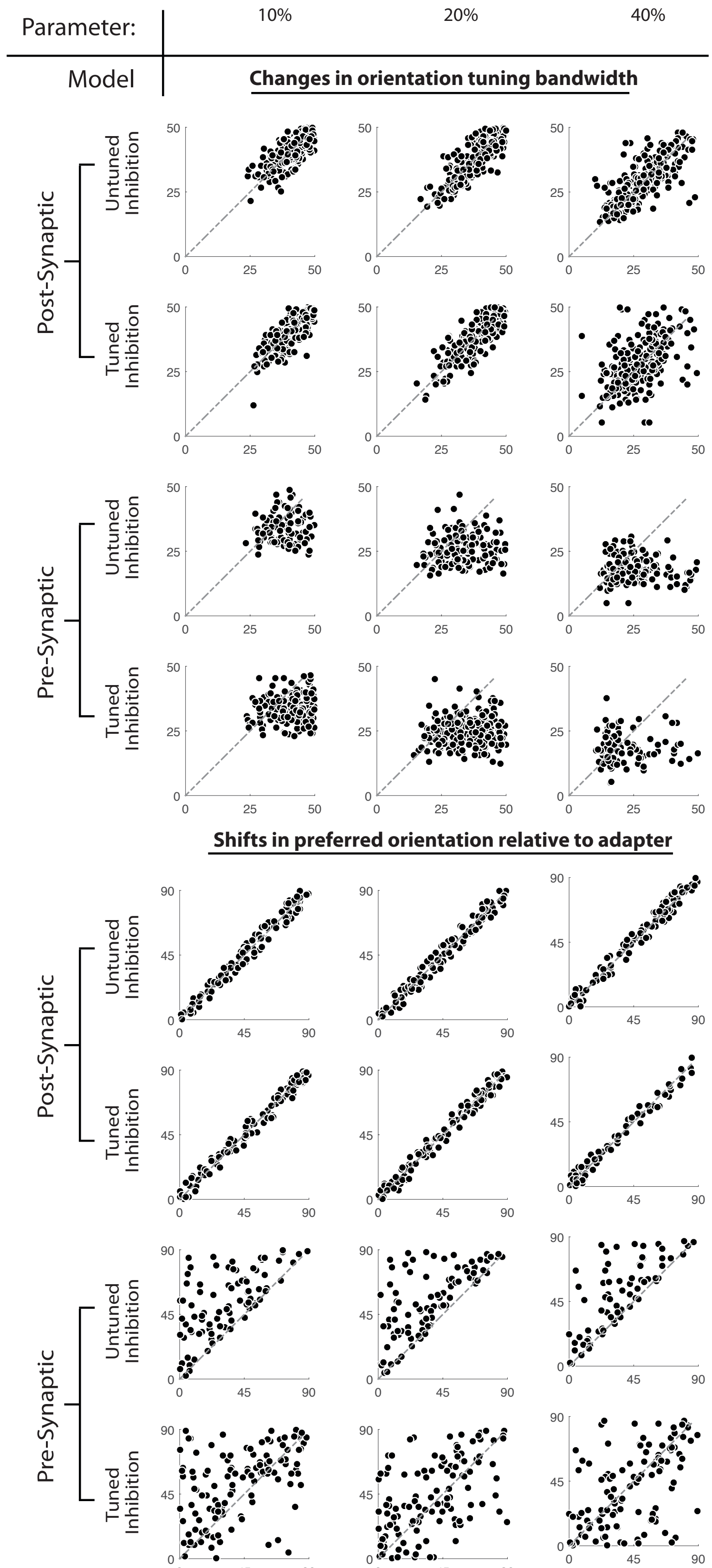
Parameter:
10%
20%
40%
Model
Changes in orientation tuning bandwidth
Post-Synaptic
Untuned Inhibition
Tuned Inhibition
Pre-Synaptic
Untuned Inhibition
Tuned Inhibition
Shifts in preferred orientation relative to adapter
Post-Synaptic
Untuned Inhibition
Tuned Inhibition
Pre-Synaptic
Untuned Inhibition
Tuned Inhibition

Fig 7.6. Model Simulations: Impact of Connectivity Rule

For the four model classes considered in the main text, we varied the connectivity rule two ways. The left column substitutes an inverted-Gaussian inhibitory connection probability for the two-Gaussian inhibitory probability used in the standard model (middle column). The right column considers a third population that receives the output of the standard model's second population (with standard connectivity rule), to approximate the effects of recurrence. The middle column reproduces Figure 7.1 of the main text for comparison. When the connectivity rule is modified, the inhibition parameter is adjusted so that the tuned-inhibition model has a baseline distribution of tuning widths that matches the physiologic data. Other model parameters taken from Table 7.1.

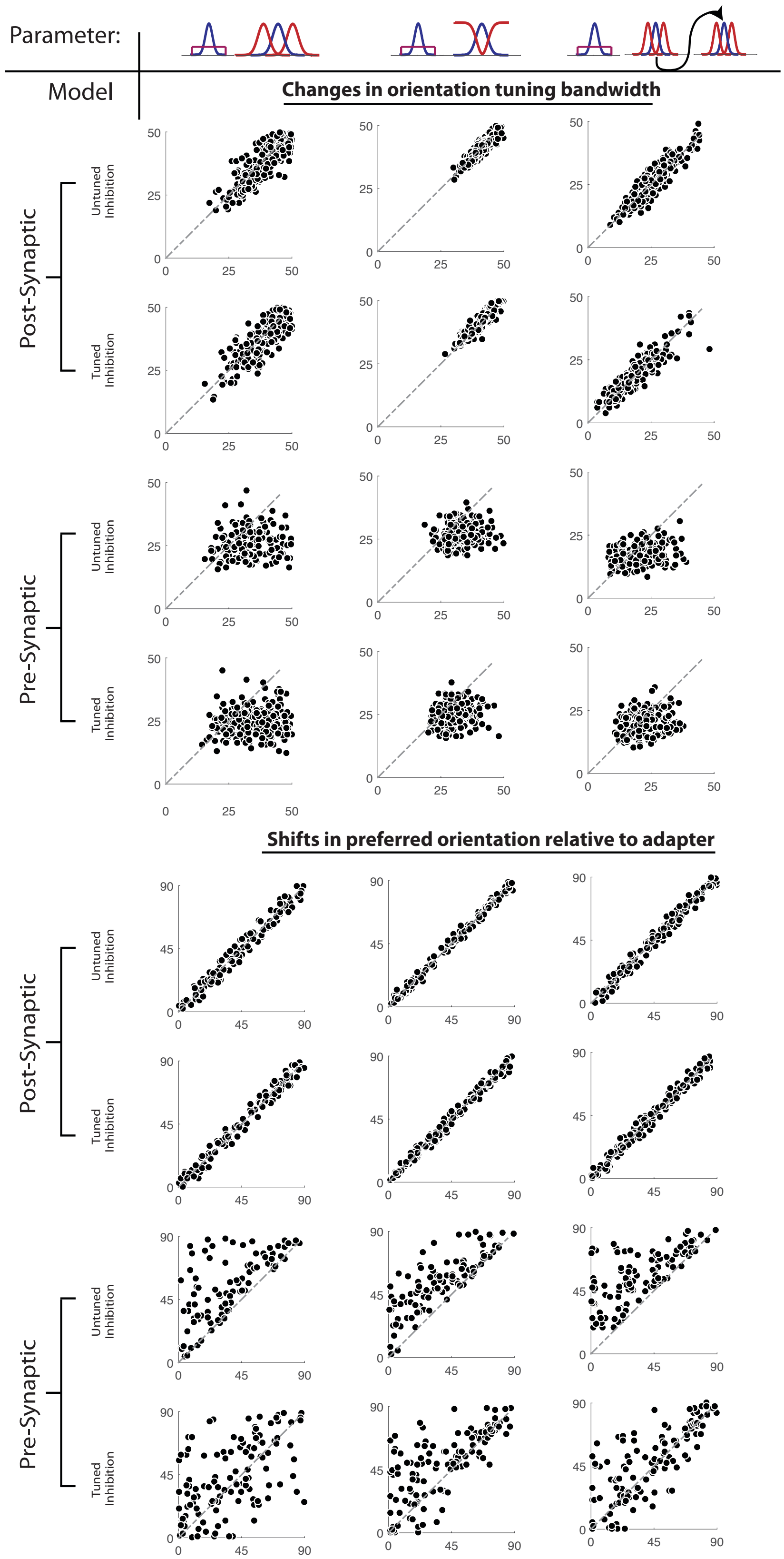
Parameter:
Model
Changes in orientation tuning bandwidth
Post-Synaptic
Untuned Inhibition
Tuned Inhibition
Pre-Synaptic
Untuned Inhibition
Tuned Inhibition
Shifts in preferred orientation relative to adapter
Post-Synaptic
Untuned Inhibition
Tuned Inhibition
Pre-Synaptic
Untuned Inhibition
Tuned Inhibition

Fig 7.7. Model Simulation: Impact of Adaptation Strength

For the four model classes considered in the main text (pre- vs. post- synaptic adaptation, untuned vs. tuned inhibition), we varied the strength of the adaptation factor from 0.2 and 0.5 (two left columns) to 1.0 (right column); third column, reproducing Figure 7.1 for comparison, shows the simulations for a value of 0.9.

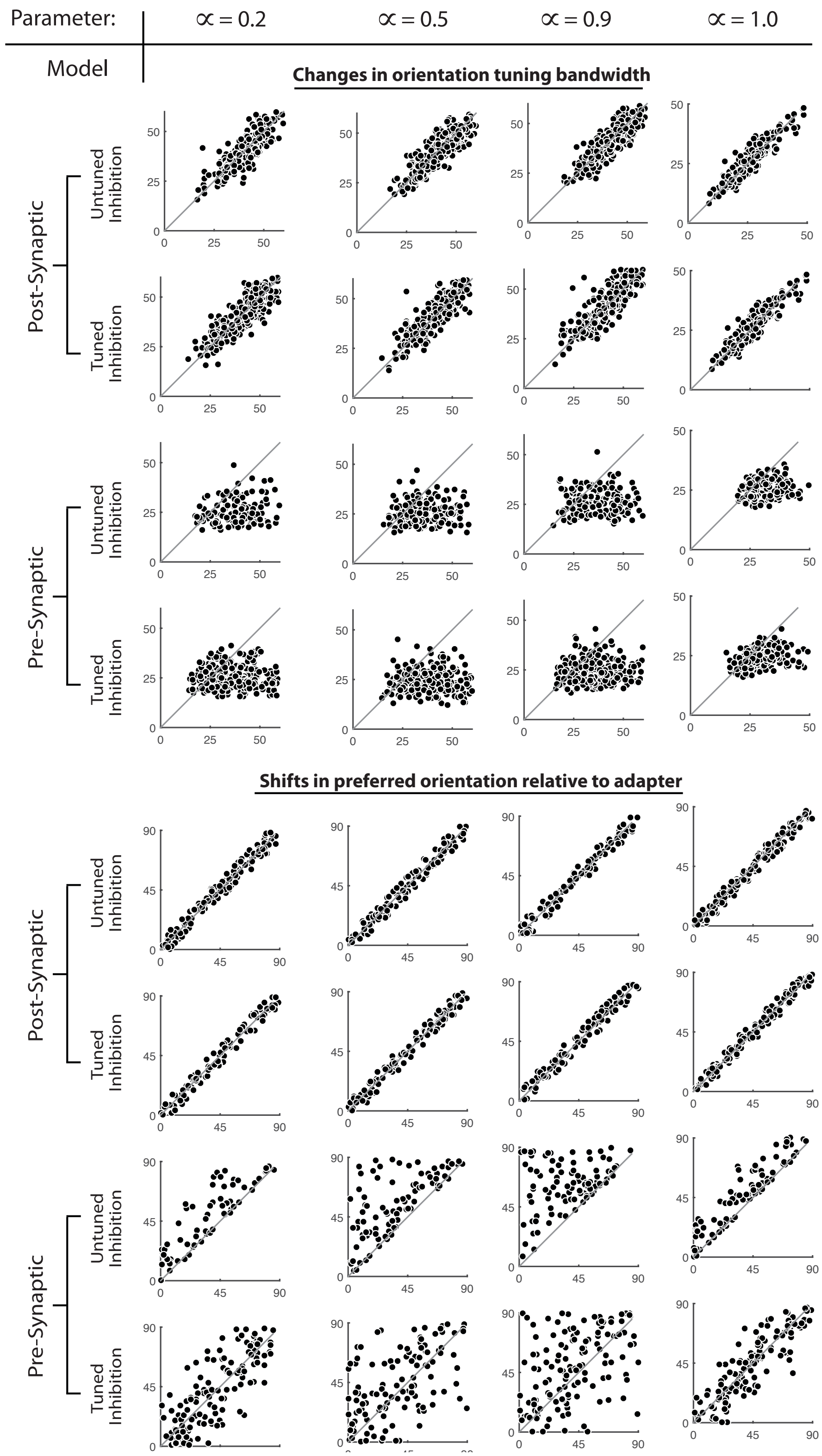

Parameter:
∝ = 0.2
∝ = 0.5
∝ = 0.9
∝ = 1.0
Model
Changes in orientation tuning bandwidth
Post-Synaptic
Untuned Inhibition
Tuned Inhibition
Pre-Synaptic
Untuned Inhibition
Tuned Inhibition
Shifts in preferred orientation relative to adapter
Post-Synaptic
Untuned Inhibition
Tuned Inhibition
Pre-Synaptic
Untuned Inhibition
Tuned Inhibition

Fig 7.8 Model Simulation: Producing Predominantly Attractive Shifts

For the four model classes considered in the main text (pre- vs. post- synaptic adaptation, untuned vs. tuned inhibition), the right column shows the effect of increasing both the amount of inhibition from the standard value of 0.2 to 0.35, and the widths of the excitatory and inhibitory connectivity probability functions were increased compared to the standard model (left column). For the tuned inhibition model with presynaptic adaptation (bottom row of each panel), this led to an increase in the fraction of neurons that showed an attractive shift. The increase was not present if only the connectivity was changed (middle column) or if only the amount of inhibition was increased (right column). Other details as in Figure 7.1.

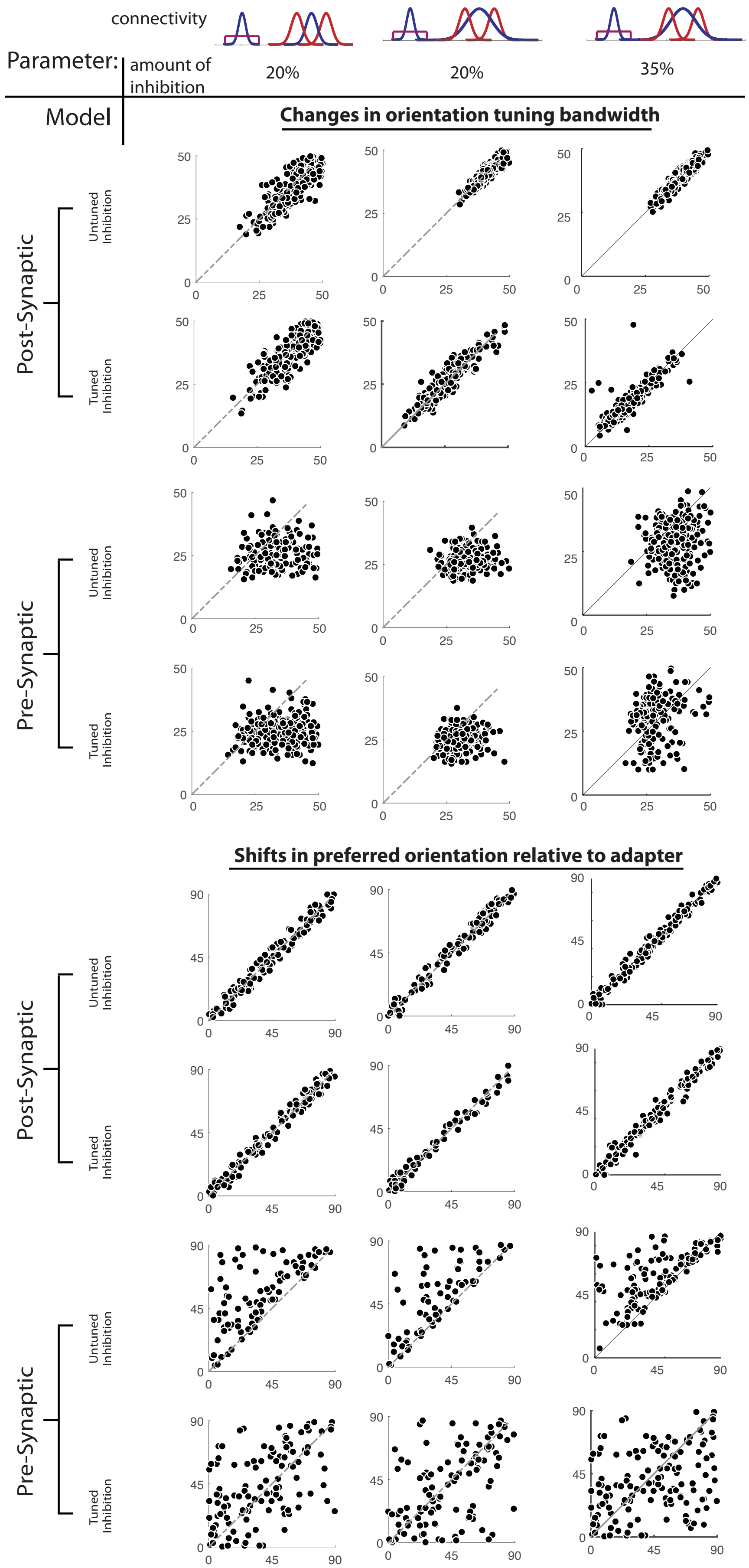
connectivity
Parameter:
amount of inhibition
20%
20%
35%
Model
Changes in orientation tuning bandwidth
Post-Synaptic
Untuned Inhibition
Tuned Inhibition
Pre-Synaptic
Untuned Inhibition
Tuned Inhibition
Shifts in preferred orientation relative to adapter
Post-Synaptic
Untuned Inhibition
Tuned Inhibition
Pre-Synaptic
Untuned Inhibition
Tuned Inhibition

DISCUSSION

To determine the characteristics of cortical networks required to account for the observed effects of adaptation, we considered four model classes. These were distinguished by the site of adaptation (i.e., post-synaptic vs pre-synaptic) and the nature of inhibition (tuned vs. untuned). Simulations showed that only the model class with tuned inhibition and pre-synaptic adaptation can account for both repulsive and attractive shifts -- basic effects of adaptation we observed and that have been widely observed by others (Kohn and Movshon, 2004a),(Patterson et al., 2013b),(Ghisovan et al., 2009b). The need for both characteristics - presynaptic adaptation and tuned inhibition - held even when we allowed two cascading levels of adaptation, thus approximating the effects of recurrence. We note that our model is at a simpler level of detail than Teich and Qian (Teich, 2002), which included spiking dynamics, but as they showed, even when these dynamics are included, untuned inhibition does not lead to attractive shifts.

This model structure accounts for several aspects of the observed diversity, with parameters drawn from the biologically plausible range. In the model as well as in the data, adaptation near the peak orientation of the model neuron induces both increases and decreases in the orientation tuning bandwidth, and the distributions of these changes are similar. Moreover, adaptation off-peak causes attractive, repulsive or no shift in the orientation tuning, again with a comparable distribution of changes in the model and the experimental data. In addition to the obvious factors (adaptation strength, inhibitory sculpting of orientation tuning), the total number of inputs that a neuron receives is relevant to this diversity. Our simulations recapitulate the observed diversity when the number of inputs lies within a broadly reasonable range (100 to 1000 inputs); outside this range, the model yields less diversity in bandwidth changes than is seen in the data.

The model also accounts for the dependence of the average orientation shift on the distance between the adapter and the preferred orientation. Specifically, in both model and data, the tuning shifts are predominantly repulsive when the adapter is within 45^0 of the preferred orientation, and the effect is maximal at a separation of 10^0-20^0. Also in both model and data, tuning shifts are predominantly attractive when the adapter is more than 75^0 away from the preferred orientation.

A final aspect of the data that the model captures is the correlation between the adaptation-induced tuning shifts and changes in firing rate. The level of correlation was present in the simulations was comparable to the data. However in the modeling statistical significance was not reached unless the number of cells in the model was increased beyond the size of the dataset. As was the case in the data, the correlation was stronger in the V2-like model – in which tuned inhibition was stronger. This is consistent with the notion that adaptation induces disinhibition of the tuned inhibitory inputs that are otherwise suppressing the response at the non-preferred orientation.

In sum, our model simulations show that both pre-synaptic adaptation and tuned inhibition are required to account for the diversity the effects of adaptation in visual areas V1 and V2.

CHAPTER 8

GENERAL DISCUSSION

The goal of the experiments in this dissertation was to study how cortical adaptation alters the representations in the visual areas V1 and V2. Our main findings in this study are: 1) adaptation changes the tuning of both broad-spiking (E cells) and narrow-spiking (I cells) in V1 and V2, 2) the effects of E and I cells are distinct, namely, in tuned inhibitory cells, attractive shifts are correlated with increases in firing during prolonged adaptation 3) adaptation induces some untuned cells to become tuned 4) at the population level, effects of adaptation to the orientation tuning are large and diverse: tuning shifts can be repulsive or attractive, and the bandwidths can increase or decrease, 5) adaptive effects in V2 go beyond effects seen in V1, and 6) the range of adaptive effects observed experimentally are only accounted for by models that include tuned inhibition and presynaptic adaptation. In addition to the main results, we develop methods to classify data from tetrode recordings on the basis of their extracellular waveshape (ie, broad-spiking putative excitatory cells vs narrow-spiking putative inhibitory cells), and location on orientation map, i.e putative pinwheel vs iso-orientation domains.

Here we consider the implications of these findings for visual function and dysfunction.

INHIBITION AND ADAPTATION

Inhibitory mechanisms have distinct roles in neuromodulatory phenomena like attention, learning and working memory (Mitchell et al., 2007; Woloszyn and Sheinberg, 2012c). Although the behavior of adaptation-induced tuning shifts was evident in both excitatory and inhibitory celltypes, the strong correlation of adaptation-induced attractive tuning shifts and increased firing rates was seen exclusively in the inhibitory subpopulation. Furthermore, a similar correlation of tuning shifts and firing rate increases emerged in the model as the fraction of tuned inhibitory inputs and their effective connectivity was increased substantially. (Figure 7.3) These findings not only corroborate prevailing theories that tuned inhibitory signals contribute heavily to sculpting cortical tuning going beyond nonspecific pooling, but also suggest that excitatory and inhibitory neurons indeed play distinctive roles in adaptation

FUNCTIONAL GOALS OF ADAPTATION

We now consider the most prominent features in our results, namely the decreases and increases in peak response amplitude and the repulsive and attractive shifts in tuning, and speculate their functional significance in visual coding.

One prominent feature of adaptation is the suppression of peak response amplitude. Functionally, this phenomenon of adaptation has been proposed to be a mechanism of gain control (Kohn, 2007; Shapley and Victor, 1978). By changing the response amplitude without changing selectivity, gain modulations allow the limited output range of the target neuron to match the dynamic range of its inputs, thus enabling the cell to encode information from a wide variety of ranges of input. At the sub-cortical level, gain control is the sole function of adaptation, and there are clear perceptual benefits. For instance in light adaptation, retinal mechanisms alter their sensitivity to match prevailing light levels. Perceptually, we are able to discriminate relatively small changes in luminance, when confronted with light intensity that varies over roughly ten orders of magnitude. This is true for contrast adaptation as well (Shapley and Victor, 1978). At the cortical level, gain control is manifested in the reductions in peak firing rates, with maximal reduction when the adapter matches the preferred stimulus. However as our data clearly show, the peak response amplitudes can increase as well, suggesting that goals of cortical adaptation may go beyond gain control mechanisms.

Another prominent aspect of our findings is that adaptation induces the tuning of cells to either shift away from the adapter (i.e repulsive shift) or move towards it (i.e attractive shift). While these may appear to be opposing phenomena in terms of tuning curves, from the perspective of the stimulus they accomplish the same goal. This is because the distance of the adapting orientation affects the direction of tuning shift. Specifically, if the adapting orientation is within $10^0 – 45^0$ away from the preferred orientation of the cell, then the shift is labelled repulsive. Effectively, if the test stimulus is within 45^0, then these cells reduce their responses to a test stimulus, thus shifting their preferences away from this test orientation. On the other hand if the adapting orientation is $>45^0$ away from the preferred orientation of the cell, then the shift is labelled attractive. Effectively, this means that in the presence of a test stimulus that is 45^0 away, these cells also shift their tuning toward the adapted orientation, which in this case is also toward the test stimulus, thereby maintaining their responses to the test stimulus. Thus the net effect at the population level is to increase the number of cells that are tuned to the off-axis to the adapter. This is consistent with the direct aftereffect and indirect aftereffect in perceived orientation that has been studied extensively (Wenderoth and Johnstone, 1988a).

This net effect of adaptation is in fact a good strategy for the visual system - the effects of adaptation should allow the visual system to make use of the regularities in the environment (i.e., persistent or recurring stimuli) to perform better. Adaptation could exploit the fact that the recent history of the sensory inputs may contain predictive information about upcoming spatiotemporal signals to optimize sensory coding strategies. Our finding that the direction of shifts in tuning depend on the distance of the adapter to the preferred orientation of cells suggest that adaptation is acting in a stimulus-dependent manner, and as we discussed can determine how they are represented in cortical neurons. Furthermore, the gain changes and tuning shifts that we describe are in fact coupled during prolonged adaptation, and suggest key directions for further perceptual studies to determine its distinctive functional benefits to visual coding.

ADAPTATION IN THE EXTRA-STRIATE CORTEX

Our finding that adaptation effects in V2 go beyond inherited effects from V1 supports the idea that adaptation affects the intrinsic processing of extrastriate cortex as well. This is consistent with finding of adaptation-induced tuning shifts in other areas including MT and V4. Specifically, attractive shifts in tuning have been demonstrated in extrastriate area MT, and some of these effects have been linked to effects to V1 (Kohn and Movshon, 2004b). However the nature and size of these stimulus-dependent shifts have been largely similar (Patterson et al., 2014) with a dependence on the stimulus size. In V4, adaptation to motion can induce direction-selective responses in neurons that normally lack such selectivity (Tolias et al., 2005b)– a phenomena we see in V1 as well.

In light of these studies of adaptation in the extrastriate cortices, our finding of adapted effects in V2 is particularly noteworthy as we find that V2 builds upon the adapted representations from V1, and not compensate for them. This is particularly relevant for explaining the complex nature of some perceptual aftereffects demonstrated by several early psychophysical studies (Wenderoth and Johnstone, 1988a). This also raises the possibility that the representation of complex features like textures and illusory contours that first emerges in V2 may be influenced by the adaptation of oriented signals that V2 inherited from its upstream source. Moreover, the existence of high-level aftereffects (induced by adaptation to faces(Webster and MacLeod, 2011), emotions(Zimmer and Kovacs, 2011), attractiveness of face (Rhodes et al., 2007)), further confirm that adaptive coding is not only a property of the early stages of sensory processing but is instead a strategy employed throughout the perceptual processing hierarchy.

Together these results suggest that adaptation in extrastriate cortices can profoundly modify response properties, corroborating psychophysical evidence that passed-on adaptation effects can affect higher-level visual processing (Dickinson and Badcock, 2013; McKone et al., 2014). It also needs to be resolved whether a similarly large diversity of adaptation effects occur under natural viewing conditions, since that would imply that neuronal response properties could potentially change profoundly even during normal vision as well.

Known dysfunctions

Given that adaptation is important for normal sensory processing, one would expect that disturbances in adaptation can lead to disturbances in perception, and there is evidence for such dysfunctions. Patients with idiopathic generalized epilepsy have impaired visual contrast gain control (Tsai et al., 2011). Modeling study of such abnormalities have attributed this phenomenon to reduced inhibitory modulation in the underlying circuitry. In this context, it is noteworthy that the parameters in our simplified models that influenced the adaptation-induced responsiveness and shifts in tuning were the one that altered the E/I balance of the network as well (Figure 7.8).

Perceptual disorders have also been attributed to dysfunctions to adaptation. Rapid visual neural adaptation, particularly adaptation to faces and visual objects has been shown to be diminished in children and adults with dyslexia (Perrachione et al., 2016). Such abnormalities in mechanisms of adaptation like gain control have been associated with other perceptual experiences in which atypical sensory processing is symptomatic, as in disorders of cortical excitability like autism spectrum disorders (Foss-Feig et al., 2013; Takarae et al., 2016), and in people who experience visual snow (McKendrick et al., 2017). At the level of cortical circuitry, dysregulations to the precise balance of excitatory and inhibitory tone has been shown to result in a wide range of sensory processes to go awry, ultimately impairing perceptual functions. Thus, given the ubiquitous nature of adaptation, and the related perceptual correlates of dysfunction to the known mechanisms like gain control, it suggests that the cortical adaptation could potentially serve as biomarker for intact cortical function.

CONCLUSION

The focus of this thesis was on the effects of adaptation in excitatory and inhibitory cells in two related cortical regions V1 and V2. Neuronal, laminar, and regional analyses revealed key aspects of the diversity of effects and their dependence of the stimulus properties.

While the functional role of adaptation in natural vision is still unclear, we have gained some insight into how adaptation affects population coding. Yet some the fundamental questions about the function of adaptation remain unanswered. In order to better resolve some of these issues, the effects of adaptation of naturalistic stimuli needs to be understood. Finally, a better knowledge of effects at different stages of visual processing, particularly extrastriate areas closely linked to perception, is crucial. Further modeling studies that include the dynamics of recurrence and experimental exploration are required to answers these questions.

REFERENCES

1. Abbonizio, G., Langley, K., and Clifford, C.W.G. (2002). Contrast adaptation may enhance contrast discrimination. Spat. Vis. *16*, 45–58.

2. Baccus, S.A., and Meister, M. (2002). Fast and slow contrast adaptation in retinal circuitry. Neuron *36*, 909–919.

3. Bachatene, L., Bharmauria, V., Rouat, J., and Molotchnikoff, S. (2012). Adaptation-induced plasticity and spike waveforms in cat visual cortex: NeuroReport *23*, 88–92.

4. Bao, M., Fast, E., Mesik, J., and Engel, S. (2013). Distinct mechanisms control contrast adaptation over different timescales. J. Vis. *13*.

5. Barlow, H.B. (2012). Possible Principles Underlying the Transformations of Sensory Messages. In Sensory Communication, W.A. Rosenblith, ed. (The MIT Press), pp. 216–234.

6. Bartho, P. (2004). Characterization of Neocortical Principal Cells and Interneurons by Network Interactions and Extracellular Features. J. Neurophysiol. *92*, 600–608.

7. Bastian, A.J. (2008). Understanding sensorimotor adaptation and learning for rehabilitation: Curr. Opin. Neurol. *21*, 628–633.

8. Bean, B.P. (2007). The action potential in mammalian central neurons. Nat. Rev. Neurosci. *8*, 451–465.

9. Bock, D.D., Lee, W.-C.A., Kerlin, A.M., Andermann, M.L., Hood, G., Wetzel, A.W., Yurgenson, S., Soucy, E.R., Kim, H.S., and Reid, R.C. (2011). Network anatomy and in vivo physiology of visual cortical neurons. Nature *471*, 177–182.

10. Bonds, A.B. (1989). Role of Inhibition in the Specification of Orientation Selectivity of Cells in the Cat Striate Cortex. Vis. Neurosci. *2*, 41–55.

11. Bonhoeffer, T., and Grinvald, A. (1991). Iso-orientation domains in cat visual cortex are arranged in pinwheel-like patterns. Nature *353*, 429–431.

12. Boynton, G.M., and Hegdé, J. (2004). Visual Cortex: The Continuing Puzzle of Area V2. Curr. Biol. *14*, R523–R524.

13. Bradley, A., Switkes, E., and De Valois, K. (1988). Orientation and spatial frequency selectivity of adaptation to color and luminance gratings. Vision Res. *28*, 841–856.

14. Burkhalter, A., and Van Essen, D.C. (1986). Processing of color, form and disparity information in visual areas VP and V2 of ventral extrastriate cortex in the macaque monkey. J. Neurosci. Off. J. Soc. Neurosci. *6*, 2327–2351.

15. Carandini, M., and Ferster, D. (1997). A tonic hyperpolarization underlying contrast adaptation in cat visual cortex. Science *276*, 949–952.

16. Carandini, M., and Ringach, D.L. (1997). Predictions of a recurrent model of orientation selectivity. Vision Res. *37*, 3061–3071.

17. Chariker, L., Shapley, R., and Young, L.-S. (2016). Orientation Selectivity from Very Sparse LGN Inputs in a Comprehensive Model of Macaque V1 Cortex. J. Neurosci. *36*, 12368–12384.

18. Clifford, C.W., Wyatt, A.M., Arnold, D.H., Smith, S.T., and Wenderoth, P. (2001a). Orthogonal adaptation improves orientation discrimination. Vision Res. *41*, 151–159.

19. Clifford, C.W.G., Webster, M.A., Stanley, G.B., Stocker, A.A., Kohn, A., Sharpee, T.O., and Schwartz, O. (2007a). Visual adaptation: neural, psychological and computational aspects. Vision Res. *47*, 3125–3131.

20. Contreras, D., and Palmer, L. (2003). Response to contrast of electrophysiologically defined cell classes in primary visual cortex. J. Neurosci. Off. J. Soc. Neurosci. *23*, 6936–6945.

21. Crowder, N.A., Price, N.S.C., Hietanen, M.A., Dreher, B., Clifford, C.W.G., and Ibbotson, M.R. (2006). Relationship between contrast adaptation and orientation tuning in V1 and V2 of cat visual cortex. J. Neurophysiol. *95*, 271–283.

22. De Valois, R.L., William Yund, E., and Hepler, N. (1982a). The orientation and direction selectivity of cells in macaque visual cortex. Vision Res. *22*, 531–544.

23. Dickinson, J.E., and Badcock, D.R. (2013). On the hierarchical inheritance of aftereffects in the visual system. Front. Psychol. *4*.

24. Dragoi, V., Sharma, J., and Sur, M. (2000a). Adaptation-Induced Plasticity of Orientation Tuning in Adult Visual Cortex. Neuron *28*, 287–298.

25. Du, J., Zhang, L., Weiser, M., Rudy, B., and McBain, C.J. (1996). Developmental expression and functional characterization of the potassium-

channel subunit Kv3.1b in parvalbumin-containing interneurons of the rat hippocampus. J. Neurosci. Off. J. Soc. Neurosci. *16*, 506–518.

26. Duong, T., and Freeman, R.D. (2007). Spatial frequency-specific contrast adaptation originates in the primary visual cortex. J. Neurophysiol. *98*, 187–195.

27. Foss-Feig, J.H., Tadin, D., Schauder, K.B., and Cascio, C.J. (2013). A Substantial and Unexpected Enhancement of Motion Perception in Autism. J. Neurosci. *33*, 8243–8249.

28. Ghisovan, N., Nemri, A., Shumikhina, S., and Molotchnikoff, S. (2009a). Long adaptation reveals mostly attractive shifts of orientation tuning in cat primary visual cortex. Neuroscience *164*, 1274–1283.

29. Gibson, J.J., and Radner, M. (1937). Adaptation, after-effect and contrast in the perception of tilted lines. I. Quantitative studies. J. Exp. Psychol. *20*, 453–467.

30. Harris, K.D., and Mrsic-Flogel, T.D. (2013). Cortical connectivity and sensory coding. Nature *503*, 51–58.

31. Hegdé, J., and Van Essen, D.C. (2000). Selectivity for complex shapes in primate visual area V2. J. Neurosci. Off. J. Soc. Neurosci. *20*, RC61.

32. Hegdé, J., and Van Essen, D.C. (2003). Strategies of shape representation in macaque visual area V2. Vis. Neurosci. *20*, 313–328.

33. Hubel, D.H., and Wiesel, T.N. (1959). Receptive fields of single neurones in the cat's striate cortex. J. Physiol. *148*, 574–591.

34. Kaufman, M.T., Churchland, M.M., Santhanam, G., Yu, B.M., Afshar, A., Ryu, S.I., and Shenoy, K.V. (2010a). Roles of monkey premotor neuron classes in movement preparation and execution. J. Neurophysiol. *104*, 799–810.

35. Kaufman, M.T., Churchland, M.M., Santhanam, G., Yu, B.M., Afshar, A., Ryu, S.I., and Shenoy, K.V. (2010b). Roles of Monkey Premotor Neuron Classes in Movement Preparation and Execution. J. Neurophysiol. *104*, 799–810.

36. Koch, E., Jin, J., Alonso, J.M., and Zaidi, Q. (2016). Functional implications of orientation maps in primary visual cortex. Nat. Commun. *7*, 13529.

37. Kohn, A. (2007). Visual Adaptation: Physiology, Mechanisms, and Functional Benefits. J. Neurophysiol. *97*, 3155–3164.

38. Kohn, A., and Movshon, J.A. (2004a). Adaptation changes the direction tuning of macaque MT neurons. Nat. Neurosci. *7*, 764–772.

39. Maldonado, P.E., Gödecke, I., Gray, C.M., and Bonhoeffer, T. (1997). Orientation selectivity in pinwheel centers in cat striate cortex. Science *276*, 1551–1555.

40. Marshall, J.F. (1984). Brain Function: Neural Adaptations and Recovery From Injury. Annu. Rev. Psychol. *35*, 277–308.

41. McCormick, D.A., Connors, B.W., Lighthall, J.W., and Prince, D.A. (1985). Comparative electrophysiology of pyramidal and sparsely spiny stellate neurons of the neocortex. J. Neurophysiol. *54*, 782–806.

42. McDougle, S.D., Bond, K.M., and Taylor, J.A. (2017). Implications of plan-based generalization in sensorimotor adaptation. J. Neurophysiol. jn.00974.2016.

43. McKendrick, A.M., Chan, Y.M., Tien, M., Millist, L., Clough, M., Mack, H., Fielding, J., and White, O.B. (2017). Behavioral measures of cortical hyperexcitability assessed in people who experience visual snow. Neurology *88*, 1243–1249.

44. McKone, E., Jeffery, L., Boeing, A., Clifford, C.W.G., and Rhodes, G. (2014). Face identity aftereffects increase monotonically with adaptor extremity over, but not beyond, the range of natural faces. Vision Res. *98*, 1–13.

45. McLaughlin, D., Shapley, R., Shelley, M., and Wielaard, D.J. (2000a). A neuronal network model of macaque primary visual cortex (V1): orientation selectivity and dynamics in the input layer 4Calpha. Proc. Natl. Acad. Sci. U. S. A. *97*, 8087–8092.

46. Mechler, F., and Ringach, D.L. (2002). On the classification of simple and complex cells. Vision Res. *42*, 1017–1033.

47. Mitchell, J.F., Sundberg, K.A., and Reynolds, J.H. (2007). Differential attention-dependent response modulation across cell classes in macaque visual area V4. Neuron *55*, 131–141.

48. Ohki, K., Chung, S., Kara, P., Hübener, M., Bonhoeffer, T., and Reid, R.C. (2006). Highly ordered arrangement of single neurons in orientation pinwheels. Nature *442*, 925–928.

49. O'Toole, B., and Wenderoth, P. (1977a). The tilt illusion: repulsion and attraction effects in the oblique meridian. Vision Res. *17*, 367–374.

50. Patterson, C.A., Wissig, S.C., and Kohn, A. (2013a). Distinct effects of brief and prolonged adaptation on orientation tuning in primary visual cortex. J. Neurosci. Off. J. Soc. Neurosci. *33*, 532–543.

51. Patterson, C.A., Duijnhouwer, J., Wissig, S.C., Krekelberg, B., and Kohn, A. (2014). Similar adaptation effects in primary visual cortex and area MT of the macaque monkey under matched stimulus conditions. J. Neurophysiol. *111*, 1203–1213.

52. Perrachione, T.K., Del Tufo, S.N., Winter, R., Murtagh, J., Cyr, A., Chang, P., Halverson, K., Ghosh, S.S., Christodoulou, J.A., and Gabrieli, J.D.E. (2016). Dysfunction of Rapid Neural Adaptation in Dyslexia. Neuron *92*, 1383–1397.

53. Peyrache, A., Dehghani, N., Eskandar, E.N., Madsen, J.R., Anderson, W.S., Donoghue, J.A., Hochberg, L.R., Halgren, E., Cash, S.S., and Destexhe, A. (2012). Spatiotemporal dynamics of neocortical excitation and inhibition during human sleep. Proc. Natl. Acad. Sci. *109*, 1731–1736.

54. Phillips, E.A., and Hasenstaub, A.R. (2016). Asymmetric effects of activating and inactivating cortical interneurons. eLife *5*.

55. Reich, D.S., Mechler, F., and Victor, J.D. (2001). Temporal Coding of Contrast in Primary Visual Cortex: When, What, and Why. J. Neurophysiol. *85*, 1039–1050.

56. Rhodes, G., Jeffery, L., Clifford, C.W.G., and Leopold, D.A. (2007). The timecourse of higher-level face aftereffects. Vision Res. *47*, 2291–2296.

57. Ringach, D.L., Shapley, R.M., and Hawken, M.J. (2002a). Orientation selectivity in macaque V1: diversity and laminar dependence. J. Neurosci. Off. J. Soc. Neurosci. *22*, 5639–5651.

58. Rossant, C., Kadir, S.N., Goodman, D.F.M., Schulman, J., Hunter, M.L.D., Saleem, A.B., Grosmark, A., Belluscio, M., Denfield, G.H., Ecker, A.S., et al. (2016). Spike sorting for large, dense electrode arrays. Nat. Neurosci. *19*, 634–641.

59. Rudy, B., and McBain, C.J. (2001). Kv3 channels: voltage-gated K+ channels designed for high-frequency repetitive firing. Trends Neurosci. *24*, 517–526.

60. Seriès, P., Stocker, A.A., and Simoncelli, E.P. (2009). Is the Homunculus “Aware” of Sensory Adaptation? Neural Comput. *21*, 3271–3304.

61. Shapley, R., and Enroth-Cugell, C. (1984). Chapter 9 Visual adaptation and retinal gain controls. Prog. Retin. Res. *3*, 263–346.

62. Shapley, R.M., and Victor, J.D. (1978). The effect of contrast on the transfer properties of cat retinal ganglion cells. J. Physiol. *285*, 275–298.

63. Shapley, R., Hawken, M., and Ringach, D.L. (2003). Dynamics of Orientation Selectivity in the Primary Visual Cortex and the Importance of Cortical Inhibition. Neuron *38*, 689–699.

64. Sharpee, T.O., Sugihara, H., Kurgansky, A.V., Rebrik, S.P., Stryker, M.P., and Miller, K.D. (2006). Adaptive filtering enhances information transmission in visual cortex. Nature *439*, 936–942.

65. Sillito, A.M. (1979). Inhibitory mechanisms influencing complex cell orientation selectivity and their modification at high resting discharge levels. J. Physiol. *289*, 33–53.

66. Skottun, B.C., De Valois, R.L., Grosof, D.H., Movshon, J.A., Albrecht, D.G., and Bonds, A.B. (1991). Classifying simple and complex cells on the basis of response modulation. Vision Res. *31*, 1078–1086.

67. Solomon, S.G., Peirce, J.W., Dhruv, N.T., and Lennie, P. (2004). Profound contrast adaptation early in the visual pathway. Neuron *42*, 155–162.

68. Somers, D.C., Nelson, S.B., and Sur, M. (1995a). An emergent model of orientation selectivity in cat visual cortical simple cells. J. Neurosci. Off. J. Soc. Neurosci. *15*, 5448–5465.

69. Sompolinsky, H., and Shapley, R. (1997a). New perspectives on the mechanisms for orientation selectivity. Curr. Opin. Neurobiol. *7*, 514–522.

70. Stavisky, S.D., Kao, J.C., Ryu, S.I., and Shenoy, K.V. (2017). Trial-by-Trial Motor Cortical Correlates of a Rapidly Adapting Visuomotor Internal Model. J. Neurosci. Off. J. Soc. Neurosci. *37*, 1721–1732.

71. Takarae, Y., Sablich, S.R., White, S.P., and Sweeney, J.A. (2016). Neurophysiological hyperresponsivity to sensory input in autism spectrum disorders. J. Neurodev. Disord. *8*.

72. Teich, A.F. (2002). Learning and Adaptation in a Recurrent Model of V1 Orientation Selectivity. J. Neurophysiol. *89*, 2086–2100.

73. Thengone, D.J., Voss, H.U., Fridman, E.A., and Schiff, N.D. (2016). Local changes in network structure contribute to late communication recovery after severe brain injury. Sci. Transl. Med. *8*, 368re5–re368re5.

74. Tkacik, G., Prentice, J.S., Victor, J.D., and Balasubramanian, V. (2010). Local statistics in natural scenes predict the saliency of synthetic textures. Proc. Natl. Acad. Sci. *107*, 18149–18154.

75. Tolias, A.S., Keliris, G.A., Smirnakis, S.M., and Logothetis, N.K. (2005a). Neurons in macaque area V4 acquire directional tuning after adaptation to motion stimuli. Nat. Neurosci. *8*, 591–593.

76. Tsai, J.J., Norcia, A.M., Ales, J.M., and Wade, A.R. (2011). Contrast gain control abnormalities in idiopathic generalized epilepsy. Ann. Neurol. *70*, 574–582.

77. Van Essen, D.C., and Maunsell, J.H.R. (1983). Hierarchical organization and functional streams in the visual cortex. Trends Neurosci. *6*, 370–375.

78. Wark, B., Lundstrom, B.N., and Fairhall, A. (2007). Sensory adaptation. Curr. Opin. Neurobiol. *17*, 423–429.

79. Webster, M.A. (2011). Adaptation and visual coding. J. Vis. *11*, 3–3.

80. Webster, M.A., and MacLeod, D.I.A. (2011). Visual adaptation and face perception. Philos. Trans. R. Soc. B Biol. Sci. *366*, 1702–1725.

81. Wei, K., and Kording, K. (2008). Relevance of Error: What Drives Motor Adaptation? J. Neurophysiol. *101*, 655–664.

82. Weliky, M., Bosking, W.H., and Fitzpatrick, D. (1996). A systematic map of direction preference in primary visual cortex. Nature *379*, 725–728.

83. Wenderoth, P., and Johnstone, S. (1988a). The different mechanisms of the direct and indirect tilt illusions. Vision Res. *28*, 301–312.

84. Whitmire, C.J., and Stanley, G.B. (2016). Rapid Sensory Adaptation Redux: A Circuit Perspective. Neuron *92*, 298–315.

85. Wilson, D.E., Whitney, D.E., Scholl, B., and Fitzpatrick, D. (2016). Orientation selectivity and the functional clustering of synaptic inputs in primary visual cortex. Nat. Neurosci. *19*, 1003–1009.

86. Wilson, D.E., Smith, G.B., Jacob, A.L., Walker, T., Dimidschstein, J., Fishell, G., and Fitzpatrick, D. (2017). GABAergic Neurons in Ferret Visual Cortex Participate in Functionally Specific Networks. Neuron *93*, 1058–1065.e4.

87. Woloszyn, L., and Sheinberg, D.L. (2012a). Effects of Long-Term Visual Experience on Responses of Distinct Classes of Single Units in Inferior Temporal Cortex. Neuron *74*, 193–205.

88. Xerri, C., Merzenich, M.M., Peterson, B.E., and Jenkins, W. (1998). Plasticity of primary somatosensory cortex paralleling sensorimotor skill recovery from stroke in adult monkeys. J. Neurophysiol. *79*, 2119–2148.

89. Xing, D., Ringach, D.L., Hawken, M.J., and Shapley, R.M. (2011). Untuned Suppression Makes a Major Contribution to the Enhancement of Orientation Selectivity in Macaque V1. J. Neurosci. *31*, 15972–15982.

90. Yamins, D.L.K., and DiCarlo, J.J. (2016). Using goal-driven deep learning models to understand sensory cortex. Nat. Neurosci. *19*, 356–365.

91. Yu, Y., Schmid, A.M., and Victor, J.D. (2015). Visual processing of informative multipoint correlations arises primarily in V2. eLife *4*, e06604.

92. Zimmer, M., and Kovacs, G. (2011). Position specificity of adaptation-related face aftereffects. Philos. Trans. R. Soc. B Biol. Sci. *366*, 586–595.